Master Thesis
TVVR 21/5009

A Laboratory-Scale Examination to Find an Optimal Application for a Groundwater Barrier Well

Tatsuya Nagino

Division of Water Resources Engineering
Department of Building and Environmental Technology
Lund University

A Laboratory-Scale Examination to Find an Optimal Application for a Groundwater Barrier Well

By:
Tatsuya Nagino

Master Thesis

Division of Water Resources Engineering
Department of Building & Environmental Technology
Lund University
Box 118
221 00 Lund, Sweden

Water Resources Engineering
TVVR-21/5009
ISSN 1101-9824

Lund 2021
www.tvrl.lth.se

Master Thesis
Division of Water Resources Engineering
Department of Building & Environmental Technology
Lund University

Swedish title:	En studie i laboratorieskala för tillämpning av optimiserad grundvattenbarriär
English title:	A Laboratory-Scale Examination to Find an Optimal Application for a Groundwater Barrier Well
Author(s):	Tatsuya Nagino
Supervisor:	Ronny Berndtsson
Examiner:	Magnus Larson
Language	English
Year:	2021
Keywords:	<Groundwater, Seawater intrusion, Countermeasure, Negative hydraulic barrier, Sea level rise, Coastal aquifer >

Acknowledgement

This thesis work is a part of my study in the master's course in the double degree program between the Department of Urban and Environmental Engineering, Kyushu University and the Division of Water Resources, Lund University.

I would like to express my gratitude to my supervisor, associate Professor Yoshinari Hiroshiro, who supported me throughout my study in the master's in Lund University and Kyushu University. This thesis would not have been completed without his kind support.

I would also like to extend my special thanks to my supervisor, Professor Ronny Berndtsson, and examiner, Professor Magnus Larsson. They kindly agreed to be my supervisor and examiner from Lund university, and gave me productive comments and advice on the thesis every time I asked them.

I also acknowledge the technical support by Mr. Oishi Hideto, a technical officer in Kyushu university. He helped me fix the experimental device and gave me many advices when I had some difficulties in my study.

My thanks should be extended to Mr. Suyama, who did the experiments with me and discussed a lot throughout the experiments. The experiments sometimes took all day long and it could not be done without his dedication.

I also appreciate Mr. Fujita, Ms. Abi Akl, and Mr. Ozaki, who basically designed the experimental device and numerical simulation model. They gave me a lot of advice in the experiments and the simulation, and I could learn a lot though the discussion with all of them.

Professor Koji Nishiyama and Mr. Kasai gave some comments on my study and kindly helped me improve the presentation of this study.

Ms. Branston kindly gave me some feedback on my writing as a native English speaker. Although it was my first paper written in English, I could complete it somehow with her advice.

Most importantly, I sincerely appreciate all the support from my family. I could learn a lot though the life in Master's in Kyushu university and Lund university thanks to them, and this thesis work would not have been done without their support. Thank you.

Abstract

Seawater intrusion has been aggravated due to anthropogenic reasons, such as sea level rise and over abstraction of groundwater, which is spoiling the groundwater sustainability. This study focused on a negative hydraulic barrier using a barrier well as a countermeasure. Two lab-scale experiments and a numerical analysis with a 2-D solute transport model were conducted to examine an optimal location for a barrier well and effects of groundwater level reduction or sea level rise on the optimal location. These experiments and simulation showed it would be better to pump saline water from a lower part of the aquifer to remediate seawater intrusion batter and faster. However, it also revealed that there was no exact optimal horizontal location for a barrier well, and instead it showed prompt remediation by an inland barrier well and better remediation rate by a coastal barrier. Groundwater level reduction or sea level rise would hinder remediation of a barrier well and aggravate the barrier well disadvantage to salinize the coastal side. Based on the simulation results, an effective barrier well application was suggested to remediate seawater intrusion faster and better, and to minimize the barrier well disadvantage to salinize the coastal side.

Table of Contents

Chapter 1: Introduction

1 Background

Although there is plenty of water on earth, about 97.2% of the total water is in the sea and 2.14% of it is frozen as glaciers or ice caps. Therefore, more than 99% of the planet's water is not available for human use (Fetter, 2014). As for the rest of water, this restricted amount of water can be used as freshwater and more than 98% of which is groundwater, which is better quality and at a more stable temperature compared to surface water in general (Fetter, 2014). Thanks to the quality and quantity, groundwater is one of the most precious water resources on earth.

Recently, however, groundwater salinization caused by seawater intrusion has been reported in many coastal areas, and that is spoiling the potential sustainability of the groundwater use. Figure 1-1 shows the fresh and saltwater interface of seawater intrusion. Because of the difference in density between freshwater and saltwater, seawater flows into the bottom of the fresh groundwater and forms saltwater wedges in coastal areas, and then the intrusion stops at an equilibrium point. However, groundwater salinization has been aggravated due to anthropogenic reasons, such as climate change and population growth. Sea level rise caused by climate change and reduction of the groundwater table caused by excessive pumping for human use break the equilibrium of the seawater intrusion. This causes the interface to enter further inland, threatening the quality and quantity of the fresh groundwater.

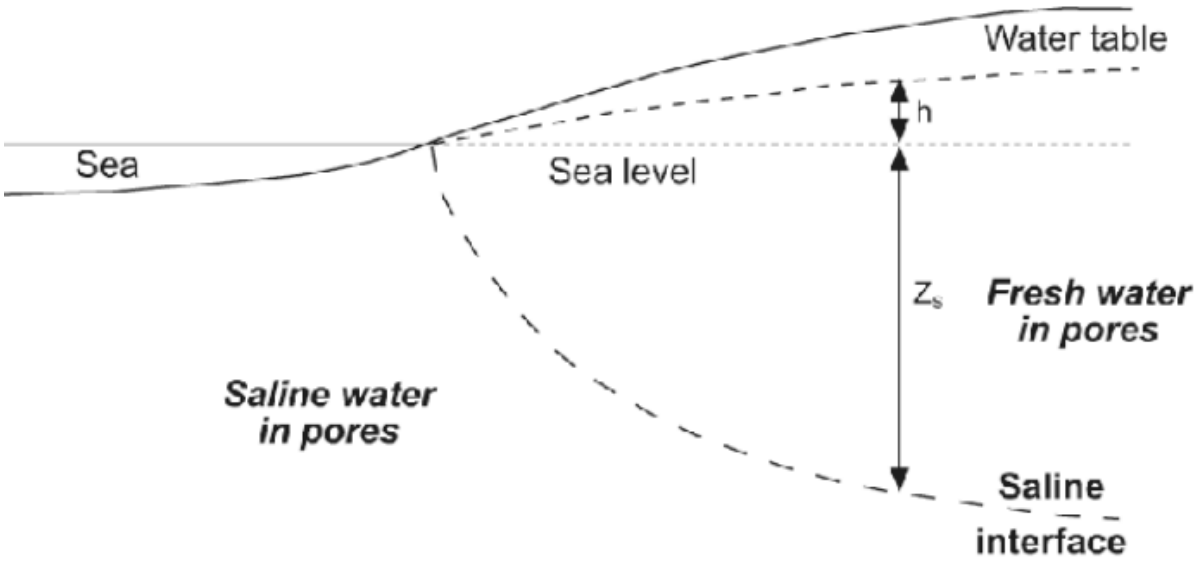

Figure 1-1: Simplified freshwater-saltwater interface in a coastal aquifer. (Ingham et al., 2006)

Ghyben and Herezberg showed the simplified equation for the depth of the saline interface in a coastal aquifer as shown in Eq. (1-1) (Fetter, 2014).

$$z = \frac{\rho_f}{\rho_s - \rho_f} h \tag{1-1}$$

where h is the height of freshwater level above sea level, and z is the depth of the fresh-saltwater interface below sea level. ρ_f and ρ_s are the densities of freshwater and saltwater, respectively. Considering the general densities of freshwater and saltwater, which are 1.000 g/cm^3 and 1.025 g/cm^3 respectively, the Ghyben-Herezberg equation can be written as;

$$z = 40h \tag{1-2}$$

This equation indicates that the reduction of the freshwater depth below sea level will be 40 times bigger than that of the freshwater depth above sea level. This is how sea level rise and over pumping can break the equilibrium and cause further seawater intrusion.

Figure 1-2 shows world population density and salinized areas reported by IGRAC as of 2009 (Costall et al., 2018). As shown in the figure, relatively high population densities are located along coastal areas, which means there are higher demands of freshwater for human activities in these areas. In fact, most of these reported salinized areas, which is colored in green in the figure, exist along the coastal areas.

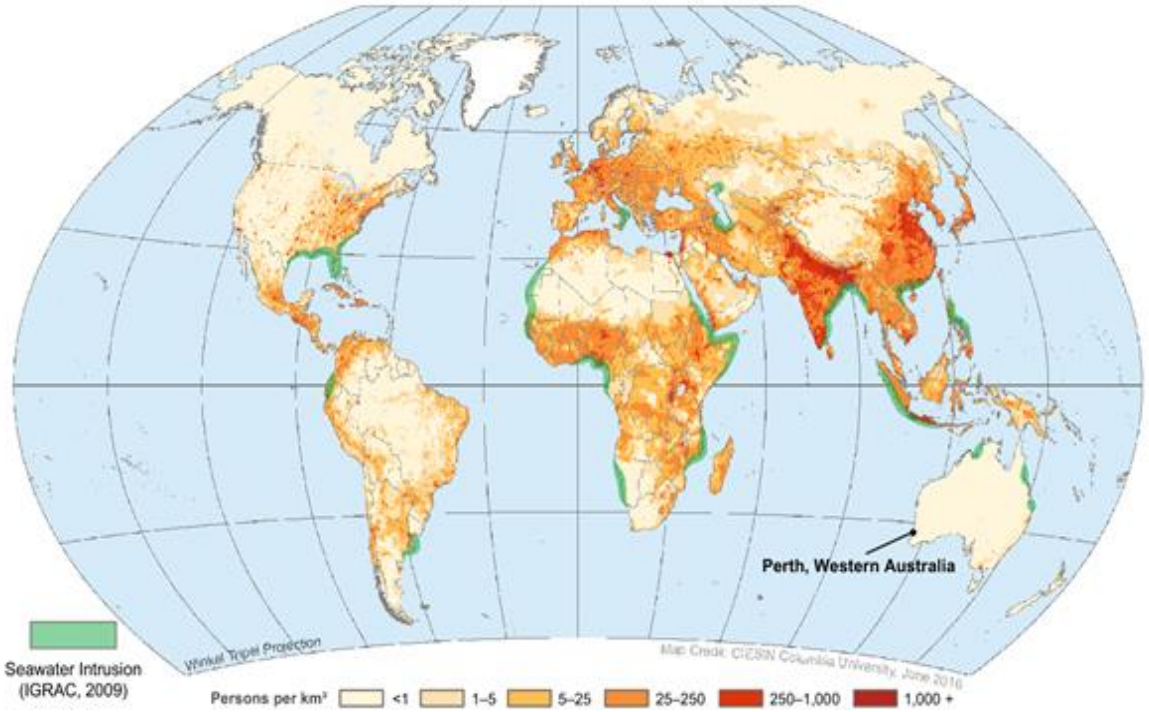

Figure 1-2: Distribution of world population density and seawater intrusion regions (Costall et at., 2018)

According to IPCC's report, global mean sea level is accelerating and will rise 1.1m by 2100 compared to the mean sea level for 1986-2005 in the worst scenario, RCP8.5 (IPCC, 2019).

Besides, United Nations predicts that the world population will be almost 10 billion by 2050 (United Nations, 2019), which could lead to further demand for freshwater. Considering these ongoing and predicted concerns, it would be inevitable for the groundwater salinization to keep deteriorating without any countermeasures. As a matter of fact, Sherif et al. (1999) revealed that 0.5 m of sea level rise would cause 9.0 km and 0.4 km of additional seawater intrusion in the Nile Delta aquifer in Egypt and the Madras aquifer in India without any countermeasures, respectively. Therefore, some remedial approaches have to be taken to maintain the sustainability of groundwater.

Several countermeasures have been studied and used to control the seawater intrusion and these approaches were categorized into these three different groups: conventional/temporary methods, physical barriers, hydraulic barriers (Hussain et al., 2019).

Reduction of pumping or relocation of pumping wells are the common examples for the conventional/temporary methods. Although these methods are the simplest and most direct approach to remediate seawater intrusion, they are usually regarded as temporary solutions because of restrictions such as difficulty to reduce water demands and unavailability of alternative land for new wells (Hussain et al., 2019).

Physical barriers, such as physical subsurface barriers and surface barriers with land reclamation, in front of the intruding seawater body prevent further seawater intrusion. However, these methods are expensive in general. Hence, hydraulic barrier approaches have been more popular than any other countermeasures (Hussain et al., 2019).

There are mainly three types of barrier in hydraulic barrier approaches: positive hydraulic barriers by recharging water, negative hydraulic barriers by pumping saline or brackish water, and the combination of these two types of barrier. These methods change the piezometric head, which enhances the seaward hydraulic gradient and then prevents or repulses the seawater intrusion. Especially in arid or semi-arid regions, negative hydraulic barriers (Figure 1-3) are easy to apply because no other water source to recharge is needed and the pumped brackish or saline water can be used in the industrial activities or even for the desalination plants. However, this negative hydraulic barrier can pump some portion of freshwater at the same time, which is the major negative aspect of this approach (Hussain et al., 2019), and yet this method is often applied without enough planning in practice (Pool et al., 2009). Furthermore, the remediation of seawater intrusion could take as long as decades or hundreds of years (Ebeling et al., 2019). Considering these negative aspects and the future when further seawater intrusion has been predicted, it will be required to find a more effective application of the seawater pumping wells in order to protect the precious fresh groundwater in the future.

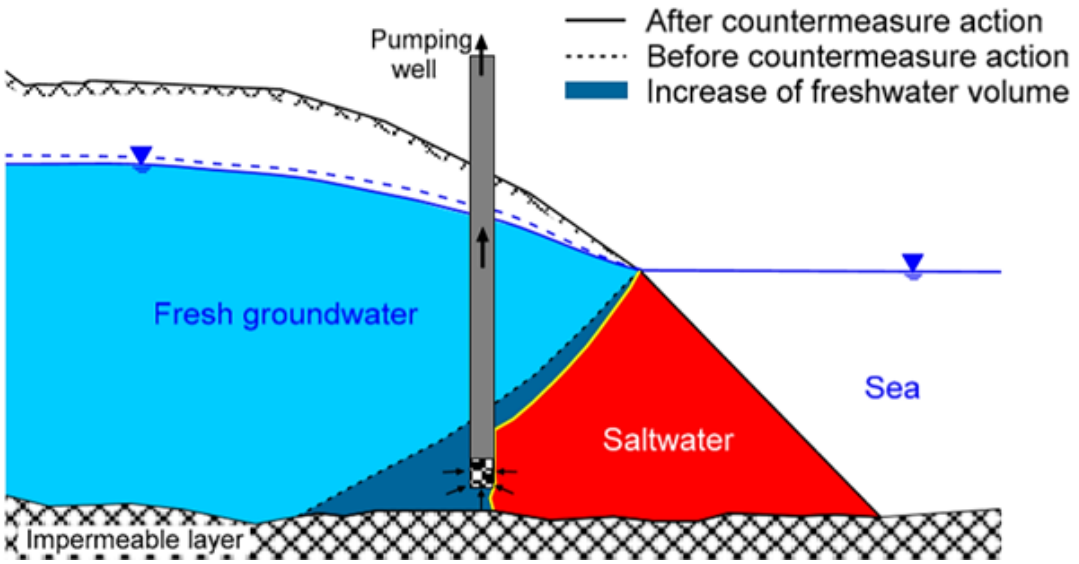

Figure 1-3: Conceptual image of saltwater pumping (Hussain et al., 2019)

2 Objectives

As mentioned above, seawater intrusion in coastal aquifers has been deteriorating mainly because of sea level rise and over extraction of groundwater, which threatens the sustainability of groundwater use. Some countermeasures have been studied and recently hydraulic barriers are more popular than the others, but a more effective application still needs to be studied considering the predicted further seawater intrusion in the future, as well as the negative aspects of saltwater pumping. This study focused on negative hydraulic barriers to find an optimal location of a barrier well instalment. Besides, effects of sea level rise or groundwater level reduction on the barrier efficiency was studied, and based on these examinations, an optimal barrier well application for the future was suggested at last.

Even though some effective conditions or locations for negative hydraulic barrier wells have been studied, these studies were conducted with only a few horizontal locations and exact relations between barrier effectiveness and well locations have not been established yet. Besides, the influence from different hydraulic heads, considering climate change or over abstraction of groundwater, on the barrier efficiency and the optimal barrier well application for the future have not yet been studied.

In this paper, two laboratory scale experiments and numerical simulations were conducted for the following three objects.

1. To find an optimal location to install a barrier well.
2. To study potential influences of groundwater level reduction and sea level rise on the barrier efficiency.
3. To find an optimal barrier well application for the future.

Chapter 2: Study Review

1 Seawater intrusion

Seawater intrusion is a lateral encroachment of seawater into coastal aquifers. As mentioned in the previous chapter, this happens because of the density difference between freshwater and saltwater and has been deteriorating due to some anthropogenic reasons, such as climate change and over pumping. This encroachment is one of the main causes of the groundwater contamination in coastal areas because groundwater can be easily contaminated by salt, in other words, a few percentage of mixing with seawater could make groundwater inadequate for human consumption, and more than five present of mixing could completely ruin the freshwater (Sherif et al., 1996) (Abd-Elhamid et al., 2015).

As shown in Figure2-1, 0.5 m of sea level rise causes 20 m reduction of the freshwater depth below the sea level based on the Ghyben-Herzberg relationship (Eq.1.2). Sherif and Singh (1999) studied the effect of climate change on seawater intrusion in two different aquifers, the Nile Delta aquifer in Egypt and the Madras aquifer in India. In the study, the effects of three different scenarios on seawater intrusion in each aquifer were simulated using a 2D-FED model: Scenario 1 where sea level rises by 0.2 m, Scenario 2 where sea level rises by 0.5 m, and Scenario 3 where the inland piezometric head reduces by 0.5 m. The results revealed that 0.5 m of sea level rise would cause 9.0 km and 0.4 km of further seawater intrusion in the Nile Delta aquifer and the Madras aquifer, respectively, and especially low concentration of saltwater was affected more than higher concentration. The reason for the huge gap of the results is because of the thickness of the aquifer, and they showed deep coastal aquifers with mild hydraulic gradients are more vulnerable against the sea level rise or over pumping of groundwater. Besides, the results showed that seawater intruded further inland in the event of 0.5 m of head loss on the land (Scenario 3) compared to 0.5 m of sea level rise (Scenario 2), which means over pumping would have bigger impacts on the seawater intrusion than seawater level rise.

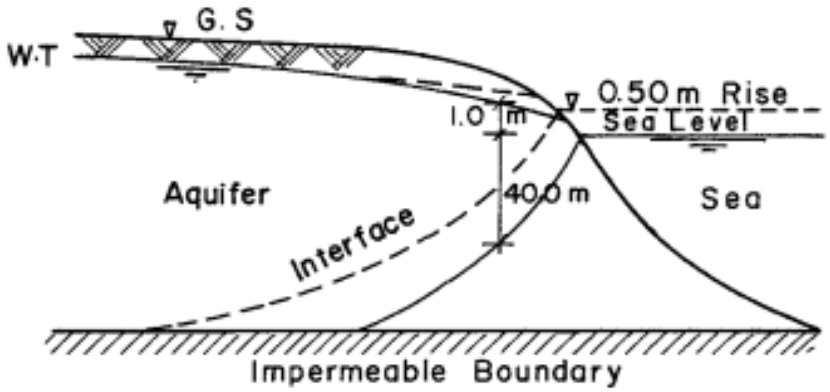

Figure 2-1: Sharp interface of seawater intrusion and sea level rise (Sherif et al., 1999).

Abd-Elhamid et al (2015) also simulated the effects of seawater rise and over pumping on seawater intrusion in the Gaza aquifer, Palestine, using a 2D-FEST model. This simulation showed that 1.0 m of sea level rise and 0.5 m of head loss on the land side can cause 500 m and 250m of further intrusion into the Gaza aquifer, respectively. However, the combination of the sea level rise and head loss on land can cause 1000 m of further intrusion.

These studies show the importance of countermeasures to the seawater intrusion, especially in arid or semi-arid regions where groundwater is the sole or main freshwater source and are vulnerable to water shortage because of the scarcity of rainfall and natural recharge.

2 Negative hydraulic barriers

Hussain et al (2019) did a comprehensive review of the countermeasures to control seawater intrusion in coastal aquifers (Hussain et al., 2019). In that review, the authors clearly mentioned that hydraulic barriers approaches are getting more popular than the other countermeasures thanks to the cost-effectiveness. Considering the lack of other water sources to recharge, negative hydraulic barriers are widely applied in arid or semi-arid regions (Sherif et al., 2001).

Sherif and Hamza (2001) evaluated the abstraction of brackish water from nine different barrier wells (3 horizontally different locations and 3 vertically different locations) in the dispersion zone as a countermeasure to seawater intrusion using a two-dimensional finite element model. The result showed that the pumping of brackish water from any points within the dispersion zone could cause a considerable remediation of the seawater intrusion, and the exact location of the barrier wells affected the distribution of the concentration in the dispersion zone to some extent. They concluded that the pumped water quality was better when the brackish water was pumped further away from the coast and in the upper horizons of the aquifer, so the location of barrier wells should be based on the required pumped water quality. However, this conclusion could lead to the reduction and loss of larger amounts of freshwater, which was reported as the major drawback of this method (Hussain et al., 2019).

To minimize the freshwater reduction, Pool and Carrera (2009) proposed a new hydraulic barrier with two extraction wells, an inland well to pump freshwater and a seaward well to pump saline water, which is also called a double pumping barrier system (Figure 2-2). This system creates a low velocity zone between the two abstraction wells with an almost horizontal hydraulic gradient, which prevents the further seawater intrusion and protects the pumped freshwater quality inland. They evaluated the effectiveness of the system with a three-dimensional variable density flow model and studied the effects of some factors, such as well locations, pumping rate, aquifer anisotropy, and aquifer thickness, on the desalination efficiency. As a result, this system would be efficient especially in thin aquifers and revealed that there was a critical pumping rate between the two wells depending on the well location. They also empirically showed the desalination efficiency would be better when the seawater

pumping well is located closer to the sea, even though it would have to be pumped at much higher rates. Besides, the overall performance of this method would be better when saltwater was pumped from the lower aquifer and freshwater was pumped from the upper aquifer.

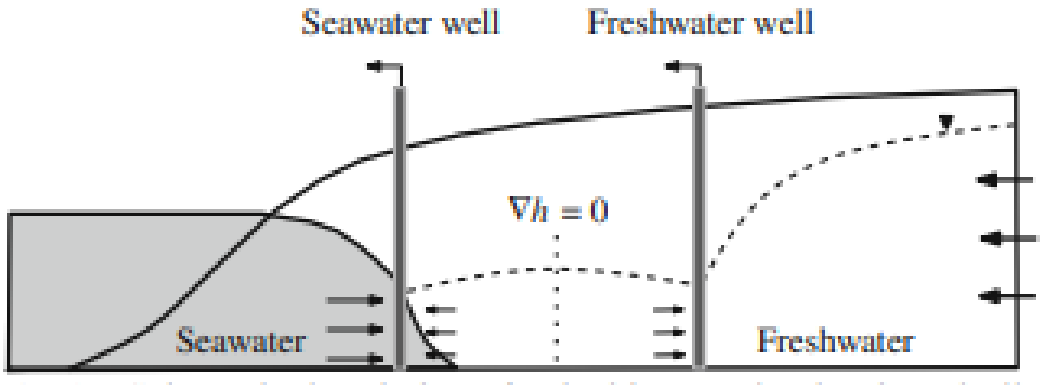

Figure 2-2: Schematic description of a double pumping barrier.

Perk et al. (2012) also studied the effects of different parameters, such as extraction rate, the number of the barrier wells, and the well locations, on the water quality from a production well. A series of three-dimensional simulations with the multidimensional hybrid Lagragian-Eulerian element model were employed to find an optimal application of the barrier wells. First, they compared the influence of the amount of saltwater extraction. The result was that extracting a greater amount of saltwater led to a better quality of freshwater at the production well. However, the gain diminished as the saltwater extraction increased. They also compared the effects of a different number of barrier wells. Three patterns of barrier wells (1, 3, and 5 barrier wells pumping the same amount of saline water in total along the coast in each pattern) were installed and the efficiencies were investigated. The result showed that pumping from a single barrier well located between the production well and the coast would be the most effective, and the other patterns could aggravate the condition. Lastly, they simulated the optimal horizontal and vertical well location. The horizontal simulation showed that pumping saline water from the horizontally midway between the production well and the coast could desalinate the production water the most, and the vertical simulation showed that pumping from the lower aquifer would desalinate the production well slightly better compared to pumping from the middle or upper aquifer, although the effects of the different vertical locations was less critical than the other factors.

Fujita (2020) and Abi-Akl (2020) pointed out that there were few experimental studies on saltwater pumping, and so they examined the effect of saltwater pumping while measuring possible freshwater intake from an inland production well in a laboratory scale experiment. The experiment clearly showed the effectiveness of this countermeasure by a barrier well and the possibility to control seawater intrusion by manipulating the pumping ratio of production

well to barrier well. Ozaki (2021) succeeded the study and numerically examined the possibility to control seawater intrusion by manipulating the pumping ratio between a production well and a barrier well. These studies clarified the existence of the critical pumping ratio to prevent seawater intrusion into the production well.

Ebeling et al. (2019) studied the potential of mixed hydraulic barriers to remediate sweater intrusion with a 2-D variable density model. Figure 2-3 shows the conceptual image of the methods. Even though it was mainly about the mixed hydraulic barrier, which is a combination of a positive and negative hydraulic barrier, it also delivered sensitivity of some geological parameters and an effective approach of the negative hydraulic barrier in the mixed barrier system, which could be beneficial for a sole negative hydraulic barrier approach as well.

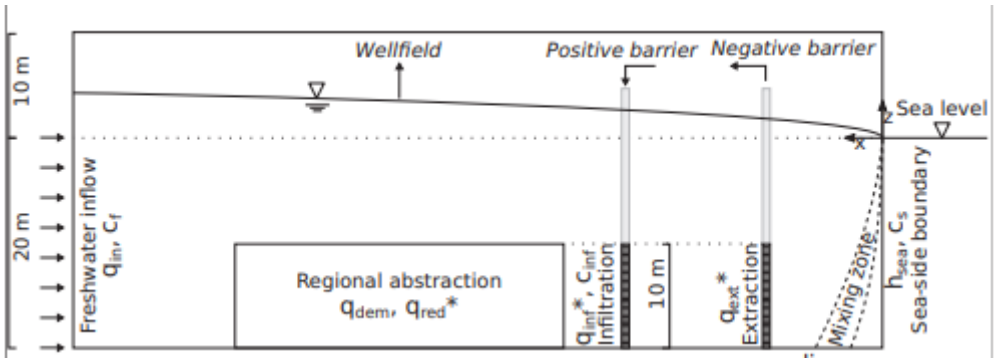

Figure 2-3: Conceptual model of the mixed hydraulic barrier simulated in the study. (Ebeling et al., 2019)

The effects of several factors, such as the well locations, injection and extraction rate, and the production rate, were investigated and the remediation potential was evaluated based on the remediation time and the reduction of the salt mass and the intrusion length. The numerical simulation results revealed that the hydraulic conductivity is one of the biggest factors for the remediation potential and the remediation could take as long as centuries in a low hydraulic conductivity. The mixed barrier could make the remediation even faster and save as much as 50.3~50.9% of the remediation time with the best combination of each factor. When it comes to the barrier well location, it concluded that it is better to install a barrier well closer to the coast for the better remediation, but the quality of the extracted water is better when it is installed inland. Once the wedge passed the barrier well, the remediation was hindered since the barrier well keeps on pulling saline water from the sea, so moving the barrier well closer to the coast or changing the extraction rate should be considered in order to gain better remediation with a mixed hydraulic barrier.

As discussed above, it is important to study an optimal application of barrier wells, considering the predicted further seawater intrusion, the too long remediation time, and the major drawback of the method taking too much freshwater from the barrier wells as well as saltwater. Even

though some studies about an optimal application of negative hydraulic barriers were conducted numerically by comparing a few horizontal well locations, there are few experimental studies about an optimal barrier well location. Moreover, the influence from different hydraulic heads, considering climate change or over pumping, on the optimal location has not been studied yet. In this study, two laboratory scale experiments were conducted to observe the difference of the barrier efficiencies by the well location and the effects of the groundwater table reduction on seawater intrusion. Furthermore, pumping from an additional number of barrier wells was simulated numerically in different hydraulic head conditions, and that way an optimal barrier well application for the future was studied.

Chapter 3: Methodology of the Experiments

In this study, Experiment 1 examined the difference of the barrier efficiencies at 4 different barrier well locations to study an optimal well location. Experiment 2 examined effects of groundwater level reduction on seawater intrusion for the future. The same laboratory equipment was used to observe the intrusion behavior in the two experiments.

In this chapter, the methodologies of the two experiments are explained. First explaining the experimental equipment and conditions, then the experimental process of each experiment.

1 Experimental equipment

Two laboratory experiments were performed in this study to examine an optimal barrier well location and effects of the hydraulic head reduction on seawater intrusion. In both experiments, the device shown in Figure 3-1 was used. This device was designed and used by Fujita (2020) and Abi-Akl (2020) and revised for this study. This device consists of three acrylic tanks, a saltwater tank on the left side, an intrusion tank in the middle, and a freshwater tank on the right side, as shown in Figure 3-1. The freshwater tank was connected to a faucet and supplied freshwater to the intrusion tank. The saltwater tank was filled with saltwater using a pump and supplied saltwater to the intrusion tank. A drainage was installed on top of each tank to keep the constant head at 30.0 cm and 31.5 cm in the seawater tank and the freshwater tank, respectively. The height of the freshwater drainage is variable, so it can change the freshwater head, which is associated with groundwater level reduction or relative sea level rise. In this experiment, a two-dimensional coordinate with X and Y-axis was defined with the origin at the bottom left corner of the aquifer section, as shown in Figure 3-1. Five wells were installed in the intrusion tank as described in Figure 3-1 at (25.0, 15.0), (25.0, 5.0), (50.0, 15.0), (75.0, 15.0) and (90.0, 5.0) on the coordinate. These wells worked as either production wells or barrier wells depending on the experiments.

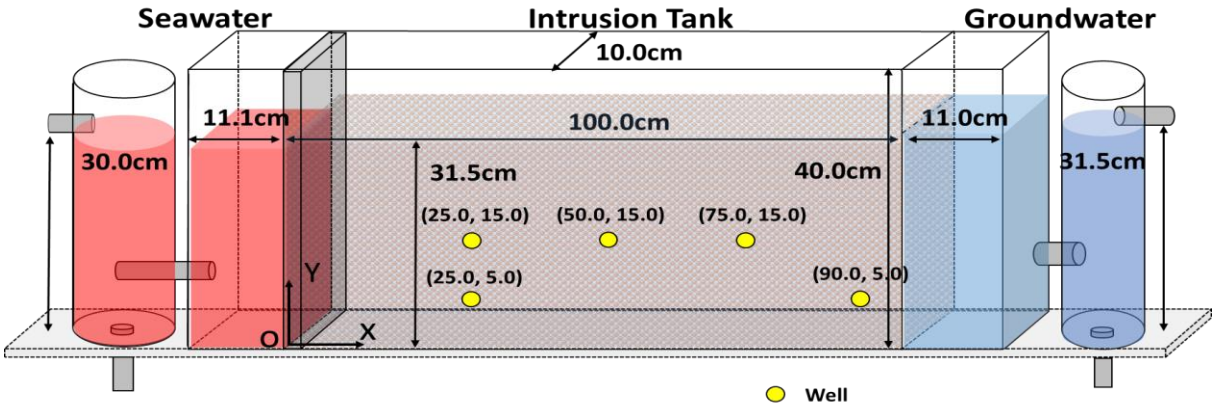

Figure 3-1: The conceptual model of the device for the experiments

2 Experimental Materials

Figure 3-2 shows the picture of the intrusion tank. As shown in the figure, the intrusion tank has three sections: a seawater supply section on the left, a freshwater supply section on the right, and a sandy aquifer section in the middle.

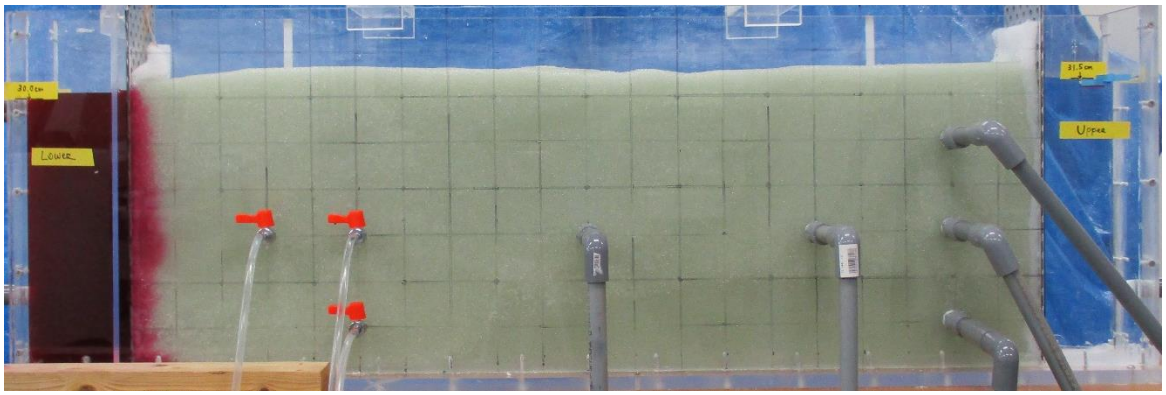

Figure 3-2: The intrusion tank

2.1 The middle section: Coastal Sandy Aquifer

The middle section of the intrusion tank was filled with glass beads, ASGB-20 made by AS ONE, up to 31.5 cm. Filters that the beads cannot go through separated each section, preventing the beads from moving from the middle. This device was designed to simulate a coastal sandy aquifer, so the glass beads were selected to have 0.71 to 1.00 mm of diameter, which belongs to the range of coarse sand as shown in the Wentworth grain size classification in Table 3-1 (Blair and McPherson, 1999). Note that these glass beads were filled while mixing with water in order to fill the void with water and prevent air entrapment in the aquifer. Then, the aquifer was assumed to be saturated and porosity of the aquifer could be estimated from the mixed water volume. The mass of the beads and mixed water were measured and divided by their densities to get the volume respectively. Once those volumes were calculated as 19.698 L for beads and 12.322 L for freshwater within the void, the porosity could be estimated to be 38.5 % by its definition, which is within the range of unconsolidated sand, as shown in Table 3-2 (Yu et al., 1993).

Hydraulic conductivity was estimated based on the Dupuit–Fawer assumptions for quasi steady-state free-surface flow in porous media (Oscar, 2011). This is the assumption where the groundwater pressure can be approximated by the hydrostatic pressure distribution when the groundwater level gradient is considerably small, because the groundwater flow direction is almost horizontal, and the flow velocity is small. Note that this assumption can be applied only when the aquifer length L is significantly larger than the head loss Δh in a free-surface aquifer as shown in Figure 3-3.

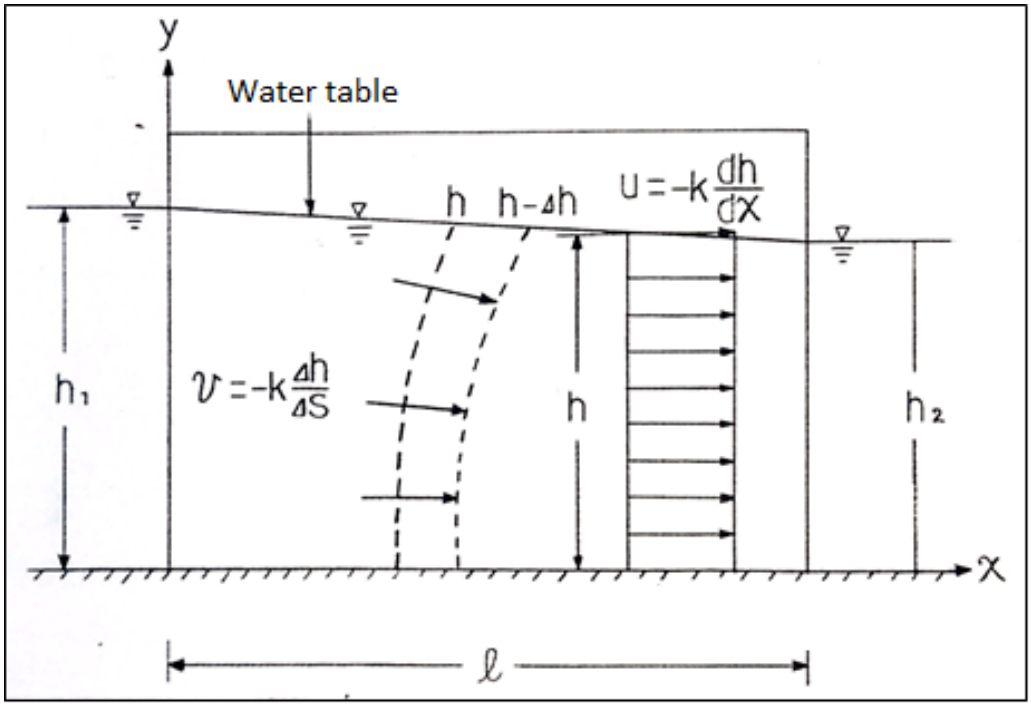

Figure 3-3: The quasi-steady flow by Dupuit-Fawer assumption (Oscar, 2011)

Horizontal velocity can be calculated by the Darcy's law, shown in Eq. (3.1), and the flow rate per width, q, can be calculated with Eq. (3.2)

$$u = -k\frac{dh}{dx} \tag{3.1}$$

$$q = uh = -kh\frac{dh}{dx} \tag{3.2}$$

By rearranging Eq. (3.2) and integrating from x=0 to x=L, where h=h_1 and h=h_2, respectively, Eq. (3.3) is obtained. Hydraulic conductivity k was then obtained by rearranging the equation into Eq. (3.4).

$$\frac{h_1^2}{2} - \frac{h_2^2}{2} = \frac{q}{k}L \tag{3.3}$$

$$k = \frac{2qL}{h_1^2 - h_2^2} \tag{3.4}$$

Before starting each experiment, overflow volume from the downstream drain in 30 seconds was measured three times and the average volume was divided by the width of 10.0 cm to calculate the flow rate per width. Table 3-3 shows the measurement results, as well as the hydraulic conductivity in the experimental device, was averaged at 0.4 cm/s.

Table 3-1: Wentworth grain size classification (Blair & McPherson, 1999)

Millimeters (mm)	Micrometers (μm)	Phi (ϕ)	Wentworth size class	
4096		-12.0	Boulder	
256		-8.0	Cobble	Gravel
64		-6.0	Pebble	
4		-2.0	Granule	
2.00		-1.0	Very coarse sand	
1.00		0.0	Coarse sand	
1/2 0.50	500	1.0	Medium sand	Sand
1/4 0.25	250	2.0	Fine sand	
1/8 0.125	125	3.0	Very fine sand	
1/16 0.0625	63	4.0	Coarse silt	
1/32 0.031	31	5.0	Medium silt	
1/64 0.0156	15.6	6.0	Fine silt	Silt
1/128 0.0078	7.8	7.0	Very fine silt	
1/256 0.0039	3.9	8.0	Clay	Mud
0.00006	0.06	14.0		

Table 3-2: The classification of porosity of deposits (Yu et al., 1993)

Soil Type	Porosity, p_t
Unconsolidated deposits	
Gravel	0.25 - 0.40
Sand	0.25 - 0.50
Silt	0.35 - 0.50
Clay	0.40 - 0.70
Rocks	
Fractured basalt	0.05 - 0.50
Karst limestone	0.05 - 0.50
Sandstone	0.05 - 0.30
Limestone, dolomite	0.00 - 0.20
Shale	0.00 - 0.10
Fractured crystalline rock	0.00 - 0.10
Dense crystalline rock	0.00 - 0.05

Table 3-3: Hydraulic conductivity (h_1=31.5 cm, h_2=30.0 cm, L=100 cm, width=10 cm in Equation (3.4))

Take	1	2	3	4	5
Flow 1 (ml/30s)	58	56	56	57	52
Flow 2 (ml/30s)	60	55	55	58	53
Flow 3 (ml/30s)	58	56	55	57	53
q (ml/s・cm)	0.196	0.186	0.184	0.191	0.176
Hydraulic conductivity (cm/s)	0.42	0.40	0.40	0.41	0.38

2.2 Freshwater supply section (the right side): Groundwater

In the freshwater supply section, the right side of the intrusion tank, tap water simulating groundwater was supplied from the freshwater tank, which is connected to a faucet. The density of the freshwater was calculated using an electrical balance and a graduated cylinder. 50 ml of tap water from the faucet was weighed, and the density was calculated by dividing its mass by 50 ml of the volume. This measurement was performed three times and the average density was defined as the density of the freshwater in this study. Table 2-3 shows the results and 0.996 g/cm^3 was used as the freshwater density in this study.

Table 2-3: Freshwater density

	Take 1	Take 2	Take 3
Mass (g/50 ml)	49.799	49.794	49.797
Density (g/cm3)	0.99598	0.99588	0.99574
Average value (g/cm3)		**0.996**	

2.3 Saltwater supply section (the left side): Seawater

In the saltwater supply section, the left side of the intrusion tank, saltwater simulating seawater was supplied from the saltwater tank. This tank pumped saltwater, which is prepared by adding commercial salt in tap water in advance. This preparation of the saltwater followed the method used by Fujita (2020) and Abi-Akl (2020) as described below.

First, the density of saltwater is expressed in Eq. (3.4) (Elizabeth et al., 2008).

$$\rho_{salt} = \frac{m_{mass} + m_f}{V_{salt} + V_f} = \rho_f + \frac{1 - \rho_f A}{\frac{1}{\frac{F_{salt}}{\rho_f} - 1} + A} \tag{3.4}$$

where, ρ_{salt} is the saltwater density, ρ_f is the freshwater density, m_{mass} is salt mass, m_f is freshwater mass, V_{salt} is the volume of salt, V_f is the volume of freshwater, F_{salt} is the mass fraction of salt, and A is the salt density. Since the solute used in this experiment was NaCL, the salt density can be approximated as follows (Simion et al., 2015):

$$A \approx -0.40064{F_{salt}}^2 + 0.37226F_{salt} + 0.29067 \quad (3.5)$$

Substituting Eq. (3.5) into Eq. (3.4) and rearranging F_{salt}, cubic F_{salt} can be expressed in Eq. (3.6):

$$-0.40064\rho_f{F_{salt}}^3 + 0.37226\rho_f{F_{salt}}^2 + (0.29067\rho_f - 1)F_{salt} + \left(1 - \frac{\rho_f}{\rho_{salt}}\right) = 0 \quad (3.6)$$

In this study, ρ_f and ρ_{salt} were set to as 0.996 g/cm^3 and 1.025 g/cm^3, respectively, and then Eq. (3.6) can be solved and three real solutions for F_{salt} can be obtained. Considering the F_{salt} is the mass fraction of salt, the range of the F_{salt} must be $0 < F_{salt} < 1$, and then the equation could have only one possible solution for F_{salt}, which is 0.0408. The required mass percent concentration of salt to get 1.025g/cm^3 at saltwater density was calculated as 4.08%.

Once the required mass percent concentration of salt was calculated, an arbitrary amount of tap water was poured in a bucket and the mass was measured with an electrical balance. Then, required salt mass was calculated to achieve the desired concentration of 4.08% with Eq. (3.7) and was mixed with the water in the bucket until it dissolved.

$$F_{salt} = \frac{m_{mass}}{m_{mass} + m_f} \quad (3.7)$$

Figure 3-4 shows the image of the prepared saltwater. For a good observation of seawater intrusion, red colorant was added in the prepared saltwater. The colorant formulation was determined by the stain test performed by Fujita (2020) and 2 g of colorant was stirred per litter of the saltwater until the color of the solution became deep red. Specific gravity of the colorant was small enough to ignore in comparison with the specific gravity of the saline solution. Considering the permeability was relatively high and advection dominant compared to diffusion in this study, it can be assumed that the salt and colorant concentration would be almost same. Therefore, it was assumed that the colored interface could accurately represent the fresh-saltwater interface. In order to confirm the density, the density of the prepared saltwater was measured in the same way as freshwater and it was found to be within the rage of 1.025 to 1.030 g/cm^3, which is a reasonable value for seawater.

Figure 3-4: Colored saltwater (Fujita, 2020).

3 Experimental processes

Before starting each experiment, the intrusion tank was filled with freshwater to make the aquifer saturated. Then, each drainage simulating wells in the aquifer was adjusted to pump required volume of water. Once the wells were adjusted and the flow became constant, a partition plate was inserted between the aquifer section and the seawater supply section in the intrusion tank to keep the aquifer saturated. Then, soon after the freshwater in the saltwater section was emptied, the prepared salt water was pumped into the saltwater tank by a pump to fill the saltwater supply section up to 30 cm.

Each experiment started when the partition was removed, and a stopwatch was used to keep track of time. To record the behavior of saltwater invasion, the intrusion tank was photographed every 10 minutes, and the length of saltwater intrusion was recorded using a ruler every 5 minutes. The first 5 minutes of every step were showing the largest intrusion, so the intrusion in the first 5 minutes was recorded with a video. Seawater in the bucket was stirred every 5 minutes in order to prevent the solute precipitation. For each step, steady-state represented a condition when the saltwater toe stopped the moving and no visual changes in salt-freshwater interface were observed for 15~20 minutes in a row.

3.1 Experiment 1: An examination of an optimal location for a barrier well.

This experiment was conducted to study an optimal barrier well location by comparing the barrier efficiencies at four different barrier well locations. Figure 3-5 shows the exact locations for the production well (Well P) and the four barrier wells (Well A, B, C, and D) to be compared in this experiment. The freshwater and saltwater heads were fixed at 31.5 cm and 30.0 cm height, respectively. This experiment consists of two steps.

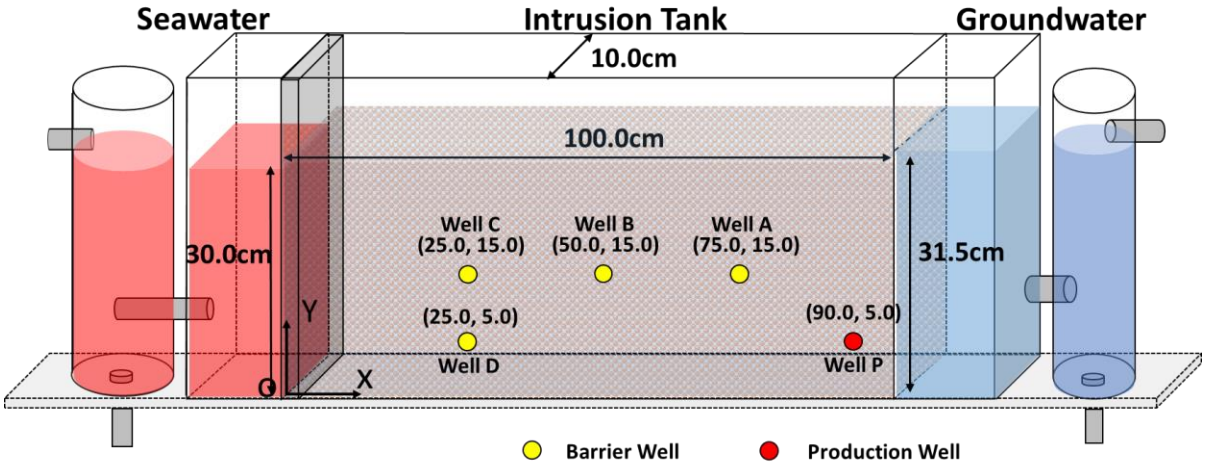

Figure 3-5: Conceptual model for Experiment 1

In the first step, freshwater was pumped from Well P, which is simulating a production well. The pumping rate was set relatively high enough to make the intrusion reach the production well.

Once the intrusion in the first step steadied, the second step could start. In this step, one barrier well out of Well A, B, C, or D, functioned as a barrier well. The barrier efficiencies were then investigated by comparing each of their critical pumping rates, which refers to a minimum pumping rate to restore the production quality.

3.2 Experiment 2: An examination of the effects of groundwater level reduction

Experiment 2 was conducted to study the effects of groundwater level reduction on seawater intrusion. Figure 3-6 shows the conceptual model for Experiment 2. In this experiment Well B and A were used and seawater intrusion process was observed in two different groundwater levels (31.5cm and 31.0cm) as shown in Figure 3-6. By comparing the difference of the intrusion behavior, such as the shape, the length, and the time, the effects of the groundwater head reduction, which is associated with over abstraction of groundwater or relative sea level rise, on seawater intrusion was studied.

This experiment consists of three steps. In the first step, seawater intrusion caused by the density difference was observed without pumping. In the second step, Well B started pumping at 3.1ml/s and further seawater intrusion was observed. In the final step, Well A started pumping at 4.8ml/s and further seawater intrusion was observed. However, Well B was working as a barrier well in this step and the effects of the barrier well was also observed in the two hydraulic head conditions.

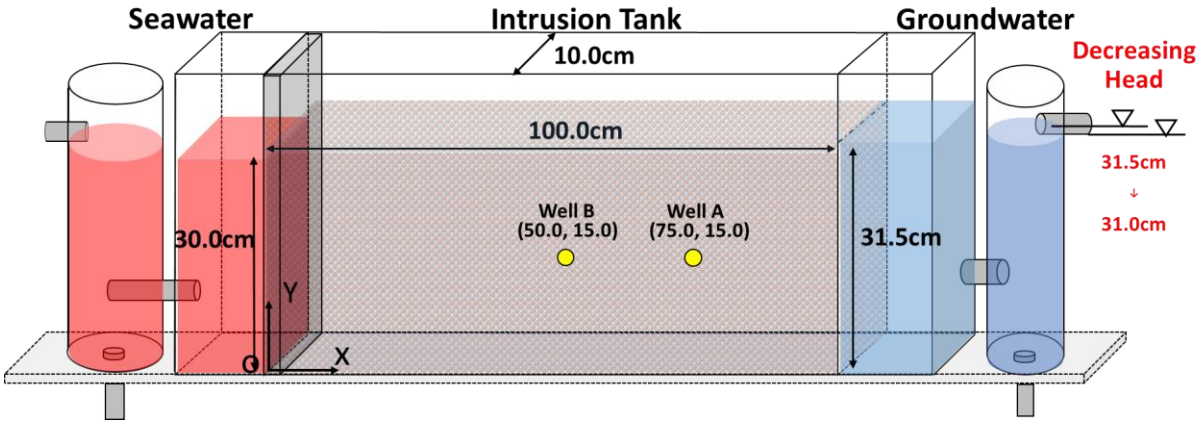

Figure 3-6: Conceptual model for Experiment 2

The results from Experiment 2 were also used to confirm the reliability of the simulation output.

Chapter 4: Experimental Results and Discussion

In this chapter, results of the two experiments are described and an optimal location to install a barrier well is discussed for the future when further seawater intrusion has been predicted.

1 Experiment 1: Examination of the difference of the barrier efficiencies at four barrier well locations.

In the first step of Experiment 1, the production well kept on pumping groundwater at the rate of 7.8 ml/s~8.0 ml/s. The process of the seawater intrusion in the first step is shown in Figure 4-1.

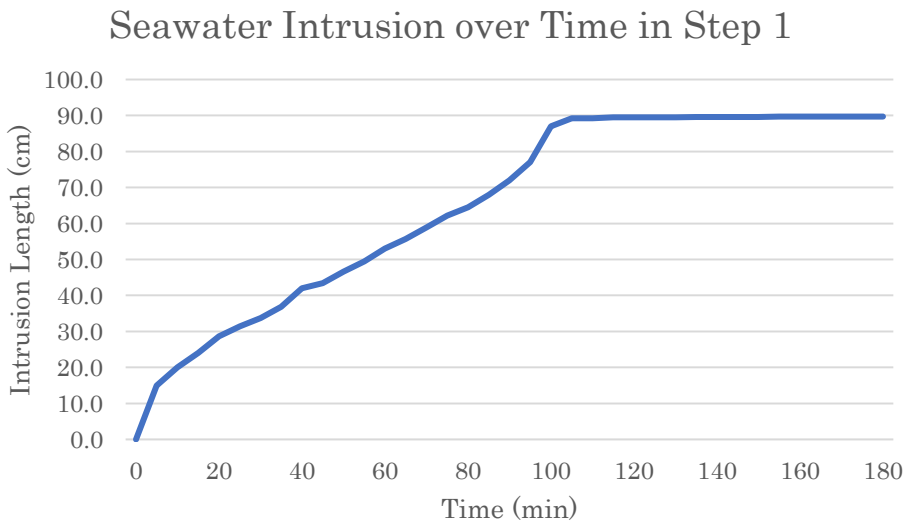

Figure 4-1: Seawater intrusion process in Step1.

The intrusion steadied in 180 minutes from the beginning. Ozaki (2021) found that seawater intruded faster at first and then it got slower gradually in his laboratory scale experiments. This happened in this experiment as well in the first 20 minutes, and the seawater wedge was accelerated again once it got closer to the production well, around 65~85 cm. This is most probably because of the pumping at the production well. Upconing towards the production well was observed in 100 minutes from the beginning and the intrusion length stopped at 89.7 cm after the upconing happened. However, seawater intrusion kept on going and the saline layer kept on getting thicker until 180 minutes, when the intrusion steadied as shown in Figure 4-2.

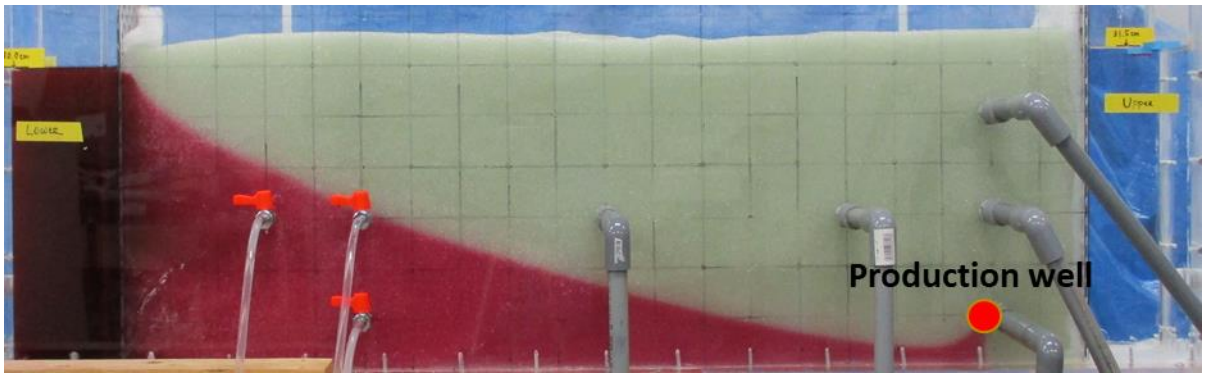

Figure 4-2: Steady state in Step1, in 180 minutes from the beginning.

In the second step, one of the barrier wells started pumping at a certain rate until the remediation stopped. The critical pumping rates, when the intrusion at the production well could not be observed visually anymore, were investigated at each barrier well in this step.

Figure 4-3 shows the barrier at Well A. Pumping at Well A did not stop seawater intrusion into the production well even when it pumped more than 65 % of the production rate. If anything, seawater intrusion in the aquifer kept on deteriorating especially around the production well after pumping at Well A as shown in the figure. This is probably because Well A worked as a production well and pulled saline water from the coast side instead of working as a barrier well preventing further seawater intrusion. Since this experiment was focusing on the remediation capacity at each well location, the observation at Well A was stopped before seawater intrusion steadied on the coast side. Even though this experiment was stopped at the pumping rate 65 % due to the limitation of the experimental device, this barrier well might have remediated the intrusion if the pumping rate got even higher.

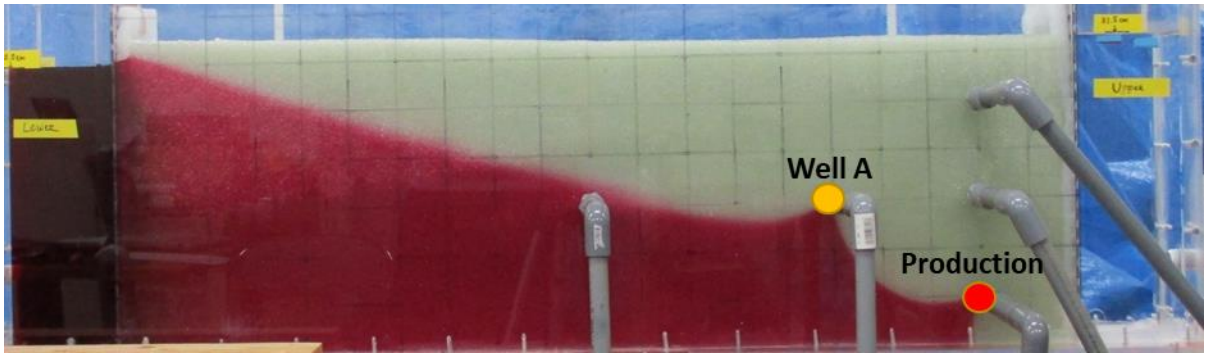

Figure 4-3: Step2 pumping from Well A at 65 % of the production rate.

Figure 4-4 shows the barrier with Well B. The seawater intrusion into the production well was stopped with the barrier when it pumped at approximately 35 % of the production. The pumping rates at the production well and the barrier well were changing within the range of 9.0~10.4 ml/s and 3.2~3.4 ml/s, respectively, and the critical pumping ratio was within the range of 32.7~37.8 % during the experiment. This fluctuation of the pumping rates was one of the

biggest uncertainties in the experiment, therefore it was constantly measured during the experiment to confirm the pumping rates and the average was used as the critical pumping ratio. However, even if this uncertainty was taken into account, the barrier efficiency was better than that of Well A, considering the low critical pumping rate to remediate the production well and the inland condition of seawater intrusion. As for the coastal side, seawater intruded furthermore compared to the initial condition of Step 2 (Steady state of Step 1). This is probably because the total amount of pumping was increased and the pumping from the barrier well pulled saline water more from the coast side, which could be one of the biggest negative effects of a barrier well.

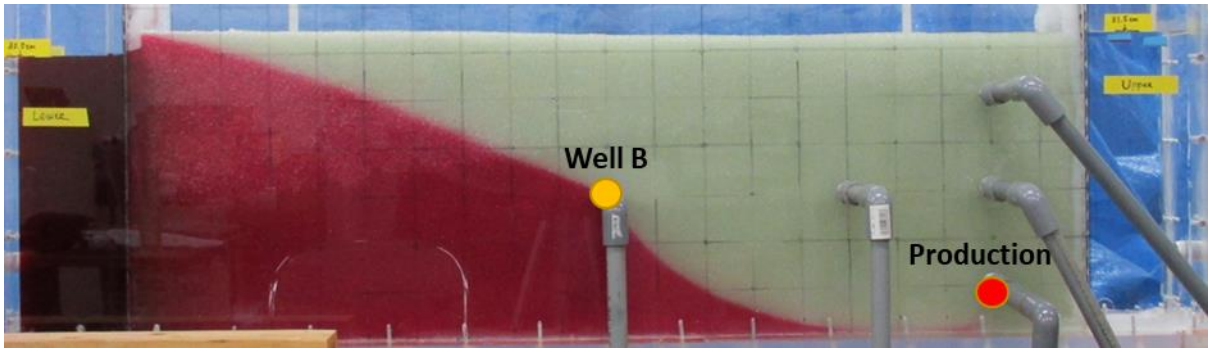

Figure 4-4: Step2 pumping from Well B at about 35 % of the production rate.

Figure 4-5 shows the barrier with Well C. The seawater intrusion into the production well was stopped when with the barrier it pumped at 30 % of the production. The critical pumping rate to prevent the seawater intrusion at the production well was slightly lower than Well B. Besides, Well C remediated seawater intrusion better than Well B, and the aggravation of the coastal salinization was not as much as Well B did.

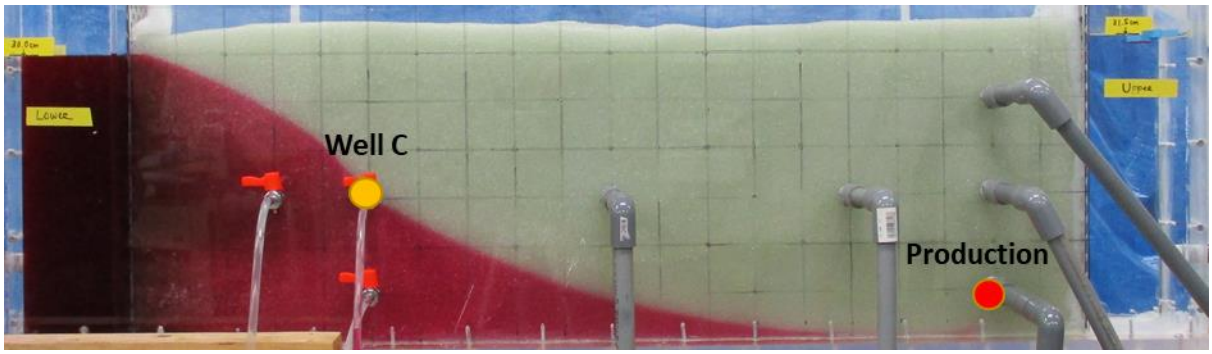

Figure 4-5: Step2 pumping from Well C at about 30 % of the production rate.

Figure 4-6 shows the barrier with Well D. Well D prevented the seawater intrusion into the production when it pumped at 29 % of the production. The uncertainty of the pumping fluctuation happened in this step again, and the pumping rates at the production well and the barrier well were changing within the range of 8.8~9.4 ml/s and 2.5~2.8 ml/s, respectively, and the critical pumping ratio was within the range of 27~30 % during the experiment. The critical

pumping rate was the lowest among the four barrier wells and the remediated aquifer condition was even better than the other wells. Even though further seawater intrusion on the coast side happened as much as Well C did, the intrusion was not intense compared to the inland wells, Well A and B.

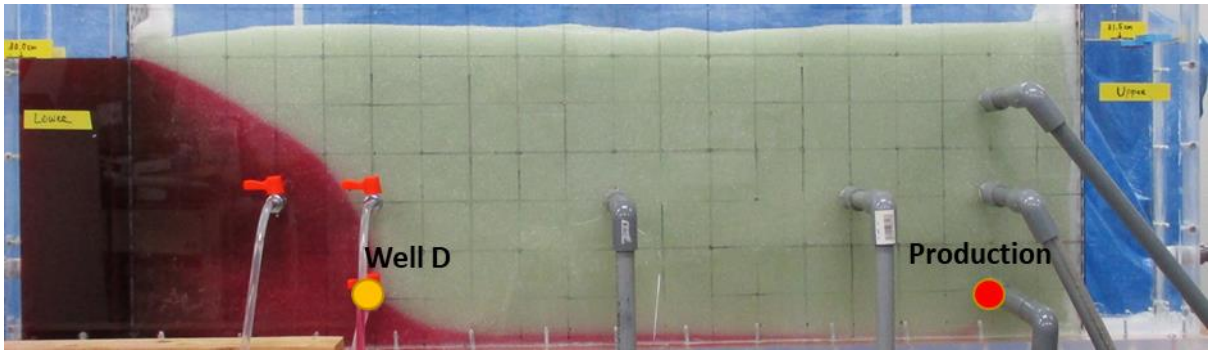

Figure 4-6: Step2 pumping from Well C at about 29 % of the production rate.

As a result of this experiment, barrier well D was the most effective considering the low critical pumping rate and the remediation in the aquifer. Comparing the horizontal locations at Well A, B, and C, Well C worked efficiently as a barrier and well A with pumping at 65 % of production did not function as a barrier at all. Therefore, it would be better to install a barrier well close to the coast and pump saline water from the lower aquifer. However, this experiment examined only three different horizontal locations, so it still needs to be studied at more locations to find out exactly where the most effective location for a barrier well is.

2 Experiment 2: Examination of the effects of groundwater level reduction on seawater intrusion.

In Experiment 2, seawater intrusion was observed in two different groundwater levels, 31.5 cm and 31.0 cm, as explained in the previous chapter. The experiment was proceeded in three steps. First, seawater intruded by the density difference between freshwater and saline water without any pumping. In the next step, Well B started pumping at 3.1 ml/s. In the final step, Well A started pumping at 4.8 ml/s as a production well and Well B worked as a barrier well at this point. This is how the behavior of seawater intrusion with a production and a barrier well was observed in the different groundwater levels.

Figure 4-7 shows the steady states of the first step and Table 4-1 shows the intrusion length over time for each groundwater level. As shown in the figure, seawater intruded further inland in 31.0 cm groundwater level and it was predictable from the Ghyben-Herzberg theory. Table 4-1 shows that the saltwater wedge steadied at 29.6 cm in 90 minutes in 31.5 cm groundwater level, but it reached 30.0 cm in 30 minutes in 31.0 cm groundwater level. This means groundwater level reduction could cause faster and further seawater intrusion.

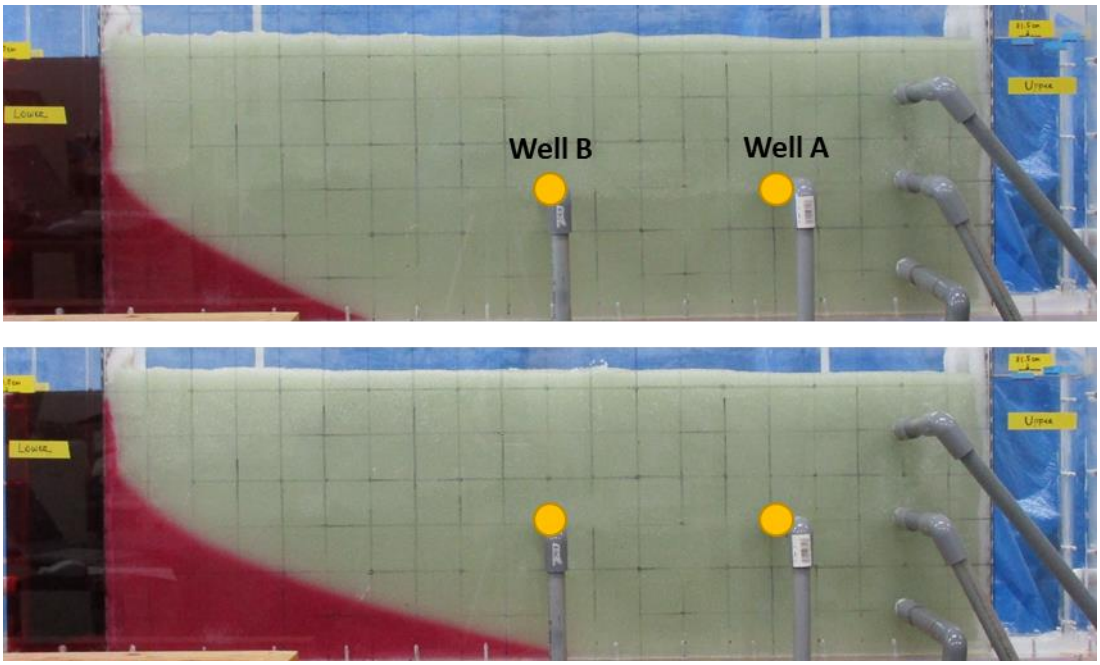

Figure 4-7: Step 1 steady state, 31.5cm (Top) and 31.0cm (Bottom) at groundwater level

Table 4-1: Intrusion length over time in Step1 in the different groundwater levels, 31.5cm and 31.0cm. (The red numbers represent the steady states)

TIME (min)	10	20	30	40	50	60	70	80	90
31.5 (cm)	13.7	19.4	22.6	25.1	26.8	27.8	28.5	29.1	29.6
31.0 (cm)	16.5	24.3	30	33.5	36.6	39.1	41.3	43.2	44.7

100	110	120	130	140	150	160	170	180
-	-	-	-	-	-	-	-	-
46	47.2	48.3	49.5	50	50.9	51.3	51.8	52.2

Figure 4-8 shows the steady states of the second step and Table 4-2 shows the intrusion length over time for each groundwater level. In this step, Well B was pumping at 3.1 ml/s and that caused further seawater intrusion. Comparing these steady conditions, seawater intruded further inland when groundwater level decreased. Although seawater intrusion deteriorated on the coast side in both cases, it was slightly more intense in the lower groundwater level.

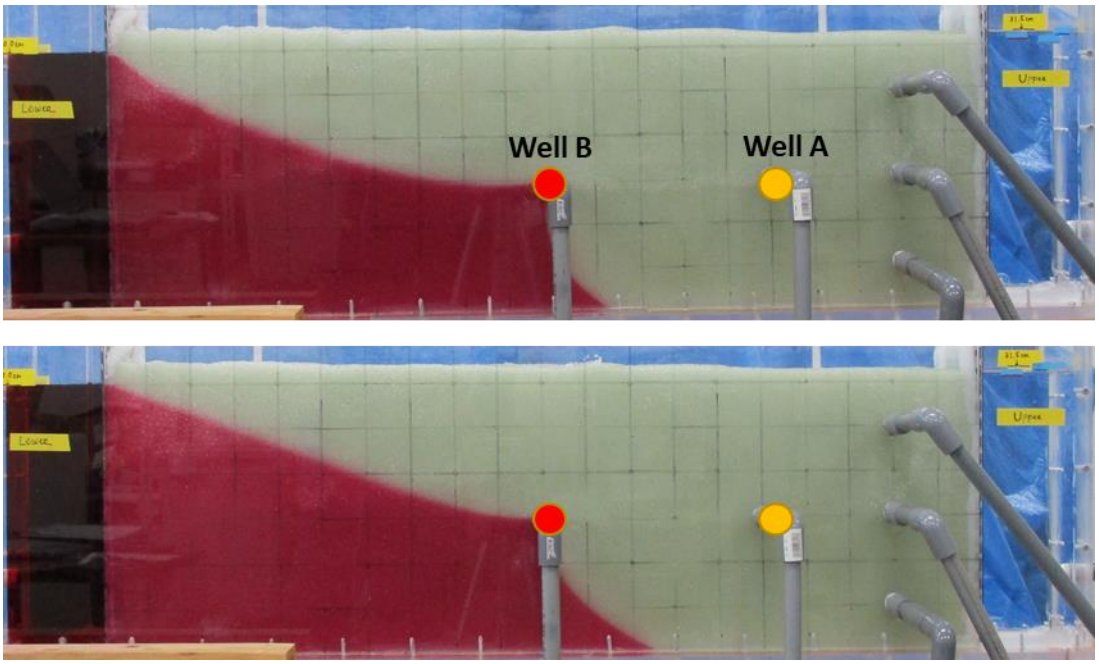

Figure 4-8: Step 2 steady state, 31.5cm (Top) and 31.0cm (Bottom) at groundwater level

Table 4-2: Intrusion length over time in Step2 in the different groundwater levels, 31.5cm and 31.0cm. (The red numbers represent the steady states)

TIME (min)	0	5	10	20	30	40	50	60	70	80	90	100	110	120
31.5 (cm)	29.6	34.3	38.4	45.4	49.8	52.4	54.4	55.8	56.2	56.4	56.6	-	-	-
31.0 (cm)	52.3	52.3	53.8	56.3	58.2	59.6	60	60.3	60.8	61.3	61.5	62	62.2	62.6

Figure 4-9 shows the steady states of the final step and Table 4-3 shows the intrusion length over time for each groundwater level. In this step, Well A was pumping at 4.8 ml/s, which caused further seawater intrusion, and also Well B was pumping at 3.1 ml/s and working as a barrier well at the same time. Saltwater wedge went further inland again due to the additional pumping at the production well for both groundwater level cases. Seawater intrusion got aggravated more on the coastal side as well, especially in the lower groundwater level case.

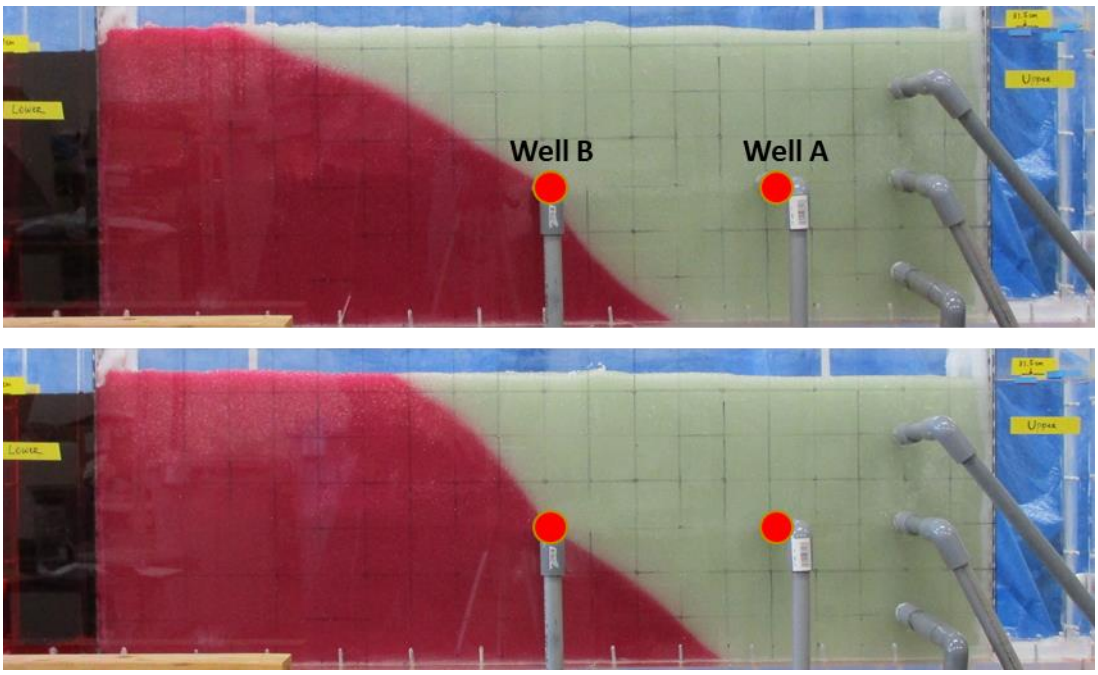

Figure 4-9: Step 3 steady state, 31.5cm (Top) and 31.0cm (Bottom) at groundwater level

Table 4-3: Intrusion length over time in Step3 in the different groundwater levels, 31.5cm and 31.0cm. (The red numbers represent the steady states)

TIME (min)	0	5	10	20	30	40	50	60	70	80	90
31.5 (cm)	56.6	59.6	61.3	61.9	63.1	63.8	63.8	62.5	62.6	63.6	64.3
31.0 (cm)	60.1	63.4	65.2	67.2	68.8	69.3	69.7	69.7	69.7	-	-

Based on the experiment, it can be predicted that groundwater level reduction or sea level rise will cause further and faster seawater intrusion in the future. Besides, the disadvantage of barrier wells aggravating the coastal salinization will be more intense because of groundwater level reduction or sea level rise.

3 Discussion

Throughout the experiments, there were several uncertainties.

First, these experiments were only observed visually. Even though pictures were taken every 10 minutes and it was regarded as the steady state when further seawater intrusion had not happened visually for more than 15minutes, it could cause some human error in judging if it was steady or not.

Secondly, it was difficult to keep the pumping rate constant or even to adjust to the required rate because the wells were just simulated by the drainage pipes without any pump. The pumping rates were controlled by opening a stopper in the pipe enough to flow the required amount of water by trial and error, and the flow rate was changing slightly throughout the

experiments, which made it difficult to find the exact value of the critical pumping ratio.

Thirdly, saline water and freshwater densities were not completely constant. Because tap water was directly used as the freshwater source, the density was measured only once before each experiment. Saline water was made based on the tap water density and confirmed to be 1.025~1.030 g/cm^3 before using in the experiments. However, considering these experiments spent long time and there was a chance that the tap water density had changed because of the temperature or the impurities, this uncertainty could have caused some error in the process of seawater intrusion since the density difference has a significant effect on seawater intrusion . However, in order to deal with these uncertainties, all pictures were carefully checked again after the experiments and the pumping rate and the tap water density were measured several times.

These two laboratory scale experiments showed the barrier efficiencies at each well, especially wells pumping from a lower aquifer and closer to the coast. However, another serious disadvantage of a barrier well, which is aggravating seawater intrusion on the coastal side, was also observed through the experiments. Although Hussain et al. (2019) stated that pumping too much freshwater is one of the biggest drawbacks of barrier wells, this another disadvantage will be serious as well, especially in the future because of groundwater level reduction or sea level rise. Considering this further deterioration in the future, installing a barrier well closer to the coast and pumping from a lower aquifer will be more important because it can prevent seawater intrusion more effectively and make the disadvantage of a barrier well smaller.

Chapter 5: Simulation Methodology

In this study, the 2-D solute transport model used by Ozaki (2021) was employed to simulate seawater intrusion process. This chapter describes the summary of the simulation algorithm used by Ozaki and the investigation method for an optimal barrier well location using the simulation model.

1 Mathematical Model

The 2-D solute transport model used by Ozaki (2021) is composed of two fundamental equations: the groundwater flow equation and the solute transport equation for advection and dispersion transport. This section explains the two fundamental equations and the discretization processes of each fundamental equation for the simulation.

1.1 Groundwater flow equation

Groundwater flow can be simulated by calculating the hydraulic head and the flow velocity in the aquifer. The hydraulic head and flow velocity in saturated-unsaturated aquifers can be calculated in two dimensions as follows:

$$(C_w + \alpha_0 S)\frac{\partial h}{\partial t} = -\frac{\partial u}{\partial x} - \frac{\partial v}{\partial y} \tag{5.1}$$

$$u = -k\frac{\partial h}{\partial x} \tag{5.2}$$

$$v = -k\left(\frac{\partial h}{\partial y} + \frac{\rho}{\rho_f}\right) \tag{5.3}$$

where t is the time period, h is the hydraulic head, k is the hydraulic conductivity, u and v are the Darcy's velocities in x and y directions, respectively, ρ is the fluid density, and ρ_f is the density of freshwater, C_w is the specific moisture capacity, S is the specific storage coefficient, and α_0 is the dummy parameter that takes 0 in the unsaturated condition and 1 in the saturated condition. Eq. (5.1) is based on a continuity equation. The specific storage coefficient represents the amount of water that is stored in soil per unit volume when the hydraulic head in the unit is raised, and it will be within 10^{-1} to 10^{-2} cm^{-1} in unconfined aquifers and 10^{-6} to 10^{-7} cm^{-1} in confined aquifers (Jinno et al., 2001). With the volumetric water content, θ, the specific moisture capacity is defined as:

$$C_w = \frac{d\theta}{dh} \tag{5.4}$$

In the saturated zone, the specific moisture capacity is equal to zero.

For the calculation of the flow in an unsaturated zone, some parameters in the unsaturated zone, such as the volumetric water content, the hydraulic conductivity, and the specific moisture capacity, have to be calculated. The following equations suggested by van Genuchten (1980)

were employed in this study to estimate the parameters for the unsaturated zone.

$$S_0 = \frac{\theta - \theta_r}{\theta_s - \theta_r} \tag{5.5}$$

$$S_e = \left[\frac{1}{1 + (\alpha|h|)^n}\right]^m \tag{5.6}$$

$$k_r = S_0^{\frac{1}{2}}\left\{1 - \left(1 - S_e^{\frac{1}{m}}\right)^m\right\}^2 \tag{5.7}$$

$$C_w = \frac{\alpha \cdot m(\theta_s - \theta)S_e^{\frac{1}{m}}\left(1 - S_e^{\frac{1}{m}}\right)^m}{1 - m} \tag{5.8}$$

where θ_r is the residual water content, θ_s is the saturated water content and α, m, and n are the coefficient of the van Genuchten formula. Referring to Jinno et al., these parameters are determined as shown in Table 5.1 (Jinno et al., 2001).

Table 5-1: Parameters for van Genuchten formula

Saturated water content		**0.385**
Residual water content		0.075
Coefficient	α	0.0491 (cm/s)
	m	0.8599
	n	7.138

1.2 2-D solute transport equation

In this study, advection, dispersion, and diffusion were taken into consideration to simulate the solute transport in two dimensions. The solute transport was simulated by calculating salt concentration. The solute transport based on advection and dispersion can be calculated in two dimensions as below:

$$\frac{\partial(\theta C)}{\partial t} + \frac{\partial(u'\theta C)}{\partial x} + \frac{\partial(v'\theta C)}{\partial y}$$
$$= \frac{\partial}{\partial x}\left(\theta D_{xx}\frac{\partial C}{\partial x} + \theta D_{xy}\frac{\partial C}{\partial y}\right) + \frac{\partial}{\partial y}\left(\theta D_{yy}\frac{\partial C}{\partial y} + \theta D_{yx}\frac{\partial C}{\partial x}\right) \tag{5.9}$$

where C is the solute concentration, θ is the volumetric water content, u' and v' are real pore velocities in x and y direction, respectively, and D_{xx}, D_{yy}, D_{xy}, and D_{yx} are dispersion coefficients. This equation is also based on the continuity equation. The volumetric water content, θ, represents the fraction of the area where water can flow, which is same as the porosity in saturated condition, so the real pore velocities are written as:

$$u' = \frac{u}{\theta}, v' = \frac{v}{\theta} \tag{5.10}$$

The product of volumetric water content and dispersion coefficient, θD_{xx}, θD_{xy}, θD_{yx}, and θD_{yy},

are calculated by the following equations.

$$\theta D_{xx} = \frac{\alpha_L u^2}{V} + \frac{\alpha_T v^2}{V} + \theta D_M \tag{5.11}$$

$$\theta D_{yy} = \frac{\alpha_T u^2}{V} + \frac{\alpha_L v^2}{V} + \theta D_M \tag{5.12}$$

$$\theta D_{xy} = \theta D_{yx} = \frac{(\alpha_{L-}\alpha_{T)}uv}{V} \tag{5.13}$$

where α_L and α_T are the longitudinal dispersion length and the transverse dispersion length, respectively, and D_M is the molecular diffusion coefficient. V is the magnitude of the velocity vector, which is written as:

$$V = (u^2 + v^2)^{\frac{1}{2}} \tag{5.14}$$

Once the salt concentration is calculated, the density of the saline water in the aquifer can be calculated with the following equation (Dierch & Kolddítz, 2002).

$$C = \frac{\rho - \rho_f}{\rho_s - \rho_f} \times 100(\%) \tag{5.15}$$

where C is the salt concentration of water, and ρ, ρ_f, and ρ_s are the density of the solution, freshwater, and saltwater, respectively.

1.3 Discretization of the groundwater equation

Eq. (5.1), the fundamental equation for groundwater flow, was discretized by the implicit finite difference method to numerically simulate the groundwater flow. Figure 5-1 shows the coordinates of the differential grids. Considering the potential head at each cell is constant, the h in Eq. (5.1) can be regarded as the pressure head. Therefore, the pressure head is calculated by the discretized equation as below:

$$\left(Cw_{i,j} + \alpha_0 S\right)\frac{h_{i,j}^{n+1} - h_{i,j}^{n}}{\Delta t} = -\frac{u_{i+1/2,j}^{n+1} - u_{i-1/2,j}^{n+1}}{\Delta x} - \frac{v_{i,j+1/2}^{n+1} - v_{i,j-1/2}^{n+1}}{\Delta y} \tag{5.16}$$

where Δt is the time increment, Δx and Δy are the grid intervals in x and y direction, respectively, n is the time level in calculation, i and j are differential nodes in x and y direction, respectively.

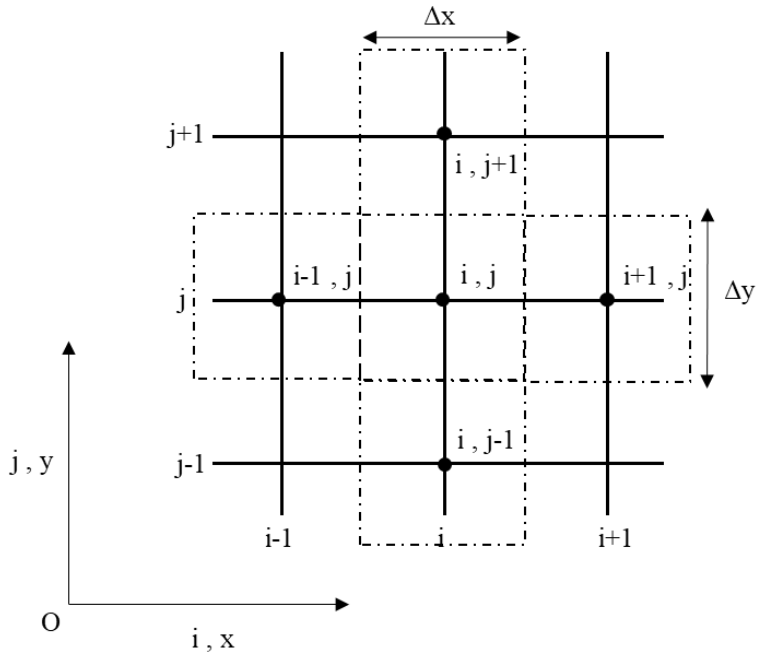

Figure 5-1: Coordinates of the differential grids

By substituting Eq. (5.2) and Eq. (5.3) into Eq. (5.16) and rearranging it for the pressure head, the pressure head at the next time step *n+1* can be calculated as the following equations Eq. (5.17) ~ (5.22).

$$h_{i,j}{}^{n+1} = \frac{(b^{n+1} + c^{n+1} + d^{n+1})\Delta t + e^{n+1} h_{i,j}{}^{n}}{a^{n+1}\Delta t + e^{n+1}} \tag{5.17}$$

$$a^{n+1} = \frac{k_{i-1/2,j}^{n+1} + k_{i+1/2,j}^{n+1}}{\Delta x^2} + \frac{k_{i,j-1/2}^{n+1} + k_{i,j+1/2}^{n+1}}{\Delta y^2} \tag{5.18}$$

$$b^{n+1} = \frac{k_{i-1/2,j}^{n+1} h_{i-1,j}{}^{n+1} + k_{i+1/2,j}^{n+1} h_{i+1,j}{}^{n+1}}{\Delta x^2} \tag{5.19}$$

$$c^{n+1} = \frac{k_{i,j-1/2}^{n+1} h_{i,j-1}{}^{n+1} + k_{i,j+1/2}^{n+1} h_{i,j+1}{}^{n+1}}{\Delta y^2} \tag{5.20}$$

$$d^{n+1} = \frac{\dfrac{k_{i,j+1/2}^{n+1}\rho_{i,j+1/2}^{n+1}}{\rho_f} - \dfrac{k_{i,j-1/2}^{n+1}\rho_{i,j-1/2}^{n+1}}{\rho_f}}{\Delta y} \tag{5.21}$$

$$e^{n+1} = \frac{Cw_{i,j}^{n+1} + Cw_{i,j}^{n}}{2} + \alpha_0 S \tag{5.22}$$

The hydraulic conductivity, *k*, and the density of the brackish water, *ρ*, are variable over time depending on the saturation or salinity, thus these values have the time step index n. The values at *i*±1/2 or *j*±1/2 are the average values between the grid points *i* and *i*±1 or j and *j*±1.

The implicit finite difference method generally requires an iterative equation for the convergence of the output. In this study, the successive over-relaxation method (SOR) is applied to the iterative computation and the equation is written as below.

$$ {}^{m+1}h_{i,j}^{n+1} = {}^{m}h_{i,j}^{n+1} + \omega\left(h_{i,j}^{n+1} - {}^{m}h_{i,j}^{n+1}\right) \tag{5.23} $$

where ω is the extrapolation factor, m is the number of iterations. The convergence of the iteration computation is judged when the difference of the pressure heads between iterative numbers m and m+1 becomes smaller than the judgement criteria ε_0.

$$ \left|{}^{m+1}h_{i,j}^{n+1} - {}^{m}h_{i,j}^{n+1}\right| < \varepsilon_0 \tag{5.24} $$

1.4 Discretization of the 2-D solute transport equation

Eq. (5.9), the fundamental equation for the 2-D solute transport, was numerically calculated based on the method of characteristics, which is developed from a conventional particle tracking technique. The method has high accuracy and stability especially when advection is dominant in the flow compared to dispersion as it was in the experimental device. Here explains the algorithm to solve Eq. (5.9) with the method of characteristics.

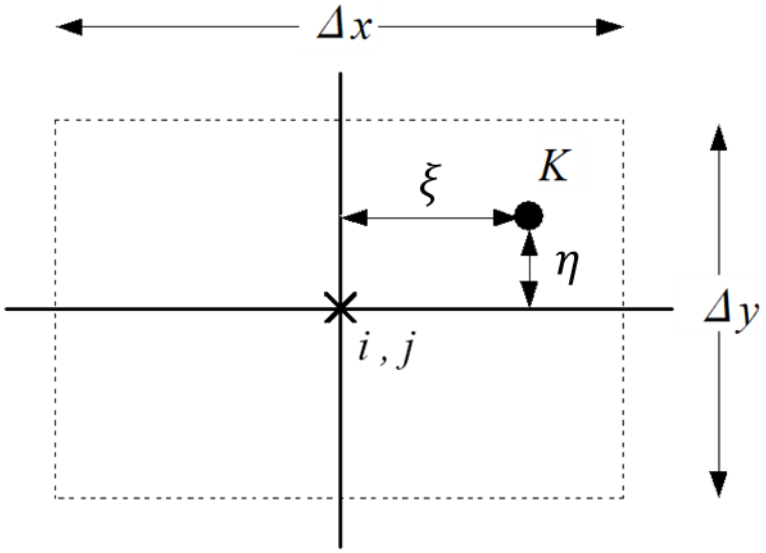

Figure 5-2: Image of the particle in a cell.

Figure 5-2 shows the image of the particle in a cell. Now given that there are M particles in a cell, the arithmetic mean of the particles in the cell is calculated as below.

$$ \overline{C_{i,j}^{n}} = \frac{1}{M}\sum_{K_i}^{M} C^{n}\left(K_i\right) \tag{5.25} $$

Where *M* is the number of particles in a cell, *K* is the identification number of the particle, *n* is the time step, $\overline{C_{i,j}^{n}}$ is the average concentration of the particles in the cell (*i* ,*j*), and $C^{n}(K)$ is the concentration of the particle *K* at time step *n*.

In the first step of the method, the particles are transported by advection, and then the average concentration of the particles in a cell can be obtained with Eq. (5.25).

The dispersion term of Eq. (5.9) is written as Eq. (5.26), and which can be discretized into Eq.

(5.27) using Eq. (5.25).

$$\frac{\partial(\theta C)}{\partial t} = \frac{\partial}{\partial x}\left(\theta D_{xx}\frac{\partial C}{\partial x} + \theta D_{xy}\frac{\partial C}{\partial y}\right) + \frac{\partial}{\partial y}\left(\theta D_{yy}\frac{\partial C}{\partial y} + \theta D_{yx}\frac{\partial C}{\partial x}\right) \tag{5.26}$$

$$\delta C_{i,j}^{n+1} = \frac{1}{\theta}\Delta t\left[\begin{array}{c} \frac{1}{\Delta x^2}\left\{D^{xx}_{i+\frac{1}{2},j}\left(\overline{C_{\iota+1,J}^{n+1}} - \overline{C_{\iota,J}^{n+1}}\right) - D^{xx}_{i-\frac{1}{2},j}\left(\overline{C_{\iota,J}^{n+1}} - \overline{C_{\iota-1,J}^{n+1}}\right)\right\} \\ + \frac{1}{4\Delta x\Delta y}\left\{D^{xy}_{i+1,j}\left(\overline{C_{\iota+1,J+1}^{n+1}} - \overline{C_{\iota+1,J-1}^{n+1}}\right) - D^{xy}_{i-1,j}\left(\overline{C_{\iota-1,J+1}^{n+1}} - \overline{C_{\iota-1,J-1}^{n+1}}\right)\right\} \\ + \frac{1}{4\Delta x\Delta y}\left\{D^{yx}_{i,j+1}\left(\overline{C_{\iota+1,J+1}^{n+1}} - \overline{C_{\iota-1,J+1}^{n+1}}\right) - D^{yx}_{i,j-1}\left(\overline{C_{\iota+1,J-1}^{n+1}} - \overline{C_{\iota-1,J-1}^{n+1}}\right)\right\} \\ + \frac{1}{\Delta y^2}\left\{D^{yy}_{i,j+\frac{1}{2}}\left(\overline{C_{\iota,J+1}^{n+1}} - \overline{C_{\iota,J}^{n+1}}\right) - D^{xx}_{i,j-\frac{1}{2}}\left(\overline{C_{\iota,J}^{n+1}} - \overline{C_{\iota,J-1}^{n+1}}\right)\right\} \end{array}\right] \tag{5.27}$$

Where $\delta C_{i,j}^{n+1}$means the variation of the concentration in a cell. Therefore, the concentration of the cell in the next time step n+1 can be calculated as below.

$$C_{i,j}^{n+1} = \overline{C_{\iota,J}^{n}} + \delta C_{i,j}^{n+1} \tag{5.28}$$

To smooth the variation of each particle concentration, the deviation of the particle from the node was interpolated as below. The variation of the concentration between the adjacent nodes is assumed liner in this study.

$$\delta C\left(x^{n+1}(K), y^{n+1}(K)\right) = \delta C_{i,j}^{n+1} + \xi\frac{\partial}{\partial x}(\delta C)_{i,j}^{n+1} + \eta\frac{\partial}{\partial y}(\delta C)_{i,j}^{n+1} \tag{5.29}$$

(i) $\xi \geqq 0$, $\eta \geqq 0$

$$\frac{\partial}{\partial x}(\delta C) = \frac{\delta C_{i+1,j}^{n+1} - \delta C_{i,j}^{n+1}}{\Delta x}, \qquad \frac{\partial}{\partial y}(\delta C) = \frac{\delta C_{i,j+1}^{n+1} - \delta C_{i,j}^{n+1}}{\Delta y} \tag{5.30}$$

(ii) $\xi \geqq 0$, $\eta \leqq 0$

$$\frac{\partial}{\partial x}(\delta C) = \frac{\delta C_{i+1,j}^{n+1} - \delta C_{i,j}^{n+1}}{\Delta x}, \qquad \frac{\partial}{\partial y}(\delta C) = \frac{\delta C_{i,j}^{n+1} - \delta C_{i,j-1}^{n+1}}{\Delta y} \tag{5.31}$$

(iii) $\xi \leqq 0$, $\eta \geqq 0$

$$\frac{\partial}{\partial x}(\delta C) = \frac{\delta C_{i,j}^{n+1} - \delta C_{i-1,j}^{n+1}}{\Delta x}, \qquad \frac{\partial}{\partial y}(\delta C) = \frac{\delta C_{i,j+1}^{n+1} - \delta C_{i,j}^{n+1}}{\Delta y} \tag{5.32}$$

(iv) $\xi \leqq 0$, $\eta \leqq 0$

$$\frac{\partial}{\partial x}(\delta C) = \frac{\delta C_{i,j}^{n+1} - \delta C_{i-1,j}^{n+1}}{\Delta x}, \qquad \frac{\partial}{\partial y}(\delta C) = \frac{\delta C_{i,j}^{n+1} - \delta C_{i,j-1}^{n+1}}{\Delta y} \tag{5.33}$$

Where $x^{n+1}(K), y^{n+1}(K)$ represent the coordinate of particle *K* and $\delta C\left(x^{n+1}(K), y^{n+1}(K)\right)$ represents the variation of the particle concentration. Therefore, the concentration of particle *K* at the next time step is calculated as:

$$C^{n+1}(K) = C^{n}(K) + \delta C^{n+1}\{x^{n+1}(K), y^{n+1}(K)\} \tag{5.34}$$

Coordinates of the particle in x and y direction after time level n+1 is:

$$x^{n+1}(K) = x^n(K) + u(K)\Delta t \tag{5.35}$$

$$y^{n+1}(K) = y^n(K) + v(K)\Delta t \tag{5.36}$$

All this process is the method of characteristics (Jinno et al., 2001), and this is how the two-dimensional solute transport with advection and dispersion can be calculated numerically.

1.5 Stability equations

Stability of the calculation must be confirmed in the finite difference method. The groundwater flow equation was discretized by the implicit finite difference method, which means the calculation is stable without any conditional. As for the 2-D solute transport equation, the following conditionals are given for the stability.

$$\frac{\Delta t D_{xx}}{\Delta x^2} < 0.47 \tag{5.37}$$

$$\frac{\Delta t D_{yy}}{\Delta y^2} < 0.47 \tag{5.38}$$

Besides, the following limitations are given to avoid the particles are transported beyond each cell length by advection during Δt:

$$\frac{\Delta t u'_{max}}{\Delta x} < 0.50 \tag{5.39}$$

$$\frac{\Delta t v'_{max}}{\Delta y} < 0.50 \tag{5.40}$$

where u'_{max} and v'_{max} are the maximum velocity in x and y direction, respectively.

Δx and Δy were decided long enough to simulate the drastic variation of the concentration in the fresh-salt water mixing zone. Then, the time step Δt which meets Eq. (5.37) ~ (5.40) was given in the simulation.

2 Conceptual Model

Figure 5-3 shows the conceptual model used to simulate seawater intrusion. As designed in the experimental device, the conceptual model has three sections; saltwater zone simulating the sea, intrusion zone simulating a coastal aquifer, and freshwater zone simulating groundwater, although the conceptual model for the simulation is in two-dimension. Additionally, a production well and several barrier wells were applied in the model in order to investigate an optimal barrier well location.

In this 2-D conceptual model, there are 8 boundaries; the saltwater boundary which has 100% constant salinity (AB), the boundaries between each section (EF and GH), the freshwater boundary which has 0% constant salinity (DC), impermeable boundary at the bottom(BC), constant head boundaries for saltwater (AE) and freshwater (DH), and groundwater surface (EH).

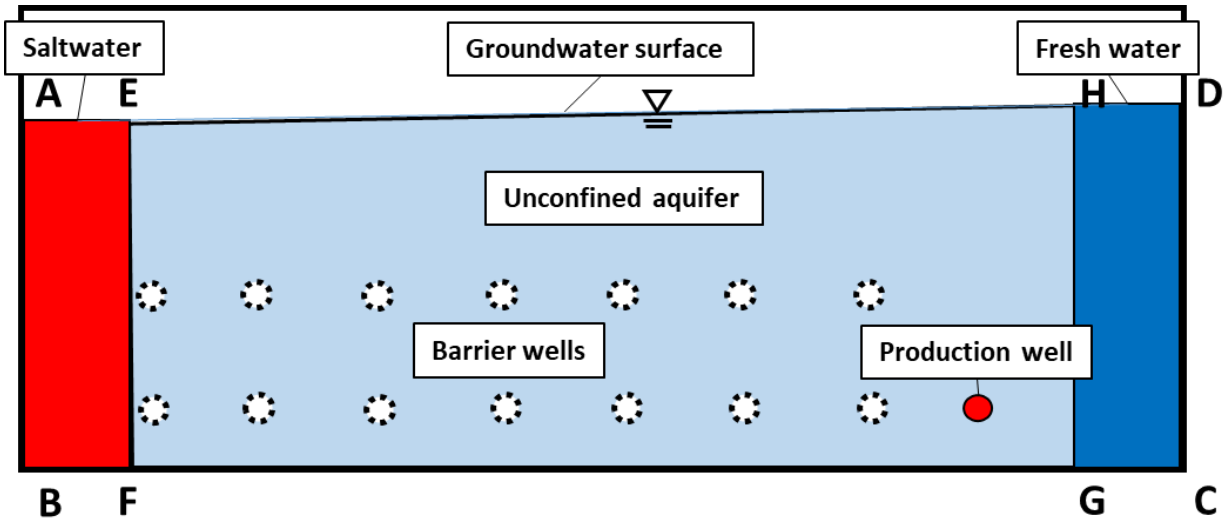

Figure 5-3: 2-D Conceptual model for the numerical simulation

3 Numerical Model

Based on the stability equations Eq. (5.37) ~ (5.40), both of Δx and Δy were designed as 0.5cm each, and Δt was set as 0.5 second. Figure 5-4 shows the image of the particle allocation in a cell. At the beginning of the simulation, four particles were allocated in each cell regularly as shown in the figure. The particles in the area simulating the saltwater supply section had 100% at particle concentration and the particles in the other areas had 0% at the concentration. Since the model simulates the experimental device, 245 cells and 81 cells were given in x and y directions respectively. The numerical model is shown in Figure 5-5 and the boundary conditions are given in Table 5-2. The coordinates of the wells were delivered in the next section.

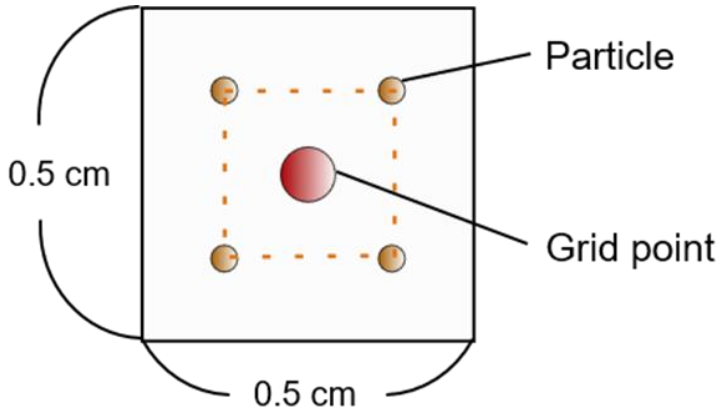

Figure 5-4: Initial allocation of the particles in a cell

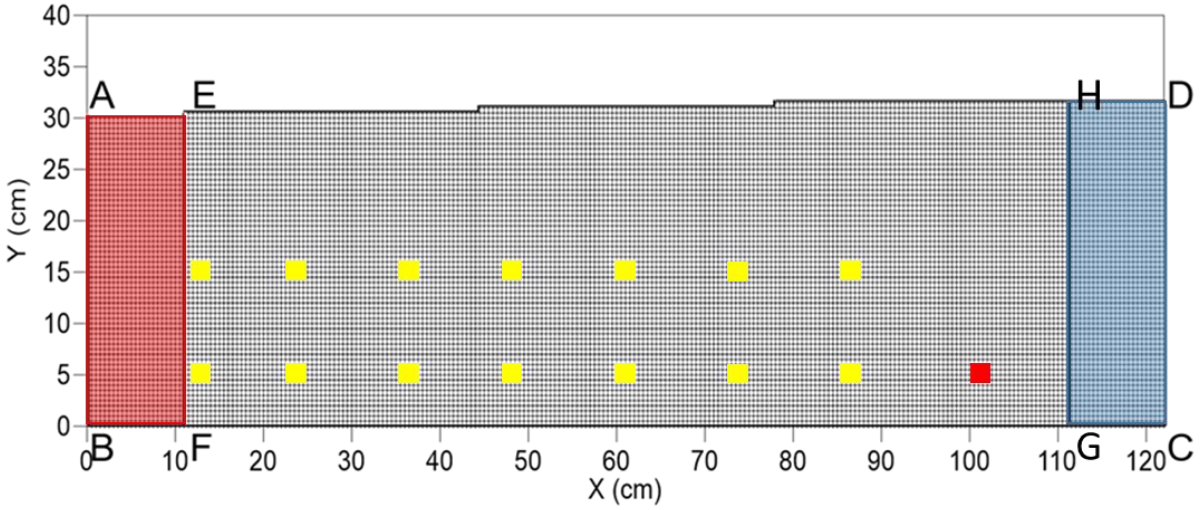

Figure 5-5: Numerical model for the simulation

The other parameters in the simulation were obtained from the experiments or referenced from the previous study (Ozaki, 2021) (Jinno et al., 2001). Table 5-3 shows the parameters used in the simulation.

Table 5-2: Boundary conditions for each boundary

Boundary		Conc.	Pressure Head
LEFT (Salt water)	AB	$C = 100\%$	$h = (H_s - y)\frac{\rho_s}{\rho_f}$
	EF	$(1)u \geq 0, \frac{\partial C}{\partial x} = 0$ $(2)u < 0, C = 100\%$	
RIGHT (Freshwater)	CD	$C = 0\%$	$h = (H_f - y)$
	GH	Eq. (5.24)	
TOP (Water Surface)	DH	$C = 0\%$	$h = (H_f - y)$
	EH	$C = 0\%$	$-k\left(\frac{\partial h}{\partial y} + \frac{\rho}{\rho_f}\right) = -q_w$
	EA	$(1)v \geq 0, \frac{\partial C}{\partial y} = 0$ $(2)v < 0, C = 100\%$	$h = (H_s - y)\frac{\rho_s}{\rho_f}$
BOTTOM (Impermeable)	BC	$\frac{\partial C}{\partial y} = 0$	$-k\left(\frac{\partial h}{\partial y} + \frac{\rho}{\rho_f}\right) = 0$

Table 5-3: Numerical and hydrological parameters for the simulation model

Time interval	Δt	0.5 (sec)
Cell length in x direction	Δx	0.5 (cm)
Cell length in y direction	Δy	0.5 (cm)
Longitudinal dispersion length	α_L	0.038 (cm)
Transverse dispersion length	α_T	0.0051 (cm)
Molecular diffusion	D_M	1.0×10^{-5} (cm2/s)
Porosity	n_e	0.385
Freshwater head	H_f	31.5 or 31.0 (cm)
Saltwater head	H_s	30.0 (cm)
Freshwater density	ρ_s	0.996 (g/cm3)
Saltwater density	ρ_f	1.025 ~ 1.030(g/cm3)
Extrapolation factor for SOR method	ω	1.6
Criteria for convergence judgement	ε_0	1.0×10^{-4}
Specific storage coefficient	S_S	0.1

4 Analysis for an Optimal Well Location using the Simulation Model

As the first phase of this study, the barrier efficiencies at the four well locations and the effects of the reduction of groundwater table were examined in the two different experiments. Before going to the second phase of the study, an analysis for an optimal well location and application, Experiment 2 was numerically simulated using the 2-D solute transport model. This simulation confirms the reliability of a simulation of seawater intrusion caused by the density difference and pumping at a production and a barrier well, as well as reduction of groundwater level, and makes it sure that the simulation model setup is reliable enough for other simulations. Therefore, once the reliability of the simulation output is confirmed, this simulation model would be able to employ for the analysis of the optimal well location.

In the last phase of this study, the barrier efficiencies of the wells at 14 locations were compared in two different groundwater level conditions, 31.5cm and 31.0cm, which is associated with over extraction of groundwater or relative seawater level rise, using the 2-D solute transport model. Figure 5-6 shows the simulation image and Table 5-4 shows the coordinates of the 14 barrier well locations. By comparing the difference of the barrier efficiencies among these well locations under the two different groundwater table conditions, an optimal barrier well location and application methods could be suggested for the future, when further seawater intrusion has been predicted. Pumping rate was decided as 8ml/s at the production well and 3.6ml/s at each barrier well, which means each barrier well pumps 45% of the production rate.

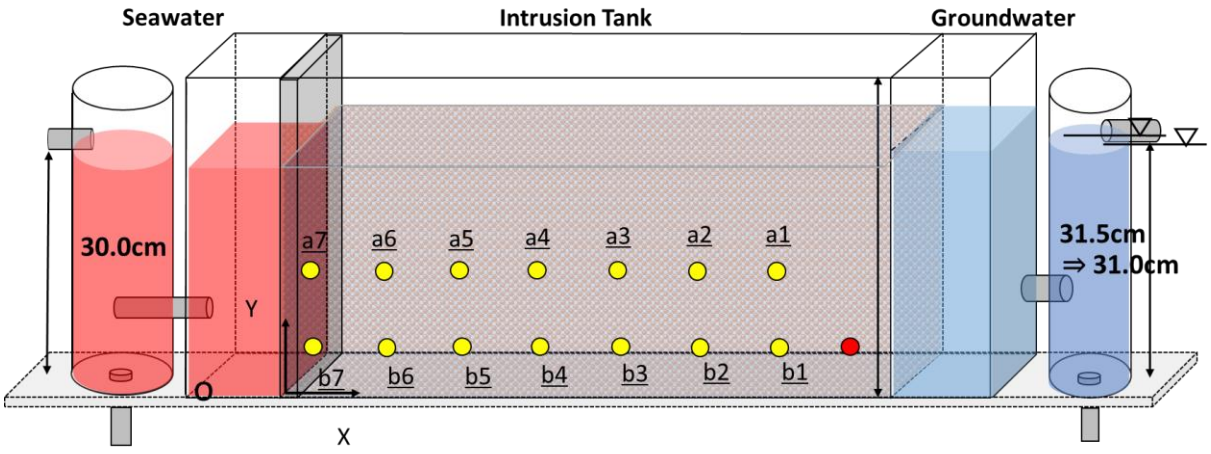

Figure 5-6: Simulation image. The red plot represents the production well at (90, 5) on the coordinate, and the yellow plots represent the barrier wells.

Table 5-4: Coordinates at the barrier well locations.

Well	a7	a6	a5	a4	a3	a2	a1
X(cm)	1	12.5	25	37.5	50	62.5	75
Y(cm)	15	15	15	15	15	15	15
Well	**b7**	**b6**	**b5**	**b4**	**b3**	**b2**	**b1**
X(cm)	1	12.5	25	37.5	50	62.5	75
Y(cm)	5	5	5	5	5	5	5

This simulation was conducted with three steps. In the first step, seawater intrusion caused by the density difference between saltwater and freshwater was simulated without any pumping. In the second step, the production well started pumping at 8ml/s. In the final step, one of the barrier wells started pumping at 3.6ml/s and worked as a barrier. All the barrier wells were simulated in the final step and each step was conducted under two different groundwater table conditions, 31.5cm and 31.0cm. Note that the other parameters on the calculation, such as densities, hydraulic conductivity, porosity, dispersion and diffusion coefficient, were assumed as the same values as the experiments.

The analysis was conducted based on the following four factors, Time1, Time2, Time3, and Remediation rate, as well as the general condition of the aquifer after the remediation. Each factor's definition was described as follows.

Time1 (min): Time when the aggravation of seawater intrusion in the coast side stops.
Time2 (min): Time when the production quality got cured by the barrier, in other words, no more seawater intrusion was observed at the production well.
Time3 (min): Time when the remediation completes.
Remediation rate (%): Remediation rate of the intrusion length by a barrier well. Note that the intrusion length at the end of Step2 were 90cm, so the rate can be calculated as below:

$$\frac{(\mathbf{90}-\boldsymbol{Intrusion\ Length\ in\ the\ steady\ state\ (cm)})}{\mathbf{90}} \times 100\ (\%)$$

Based on the analysis, the optimal well location to remediate seawater intrusion could be suggested. Besides, the effects of the groundwater head reduction on the optimal location were discussed and an effective barrier well approach to remediate groundwater sustainability was suggested for the future based on the situation and experimental results.

Chapter 6: Simulation Results and Discussion

This chapter consists of three sections: a simulation of the experiment, an analysis of an optimal well location using the 2-D simulation model, and a suggestion of an efficient barrier well application. First, in the simulation part of the experiment, the simulation results were compared to the results of Experiment 2 to confirm the model reliability. Then, in the analysis section, barrier efficiencies at 14 well locations, in two different ground water level conditions, were analyzed to examine an optimal well location and the effects of the groundwater level reduction on the optimal location. Finally, an effective application for a barrier well was suggested based on the simulation results, and the effectiveness was examined using the simulation model.

1 Simulation of Experiment 2

In this section, Experiment 2 was simulated using the 2-D solute transport model. The simulation results were compared to the experimental results to confirm the model reliability.

Experiment 2 was simulated in three steps. In Step 1, the density difference between freshwater and saltwater caused seawater intrusion. In Step 2, additional intrusion was caused by pumping from Well B at 3.1 ml/s. In Step 3, Well A pumped at 4.8 ml/s as a production well and Well B functioned as a barrier well to prevent further seawater intrusion. All the steps were simulated in two different groundwater levels, 31.5 cm and 31.0 cm. Note that saltwater density was set as 1.028 g/cm^3, 1.026 g/cm^3, and 1.025 g/cm^3 in Step1, 2, and 3, respectively, based on the experiment. Since Experiment 2 used a barrier well and a production well in two different groundwater levels, the simulation of Experiment 2 could confirm the reliability of the simulation of seawater intrusion with these external factors.

Figure 6-1, 2, and 3 show the seawater intrusion process with the salinity distribution in each step for 31.5 cm groundwater level. As shown in the figures, the intrusion process and the general shape of the saltwater wedge were reproduced with high accuracy by the simulation model. The intrusion lengths over time in each step are described in Figure 6-4. There was a slight error in the intrusion lengths, especially in Step 3. This is probably because of the limitations in the experiment, such as the fluctuation of the pumping, the density difference, and human error, as well as the potential calculation error. The intrusion length was measured numerically in the simulation, even though it was measured visually in the experiment, which also might be the cause of the error. However, the simulation model could calculate the general intrusion behavior over time with high accuracy considering the shape of the interface and the intrusion length. The maximum error in the steady state was 4.2 cm and it was regarded as plausible considering the scale of the experimental device and the simulation model.

Figure 6-5, 6, and 7 show the seawater intrusion process with the salinity distribution in each

step for 31.0 cm groundwater level. The intrusion behavior was simulated with high accuracy in this groundwater level as well, as shown in the figures. The aggravation of the salinization in the coast side in Step3, which was observed in the experiment, was also shown in the simulation. Figure 6-8 shows the intrusion length over time in each step for 31.0 cm groundwater level. Even though slight errors were observed again, this is most probably caused by the same reasons as outlined above. Note that the color label for each figure is the same as the one shown in Figure 6-3.

The simulation of Experiment 2 showed that the 2-D solute transport model can simulate seawater intrusion with a production well and a barrier well in different groundwater level conditions over time with high accuracy. Therefore, it can be assumed that this simulation model is reliable enough to employ for the analysis of an optimal well location for the further.

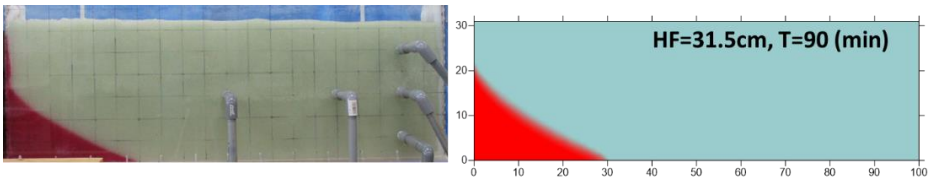

Figure 6-1: Step1 for 31.5 cm groundwater level.

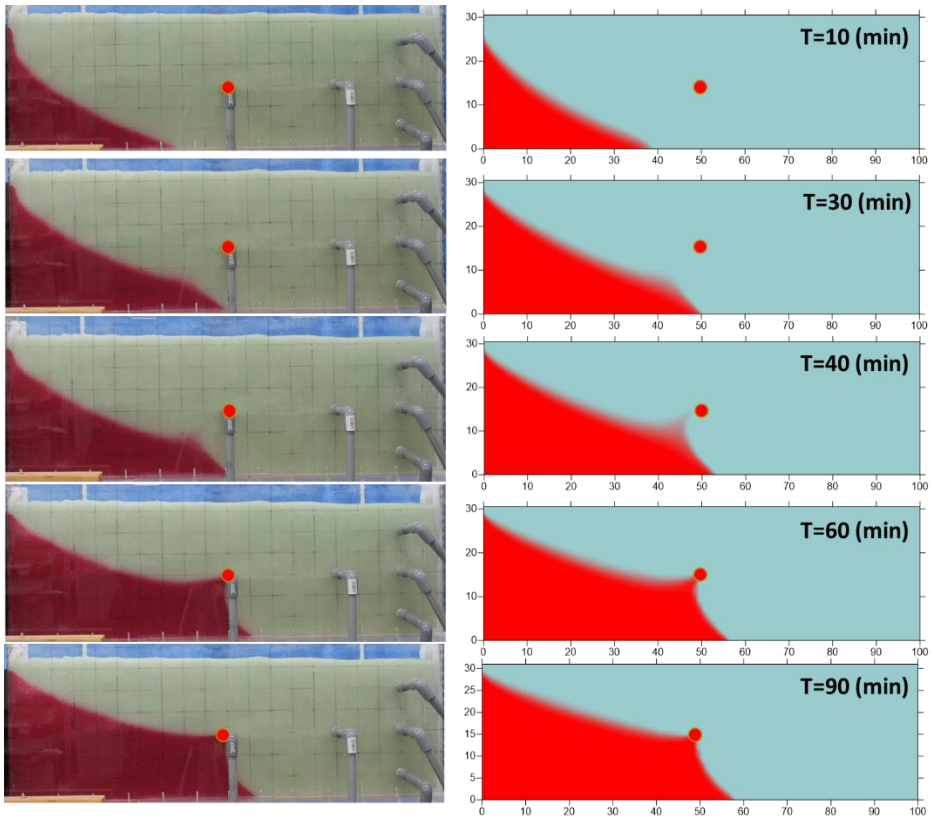

Figure 6-2: Step2 for 31.5 cm groundwater level.

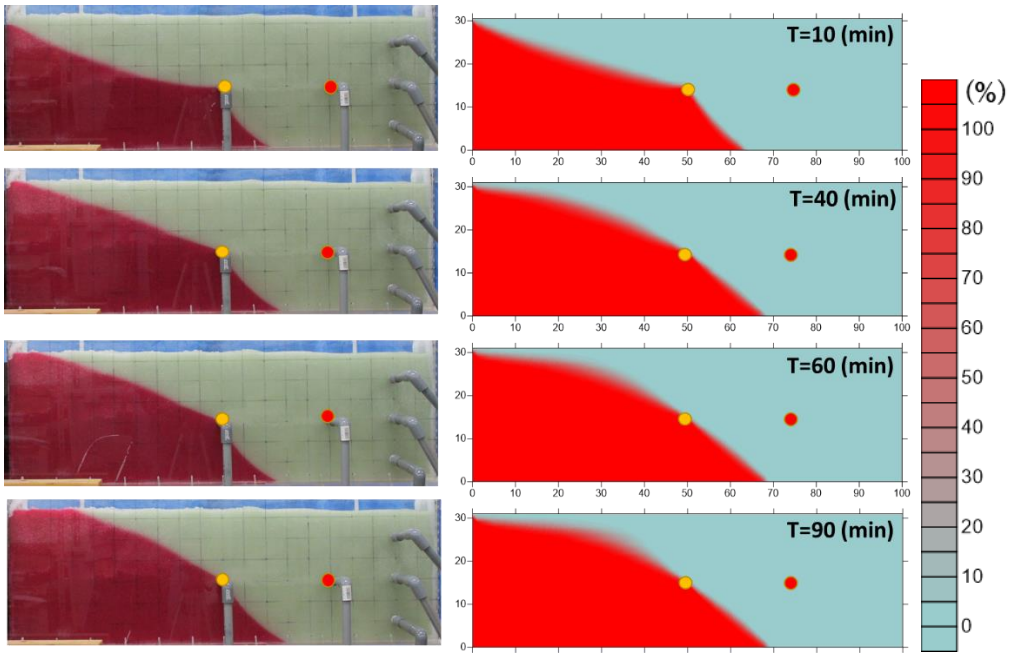

Figure 6-3: Step3 for 31.5 cm groundwater level.

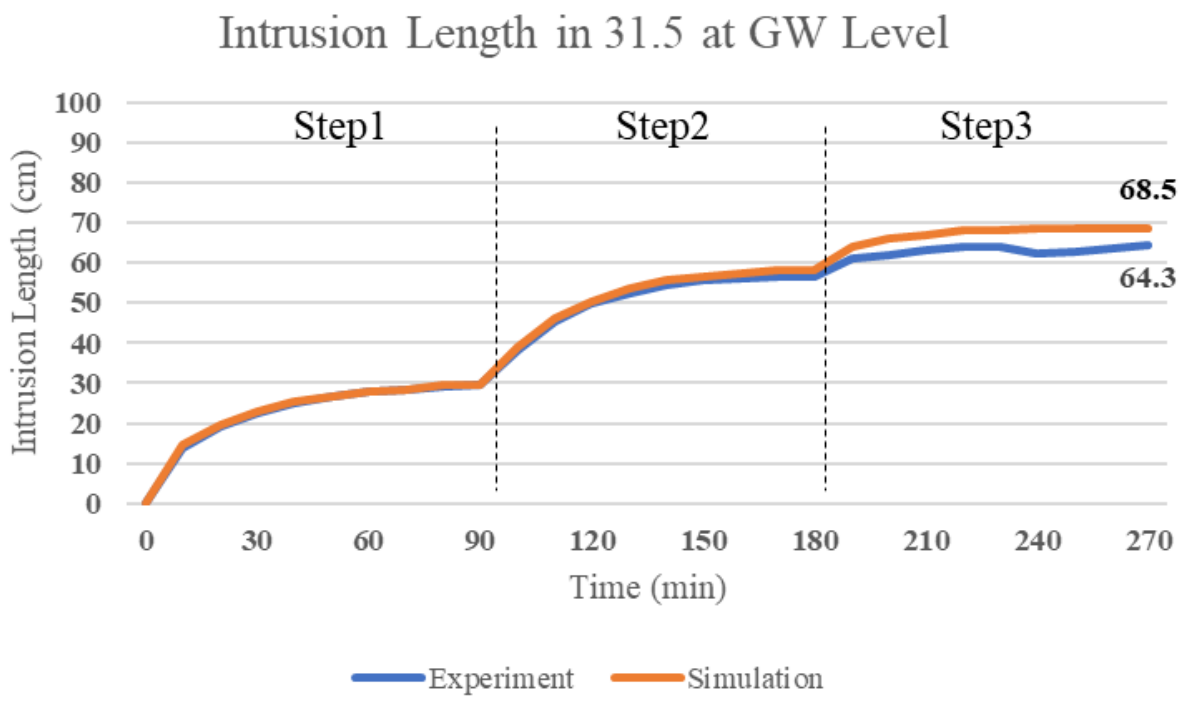

Figure 6-4: The intrusion length over time in each step in 31.5 cm at groundwater level

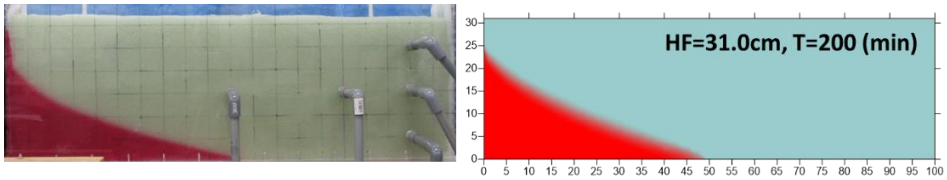

Figure 6-5: Step1 for 31.0 cm groundwater level.

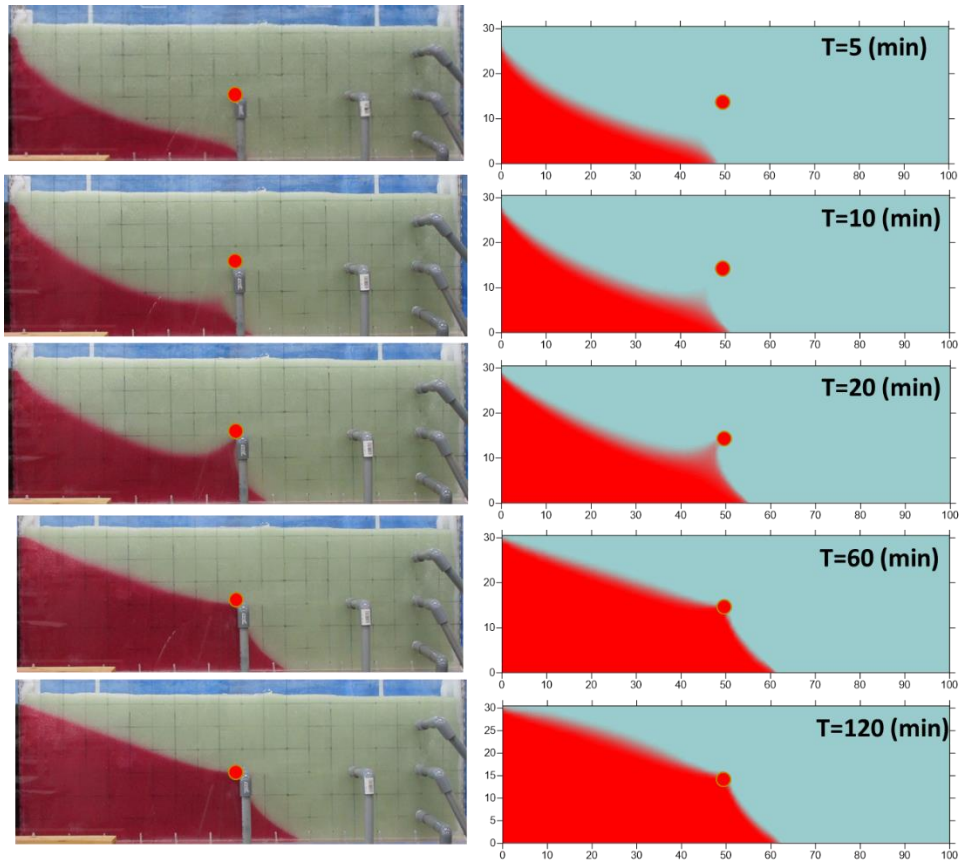

Figure 6-6: Step2 for 31.0 cm groundwater level.

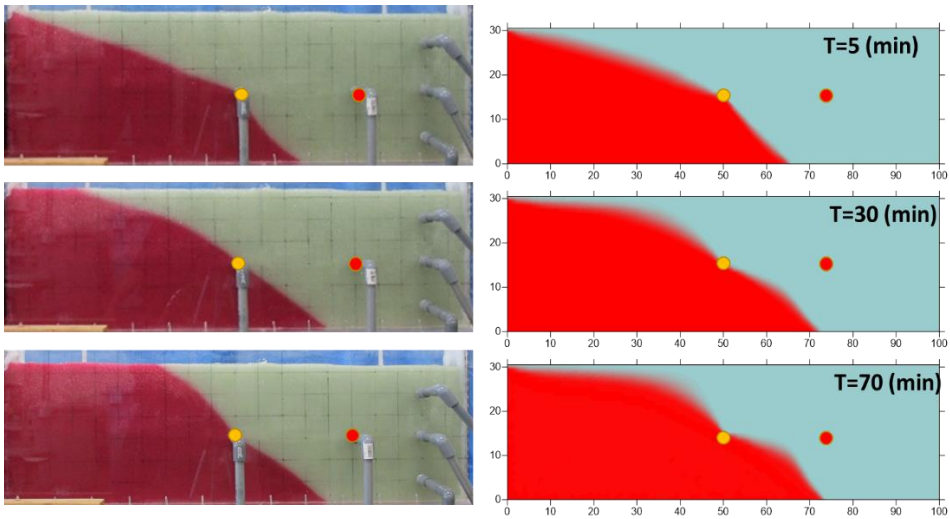

Figure 6-7: Step3 for 31.0 cm groundwater level.

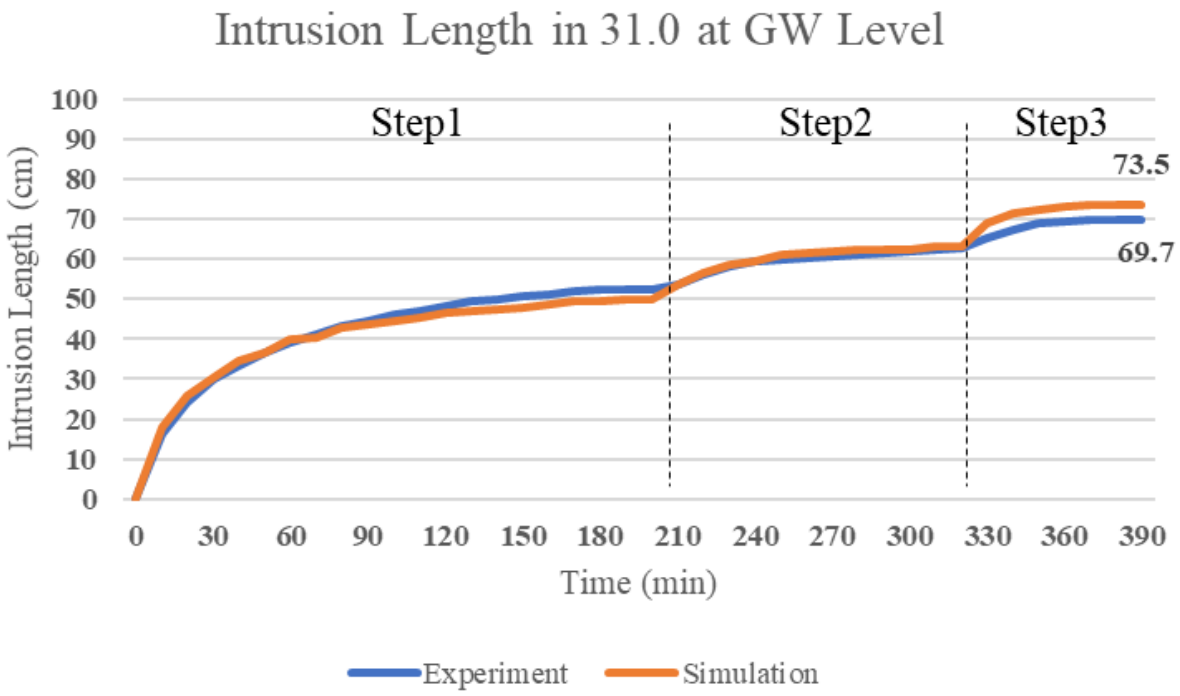

Figure 6-8: The intrusion length over time in each step in 31.0 cm at groundwater level

2 A numerical analysis of an optimal barrier well location

This section describes the results of the numerical analysis of an optimal barrier well location. The simulation was conducted in two different groundwater level conditions with three steps: Step 1, Seawater intrusion caused by the density difference; Step 2, further seawater intrusion caused by pumping from the production well at 8.0 ml/s; Step 3, remediation by a barrier well pumping at 3.6 ml/s (45 % of the production rate). The barrier efficiencies at each well location were then analyzed, and the effects of the groundwater level reduction on the optimal well location were discussed below. The analysis was conducted based on the four factors, Time 1, Time 2, Time 3, and Remediation rate, as well as the general shape of seawater intrusion as explained in the previous chapter. All the simulation results were described in Appendix-1.

2-1 Simulation results of Step 1 and Step 2.

In Step 1, seawater intrusion caused by the density difference was simulated in different groundwater levels, 31.5 cm and 31.0 cm. This is completely the same process as Step 1 of Experiment 2, which was accurately simulated with the model as described in the previous section. As discussed in the experiment chapter and described in the previous section, the groundwater level reduction caused further and faster seawater intrusion.

In Step 2, further seawater intrusion caused by groundwater production was simulated in the two groundwater levels. Figure 6-9 shows salinity distributions in each steady state of this step.

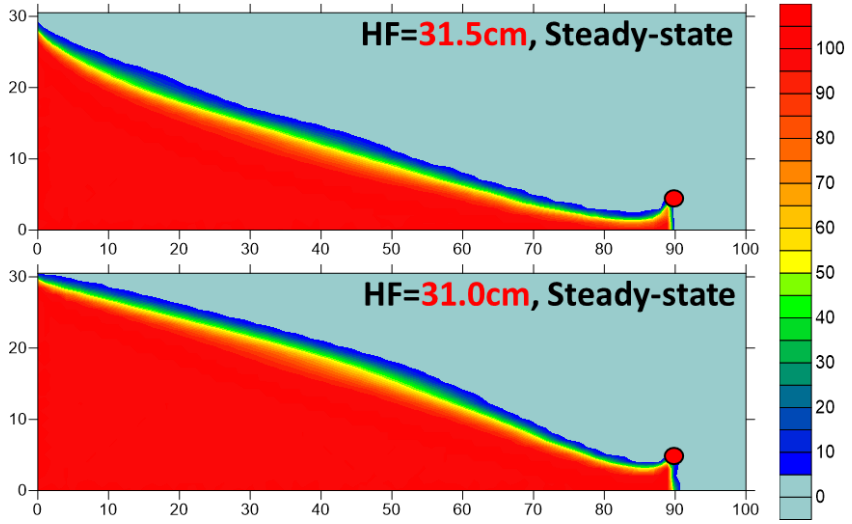

Figure 6-9: Steady states in Step 2 for 31.5 cm (Top) and 31.0 cm (Bottom) at groundwater level.

As shown in the figure, intrusion lengths were both 90 cm from the coast. However, the thickness of the saline water in the aquifer was grater in the 31.0 cm groundwater level. The same phenomenon was observed after Well B started pumping in Step 2 of Experiment 2, especially on the coast side. Therefore, groundwater level reduction surely causes further seawater intrusion and expands the salinized area in the aquifer, even if the intrusion length does not change.

2-2 Simulation results of Step 3 for 31.5 cm groundwater level.

Once the intrusion steadied in Step 2, a barrier well started pumping at 3.6 ml/s (45 % of the production), and then the barrier efficiency at each well location was investigated. Figure 6-10 shows the remediation process with the barrier well at b4. This result also shows the times explained above, Time 1, Time 2, and Time 3.

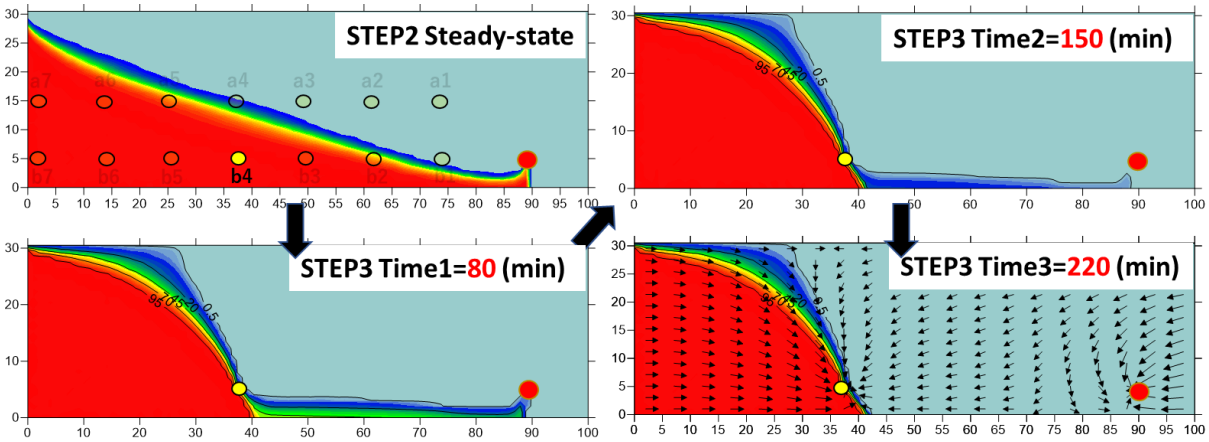

Figure 6-10: Salinity distribution with the barrier well at b4. (31.5cm groundwater level)

As shown in the figure, the barrier well pulled saline water from the coast side and made the coastal aquifer more salinized. The aggravation stopped after 80 minutes from the beginning of Step 3 (Time 1). Although the production well kept on pumping saline water after Time 1, it was completely restored by 150 minutes (Time 2). However, less than 20 % salinity remained to be cured inland after Time2, and it took 220 minutes in total to complete the remediation (Time 3). At the end of the remediation, seawater intrusion length was 42 cm from the coast, so the remediation rate of the intrusion length was 53.3 %. Note that the arrows on the figure at Time 3 represent the velocity vector in Step 3.

Table 6-1 and 6-2 show the results of Time 1, Time 2, Time 3, and the remediation rate at each barrier well location. Note that here the dashes (–) represent no data because the barrier well did not work enough to observe the data. For example, the barrier at a6 did not remediate seawater intrusion from the production well, and it was too close to the coast to observe the salinization in the coast side. Therefore, these times could not be measured at the well location.

Table 6-1: Results at each well location at depth a (15 cm from the bottom).

HF=31.5cm	a7	a6	a5	a4	a3	a2	a1
Intrusion length （cm）	90	90	62	65	90	90	90
Remediation rate （%）	0	0	31.1	27.8	0	0	0
Time 1 (min)	-	-	40	70	90	130	190
Time 2 (min)	-	-	300	200	-	-	-
Time 3 (min)	-	-	430	270	-	-	-

As shown in Table 6-1, the barrier well at a1, a2, a3, a6, and a7, did not remediate the intrusion length. At a1, the barrier well pulled saline water from the coast and the salinity of production water increased. This result corresponds with the result of Experiment 1. As for a2, a6, and a7, salinity around the production well hardly changed and the production well kept on pumping saline water even in the steady states. Although the barrier at a3 worked properly in the experiment and seemed not to remediate seawater intrusion well in the simulation, the barrier decreased salinity around the production well to less than 5% and the remediation stopped in 190 minutes. This is probably the reason why the barrier well at a3 seemed to have restored the production quality in the experiment visually, but it did not fully restored the intrusion length in the simulation. As for the barrier wells at a4 and a5, these barriers remediated the intrusion length by 27.8 % and 31.1 %, respectively. Although the remediation rate was slightly better at a5 compared to a4, Time 2 and Time 3 were even faster at a4.

Table 6-2: Results at each well location at depth b (5 cm from the bottom).

HF=31.5cm	b7	b6	b5	b4	b3	b2	b1
Intrusion length （cm）	-	18.5	30	42	54	66	79
Remediation rate （%）	-	79.4	66.7	53.3	40.0	26.7	12.2
Time 1 (min)	-	-	50	80	90	120	190
Time 2 (min)	-	1040	280	150	120	90	10
Time 3 (min)	-	1520	380	220	140	110	40

At depth b, all the well locations apart from b7 functioned as a barrier well, as shown in Table 6-2. The results clearly show the remediation rate is better when the barrier well is closer to the coast. The barrier at b7 as well as a7 did not function as intended since these barrier wells were too close to the coast with the constant head at 30 cm, and most of the pumped water at the barrier wells was pulled directly from the sea instead of the saline water in the aquifer. Figure 6-11 shows the velocity distribution and the conceptual images with the barriers at b6 and b7. Although the barrier wells closer to the coast remediated the intrusion length better, the remediation time (Time2 and Time3) took even longer than inland barrier wells, especially at b6. In other words, inland barrier wells can remediate the production quality promptly and coastal barrier wells can remediate seawater intrusion length better after a longer time. These results show the better remediation by a barrier well close to the coast and the prompt remediation by an inland well, but also revealed that the barrier would not function if it is too close to the coast since it would pump saline water directly from the sea more so than inland salinity.

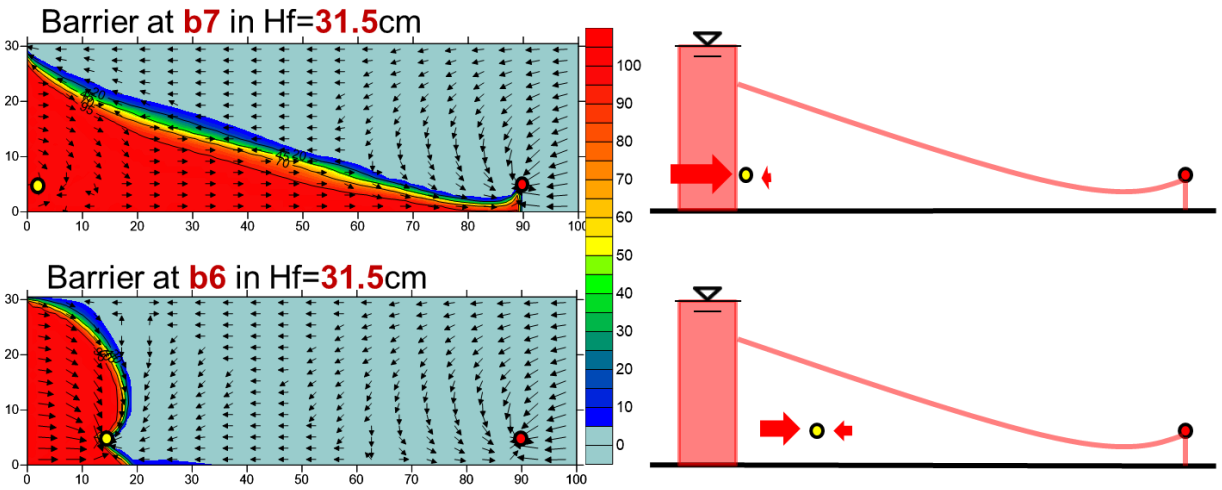

Figure 6-11: Velocity distribution with the barrier at b6 and b7, and the conceptual images.

Comparing the two depths, a and b, the barrier wells at depth b worked better in terms of the remediation rate and time. However, the further salinization on the coast side was caused by a barrier well in any depth, and the intensity and the time of the coastal salinization (Time1) were almost the same despite the depth of the barrier well. As observed in the experiments, the simulation also showed that the inland barrier wells salinized the coast side more than the coastal barrier wells. Considering the remediation rate and the further salinization in the coastal side by a barrier well, it seems to be better to install a barrier well closer to the coast. However, the remediation time would be even longer when the barrier well is too close to the coast and an inland barrier well would work even faster. Therefore, it can be clearly suggested to pump saline water from the lower part of the aquifer, but not necessarily better to install a barrier well close to the coast.

2-3 Simulation results of Step3 for 31.0cm groundwater level.

Figure 6-12 shows the remediation process with the barrier well at b4 for 31.0 cm groundwater level.

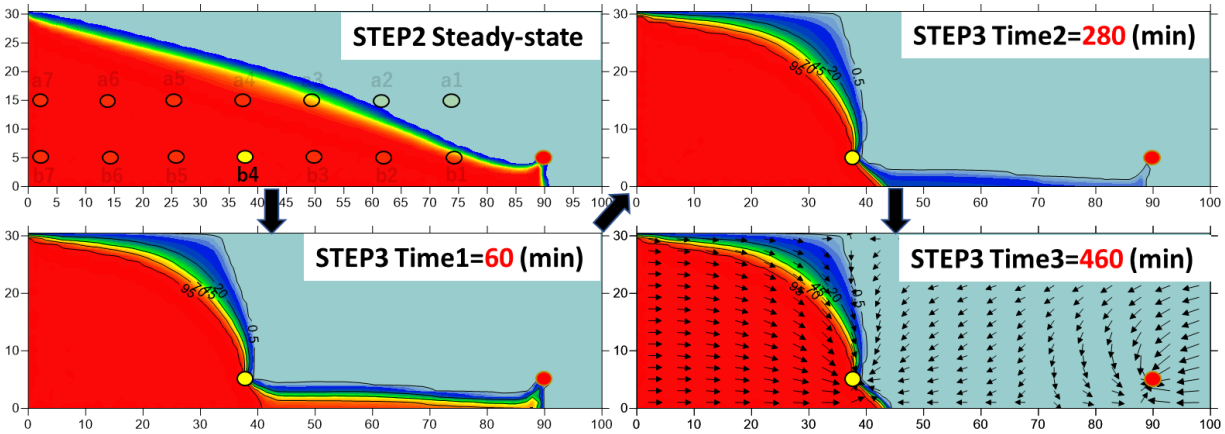

Figure 6-12: Salinity distribution with the barrier well at b4. (31.0cm groundwater level)

The barrier well at b4 remediated seawater intrusion properly even after the groundwater level reduction. The remediation rate of the intrusion length was 52.2 %, which was almost the same as that for 31.5cm groundwater level. However, salinization on the coast side expanded more due to the reduction of the groundwater level, which corresponds with the results of Experiment 2. Besides, Time 2 and Time 3 took almost twice as long as the corresponding times for 31.5 cm groundwater level. Therefore, groundwater level reduction could hinder remediation of a barrier well and provoke more intense seawater intrusion on the coastal side.

Table 6-3 and 6-4 show the results of Time 1, Time 2, Time 3, and the remediation rate, at each barrier well location.

Table 6-3: Results at each well location at depth a (15 cm from the bottom).

HF=31.0cm	a7	a6	a5	a4	a3	a2	a1
Intrusion length（cm）	90	90	90	90	90	90	90
Remediation rate（%）	0	0	0	0	0	0	0
Time 1 (min)	-	-	30	40	50	80	120
Time 2 (min)	-	-	-	-	-	-	-
Time 3 (min)	-	-	-	-	-	-	-

When a barrier was at depth a, seawater intrusion was not remediated at all and salinity around the production well was more than 90 % in all cases, and if anything, the barrier aggravated salinization on the coastal side. Hence, pumping from an upper part of the aquifer could become less effective by groundwater level reduction or sea level rise in the future.

Table 6-4: Results at each well location at depth b (5 cm from the bottom).

HF=31.0cm	b7	b6	b5	b4	b3	b2	b1
Intrusion length（cm）	-	-	31	43	55	67	81.5
Remediation rate（%）	-	-	65.6	52.2	38.9	25.6	9.4
Time 1 (min)	-	-	50	60	70	80	120
Time 2 (min)	-	-	980	280	160	100	100
Time 3 (min)	-	-	1460	460	210	130	230

On the other hand, the barrier wells at depth b still remediated the intrusion as much as they did before the groundwater level reduction. However, the remediation times (Time 2 and Time 3) took longer after the groundwater level reduction. This likely resulted in a decrease in hydraulic gradient, which hindered the repulsion with the seaward flow. The barrier well at b6 slightly decreased salinity around the production well but could not fully restore the production water quality. This is because of the same reason why the barriers at b7 and a7 would not function as barrier wells. In other words, the groundwater level reduction caused further seawater intrusion and expansion of the area where a barrier well takes too much seawater

directly from the sea as shown in Figure 6-12. Therefore, it would be better not to install a barrier well too close to the coast since it could be less effective to remediate inland seawater intrusion.

Although the remediation time was faster as the barrier well was inland basically, the remediation time (Time3) at b1 took longer than expected in the simulation. Figure 6-13 shows the velocity distribution around the production well and the barrier well at b1 in the two different groundwater level conditions. As shown in the figure, the groundwater level reduction slowed down the horizontal flow towards the barrier well, especially around the red dashed line shown in the figure. Because there is almost no horizontal flow around this line, the remediation took longer than the barrier by the well at b2, which was expected to take longer to remediate seawater intrusion.

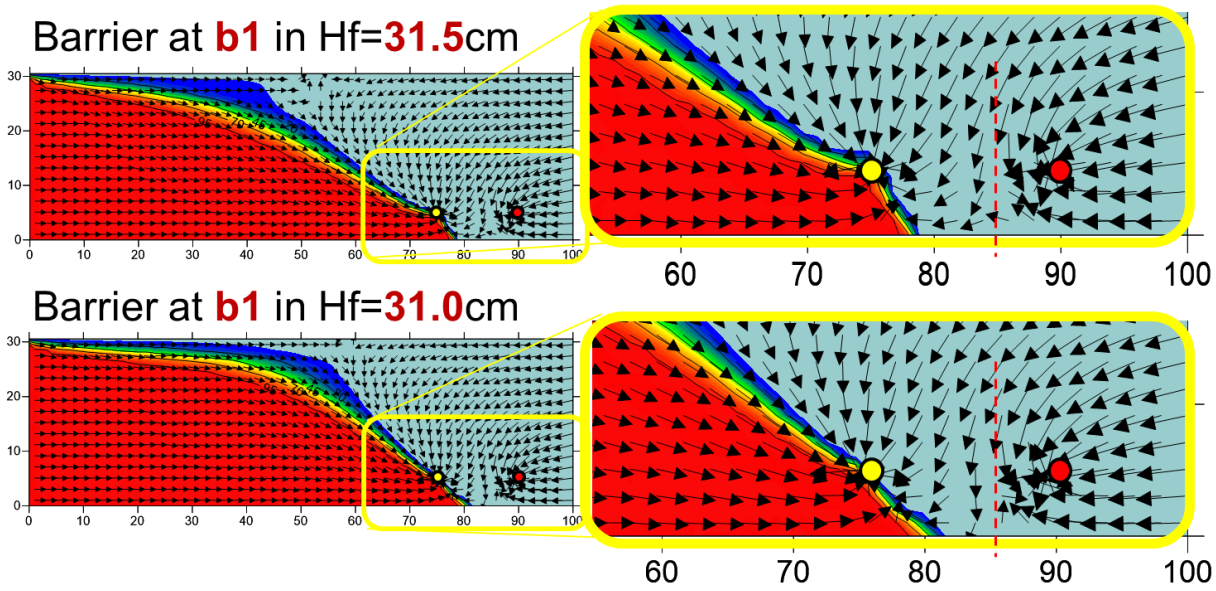

Figure 6-13: Velocity distribution around the production well and the barrier well at b1.

Figure 6-14 shows the time to remediate the equiconcentration line for 95 %, 70 %, 45 %, 20 %, and 0 % by the barrier wells at b1, b2, b3, b4, and b5 in each groundwater level condition. The figure clearly shows that the groundwater level reduction hindered the remediation efficiency especially at the wells close to the coast. Even though barrier wells close to the coast can remediate high concentration zones as fast as the other well locations, it takes even longer time to remediate the low concentration zone than the other wells.

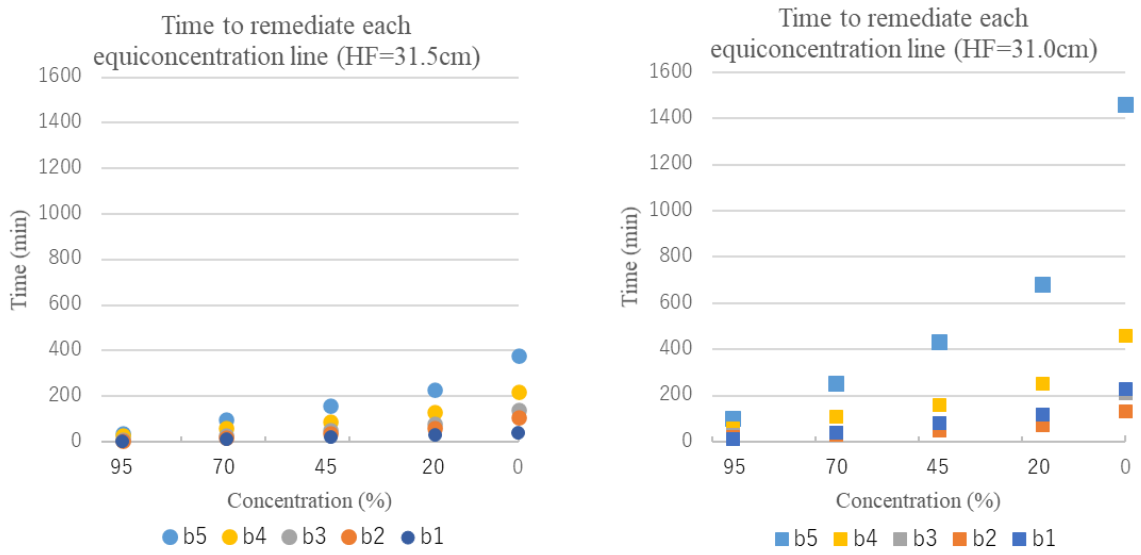

Figure 6-14: Time to remediate each equiconcentration line back to the barrier well

The results of the simulations revealed that there was no exact optimal location to install a barrier well. However, it showed prompt remediation by an inland barrier well, and better remediation rate by a coastal barrier well instead. Besides, coastal barrier wells can minimize the barrier well disadvantage of aggravating coastal salinization, even though they would not function if they were too close to the coast. Barrier wells at depth b showed better remediation rate and time compared to those at depth a even after the groundwater level reduction. However, the groundwater level reduction would hinder the remediation and aggravate the disadvantage of a barrier well to salinize the coastal side more. Considering the results and the fact remediation of seawater intrusion takes as long as decades or centuries in a practical scale, it would be required to find an effective barrier well approach to remediate seawater intrusion faster and better, and to minimize the disadvantage of a barrier well to aggravate the coastal salinization.

3 A suggestion of an optimal barrier well application for the future

Although there are some approaches to make the remediation faster already, such as controlling the pumping volume at the production or barrier wells and applying a mixed barrier system (Ebeling et al., 2019), this study focuses on barrier well locations. Given that other alternative water sources are not available and groundwater pumping cannot be stopped in an arid or semi-arid area, other approaches to remediate seawater intrusion faster without any other water source would be required.

In this study, I suggest a new barrier well application where an operational barrier well is shifted from inland to the coast step by step. This approach takes advantage of the prompt remediation by an inland barrier well and the high remediation rate by a coastal barrier well. The simulation in this section evaluates the effectiveness of this approach in 31.0 cm groundwater level.

Figure 6-15 shows the conceptual image of this approach and the remediation process. Since the barrier well at b1 took a long time for the remediation due to the slowdown of the horizontal flow as explained in the previous section, the barrier well at b2 is used for the first inland barrier (Step1). Once the remediation with the barrier well at b2 completes, the pump at b2 is stopped and the barrier well at b3 starts the operation until the remediation completes (Step2). Then, the operational barrier well is shifted to the next one in the same way and remediate seawater intrusion back to the barrier well at b4 (Step3). At last, the operational barrier well at b4 stops the pumping and the barrier well at b5 starts the operation until the remediation completes (Step4).

Step1 is the same process as the conventional approach that was simulated in the previous section and the remediation completed in 130 minutes. In Step2, the remediation by the well at b3 completed in 40 minutes. At the beginning of Step2, seawater intrusion toe encroached inland slightly, and then it was remediated gradually. This encroachment also happened at the beginning of the other steps, and it was intense especially in Step4. Figure 6-16 shows the image of the encroachment of the toe in Step4. The figure shows that the low concentration zone intruded inland, even though the barrier remediated the high concentration zone fast. This is probably because the intrusion toe with low concentration (less than 20%) reached the point where the production well can take as shown by the red dashed line, and the production well pulled only that low concentration zone, which makes the remediation time longer. Although upconing was caused by the production well, the salinity around the production well was less than 0.5% and it did not affect the production quality.

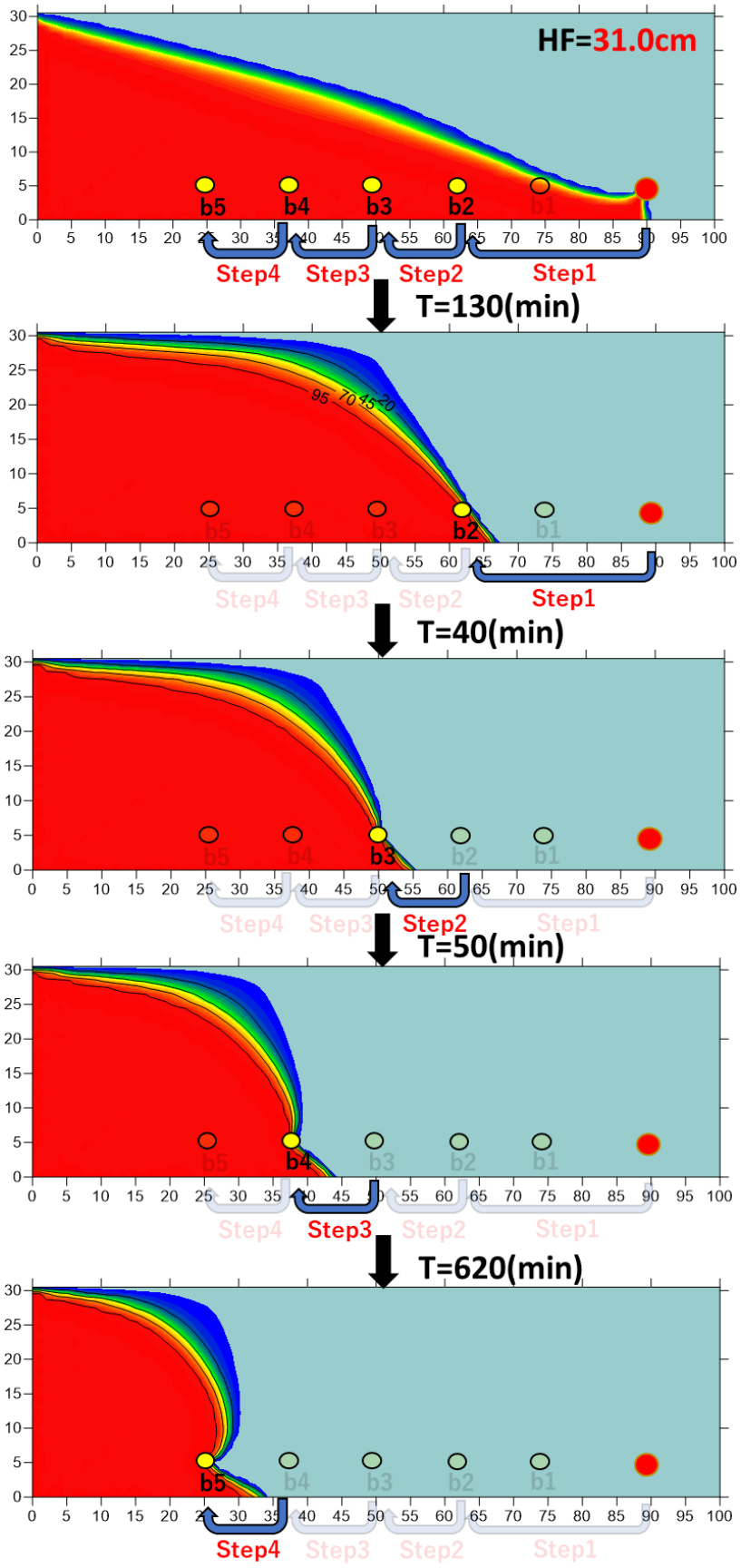

Figure 6-15: The remediation process by the suggested approach.

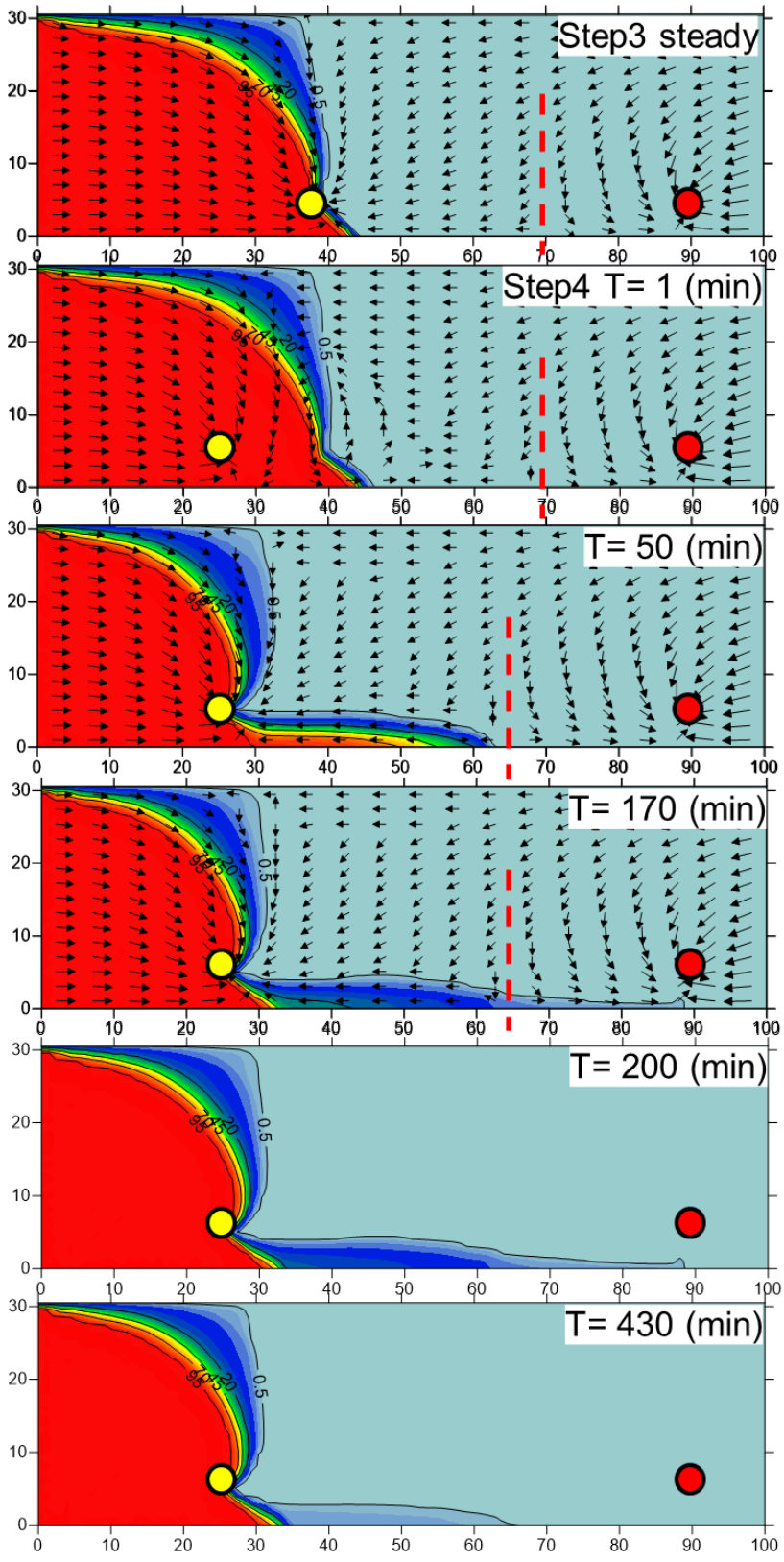

Figure 6-16: The image of the encroachment of the toe in Step4.

Despite the encroachment in each step, the remediation time was still even faster than the remediation by the conventional approach. Table 6-5 shows the cumulative remediation time at each location by the suggested approach and the conventional approach that is simulated in the previous section. Since the suggested approach prevents seawater intrusion into the production well in Step1, Time2 was not measured in the other steps. Remediation time at b2 did not have any difference because the first step was completely the same as the conventional approach. However, the remediation time at b3 by the suggested approach was 40 minutes faster than that of the conventional approach. In the same way, the suggested approach saved 240 minutes and 620 minutes to remediate seawater intrusion at b4 and b5, respectively.

Table 6-5: Remediation time by the conventional approach and the suggested approach.

	Conventional		**Suggestion**	
Barrier well	**Time2 (min)**	**Time3 (min)**	**Time2 (min)**	**Time3 (min)**
b2	**100**	**130**	**100**	**130**
b3	**160**	**210**	**-**	**170**
b4	**280**	**460**	**-**	**220**
b5	**980**	**1460**	**-**	**840**

As a conclusion of this simulation, it was clearly shown that the suggested approach, where the operational barrier well was shifted from inland to the coast step by step, would expedite the remediation at each step. Besides, considering the coastal barrier well was used in the last step, this method would remediate the intrusion length better and minimize the disadvantage of a barrier well to salinize the coastal side.

However, all the simulation in this study was conducted on a laboratory scale two dimensionally. Although this study revealed the potential of the suggested method, it still needs to be studied in a practical scale in three-dimension to employ the suggested approach in practice.

Chapter 7: Conclusions

In this study, an optimal barrier well location and effects of groundwater level reduction on the optimal location were investigated through the two laboratory scale experiments and the numerical simulation. Besides, based on the simulation results, an effective barrier well application was suggested for the future and its effectiveness was examined.

Thorough Experiment 1, where the barrier efficiencies at four different barrier well locations were compared, it was shown that the coastal barrier well can remediate seawater intrusion at lower pumping rate than the inland barrier well. Furthermore, the barrier well pumping from the lower part of the aquifer remediated seawater intrusion the most among the four barrier wells. Even though this experiment showed the effect of the barrier wells, salinization deteriorated on the coast side in all the cases of this study, since the barrier well pulled saline water from the coast. It was found as another disadvantage of negative hydraulic barriers. However, this study also revealed that the coastal barrier wells can minimize the disadvantage.

In Experiment 2, where the impact of the groundwater level reduction on seawater intrusion was examined, further seawater intrusion was caused in the coastal side as well as the intrusion length. Especially when a barrier well was employed at 31.0cm groundwater level, the disadvantage aggravating the coastal salinization was more severe. Therefore, sea level rise or over abstraction of groundwater would cause further seawater intrusion and aggravate the disadvantage of a barrier well.

Considering these experimental results, it would be better to install a barrier well closer to the coast and pump groundwater from the lower part of the aquifer in the future because the well location is more effective to remediate seawater intrusion and also diminishes the disadvantage to aggravate the coastal salinization.

The simulation model successfully reproduced the experimental results with high accuracy. The optimal well location analysis showed that the barrier wells pumping from the lower part of the aquifer remediated seawater intrusion better in terms of the remediation rate and time. The simulation also revealed that there is no exact optimal horizontal location to install a barrier well, and a barrier well close to the production well can remediate seawater intrusion promptly and a barrier well close to the coast can remediate seawater intrusion better and minimize the disadvantage to salinize the coast side. However, the groundwater level reduction hindered the remediation and provoked more intense salinization in the coast side as the negative effect of the barrier well. Therefore, a new barrier well approach would be required to remediate seawater intrusion better and faster, and also to minimize the disadvantage of a barrier well.

Based on the simulation results, an effective barrier well application method was suggested to

make the remediation more efficient and faster for the future. In the suggested application method, an operational barrier well is shifted from inland to the coast step by step, in other words, use the inland barrier well at first and then change it to the coastal one gradually once the remediation by the barrier well completes. This is how the suggested method can take advantage of the prompt remediation by an inland barrier well and the better remediation rate by a coastal barrier well. In fact, the suggested method could expedite the remediation and the final condition in the aquifer was as good as the remediation by a coastal barrier well.

However, this study was conducted only on a laboratory scale and simulated in two dimensions. Even though the potential of the suggested method to expedite the remediation was shown in this study, it still needs to be studied more on a practical scale three dimensionally in order to apply the method in practice.

References

Abd-Elhamid, H.F., Javadi, A.A., & Qahman, K.A. (2015). Impact of climate change and sea level rise on seawater intrusion in Gaza aquifer (Palestine). *Journal of Water and Climate*, 6(4): jwc2015055

Abi-Akl, C. (2020). Experimental Laboratory Observation of the Effectiveness of the Saltwater Pumping from Barrier Well as a Countermeasure to Salinization

Blair, T.C., & McPherson, J.G. (1999). Grain-size and textural classification of coarse sedimentary particles. *Journal of Sedimentary Research*, 69(1), pp.6-19.

Castro-Orgaz, O. (2011). Steady free-surface flow in porous media: generalized Dupuit–Fawer equations, *Journal of Hydraulic Research*, 49(1), pp.55-63, DOI: 10.1080/00221686.2010.526758

Costall, A., Harris, B., & Pigois, J.P. (2018). Electrical Resistivity Imaging and the Saline Water Interface in High-Quality Coastal Aquifers. *Survey in Geophysics*, 39, pp. 753-816.

Dierch, H.j.G. & Kolditz, O. (2002). Variable-density flow and transport in porous media: approaches and challenges. *Advances in Water Resources*, Vol.25, 8-12, pp.899-944. DOI:10.1002/(SICI)1099-1085(19990615)13:8<1277: AID-HYP765>3.0.CO;2-W

Ebeling, P., Handel, F., & Walther, M. (2019). Potential or mixed hydraulic barriers to remediate seawater intrusion. *Science of the Total Environment*, 693, 133478

Elizabeth, L.E., Miguel, A., Maria, G. & Eduardo, A. (2008). A model for calculating the density of aqueous multicomponent electrolyte solutions. *Journal of The Chilean Chemical Society*, 53(1), pp.1404-1409. DOI:10.4067/S0717-97072008000100015

Fetter, C.W. (2014). Applied hydrogeology. 4th ed. Pearson, pp.15-16, 367-369.

Fujita, Y. (2020). Laboratory-scale investigation about examination of effectiveness of barrier well to prevent saltwater intrusion and possible water intake of production well (In Japanese)

Hussain, M.S., Abd-Elhamid, H.F., Javadi, A.A., & Sherif, M.M. (2019). Management of Seawater Intrusion in Coastal Aquifers: A Review. *Water*, 11, 2467.

Ingham, M., Mcconchie, J. & Cozens, N. (2006). Measuring and monitoring saltwater intrusion in shallow unconfined coastal aquifers using direct current resistivity traverses. *Journal of Hydrology*. New Zealand. 45(2). pp.69-82.

IPCC (2019). Sea Level Rise and Implications for Low-Lying Islands, Coasts and Communities. In: IPCC Special Report on the Ocean and Cryosphere in a Changing Climate [H.-O. Po¨rtner, D.C. Roberts, V. Masson-Delmotte, P. Zhai, M. Tignor, E. Poloczanska, K. Mintenbeck, A. Alegría, M. Nicolai, A. Okem, J. Petzold, B. Rama, N.M. Weyer (eds.)]. In press.

Jinno, K., Momii, K., Fujino, K., Nakagawa, K., Hosokawa, T., Egusa, N., & Hiroshiro, Y. (2001). Numerical analysis of mass transport in groundwater (In Japanese). *Kyushu University Press*. pp.1-99.

Ozaki, S. (2021). Effectiveness of Barrier Well by Pumping Ratio Control for Saltwater Intrusion: Lab Scale Experiments and Numerical Modeling

Park, S., Kim, J., Yum, B., & Yeh, G. (2011). Three-Dimensional Numerical Simulation of Saltwater Extraction Schemes to Mitigate Seawater Intrusion due to Groundwater Pumping in a Coastal Aquifer System. *Journal of Hydrologic Engineering*, 17, 10-22.

Pool, M., & Carrera, J. (2010). Dynamics of negative hydraulic barriers to prevent seawater intrusion. *Hydrogeology Journal*, 18(1), pp.95-105. DOI 10.1007/s10040-009-0516-1

Sherif, M., & Hamza, K. (2001). Mitigation of seawater intrusion by pumping brackish water. *Transport in Porous Media*, 43(1), pp.29-44.

Sherif, M, M. & Singh, V, P. (1996). Saltwater Intrusion. Hydrology of Disasters Water Science and Technology Library, Vol. 18, Kluwer Academic Publishers, pp.269-319

Sherif, M.M. & Singh, V, P. (1999). Effect of climate change on sea water intrusion in coastal aquifers. *Hydrological Processes*,13(8): pp.1277 – 1287.

Sherif, M, M. & Singh, V, P. (2002). Effect of Groundwater Pumping on Seawater Intrusion in Coastal Aquifers. *Agricultural science*. 7(2): pp.61-67, 2002.

Simion, A.I., Grigoraş, C., Roşu, A., & Gavrilă, L. (2015). Mathematical modelling of density and viscosity of nacl aqueous solutions. *Journal of Agroalimentary Processes and Technologies*. 21(1), pp.41-52.

United Nations (2019). World Population Prospects 2019, Department of Economic and Social Affairs Population Dynamics. Accessed on 28th May 2021, Available at https://population.un.org/wpp/Graphs/DemographicProfiles/Line/900

Yu, C., Loureiro, C., Cheng, J.J., Jones, L.G., Wang, Y.Y., Chia, Y.P., & Faillance, E. (1993). Data collection handbook to support modeling the impacts of radioactive material in soil.

United States. doi:10.2172/10162250.

Appendix-1 Simulation results

This section describes salinity distributions for each simulation. All the figures were edited with Surfer version 10.4.799. The barrier wells which did not function as intended and did not have remediation time data were described in 200 (mins) conditions. As for the other wells, the aquifer conditions at Time 1, Time 2, and Time3 were described in the figures. Note that the color label for each figure was the same as the one shown in Figure 1-a1.

1 Simulation results for 31.5 cm groundwater level

1-1 Barrier wells at depth a

a1

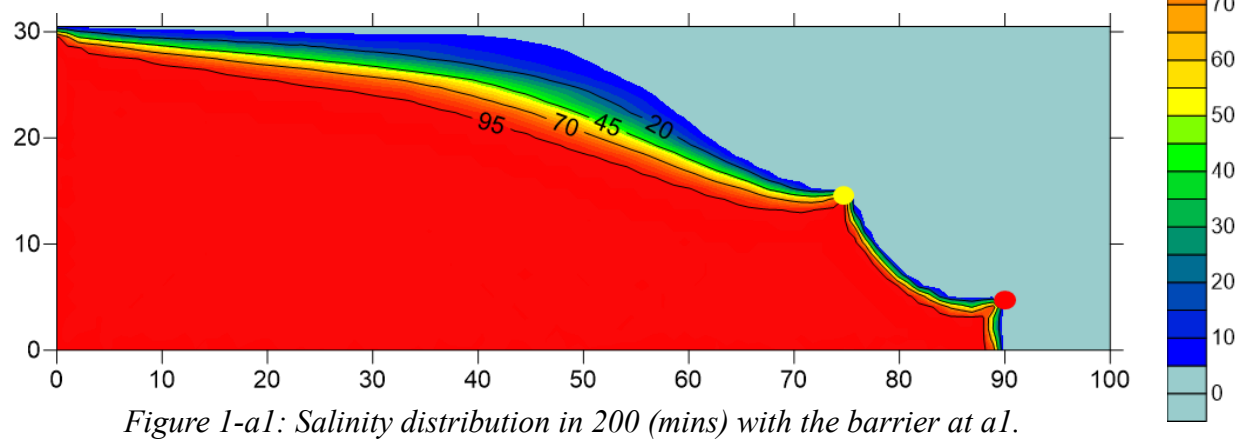

Figure 1-a1: Salinity distribution in 200 (mins) with the barrier at a1.

a2

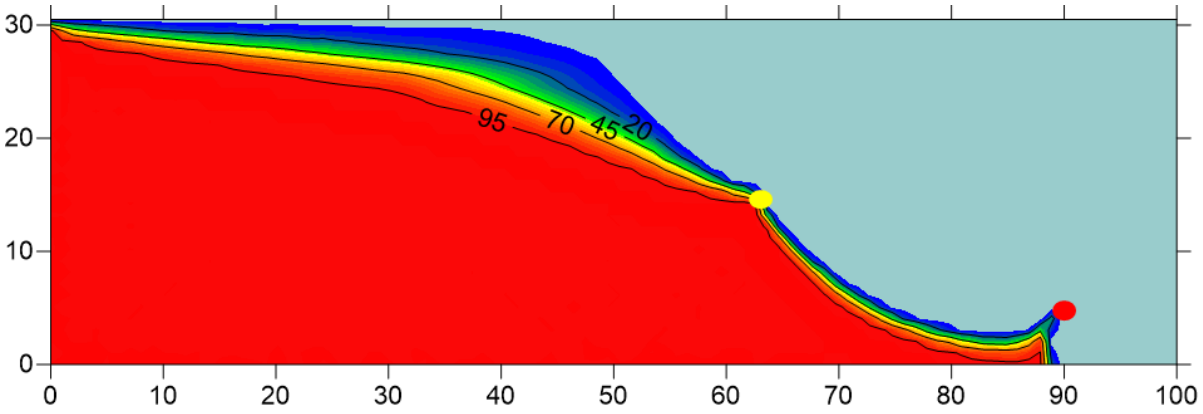

Figure 1-a2: Salinity distribution in 200 (mins) with the barrier at a2.

a3

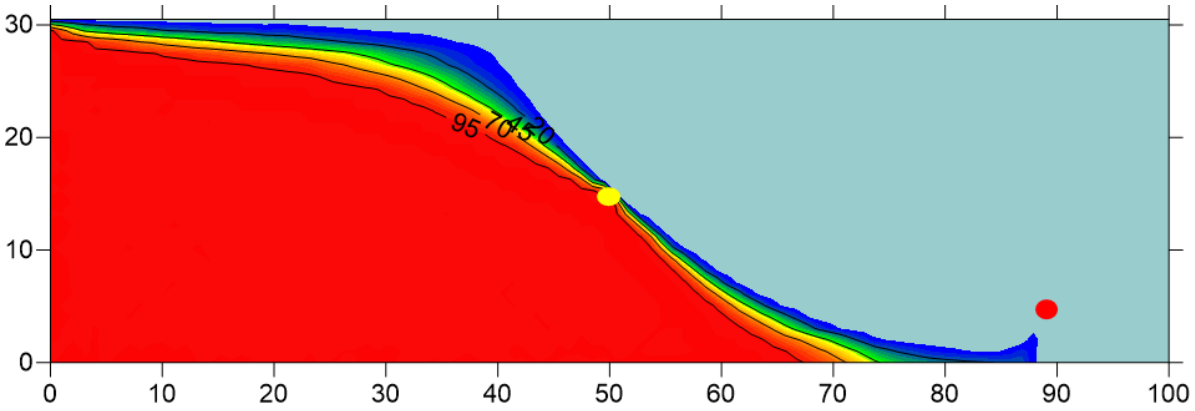

Figure 1-a3: Salinity distribution in 200 (mins) with the barrier at a3.

a4

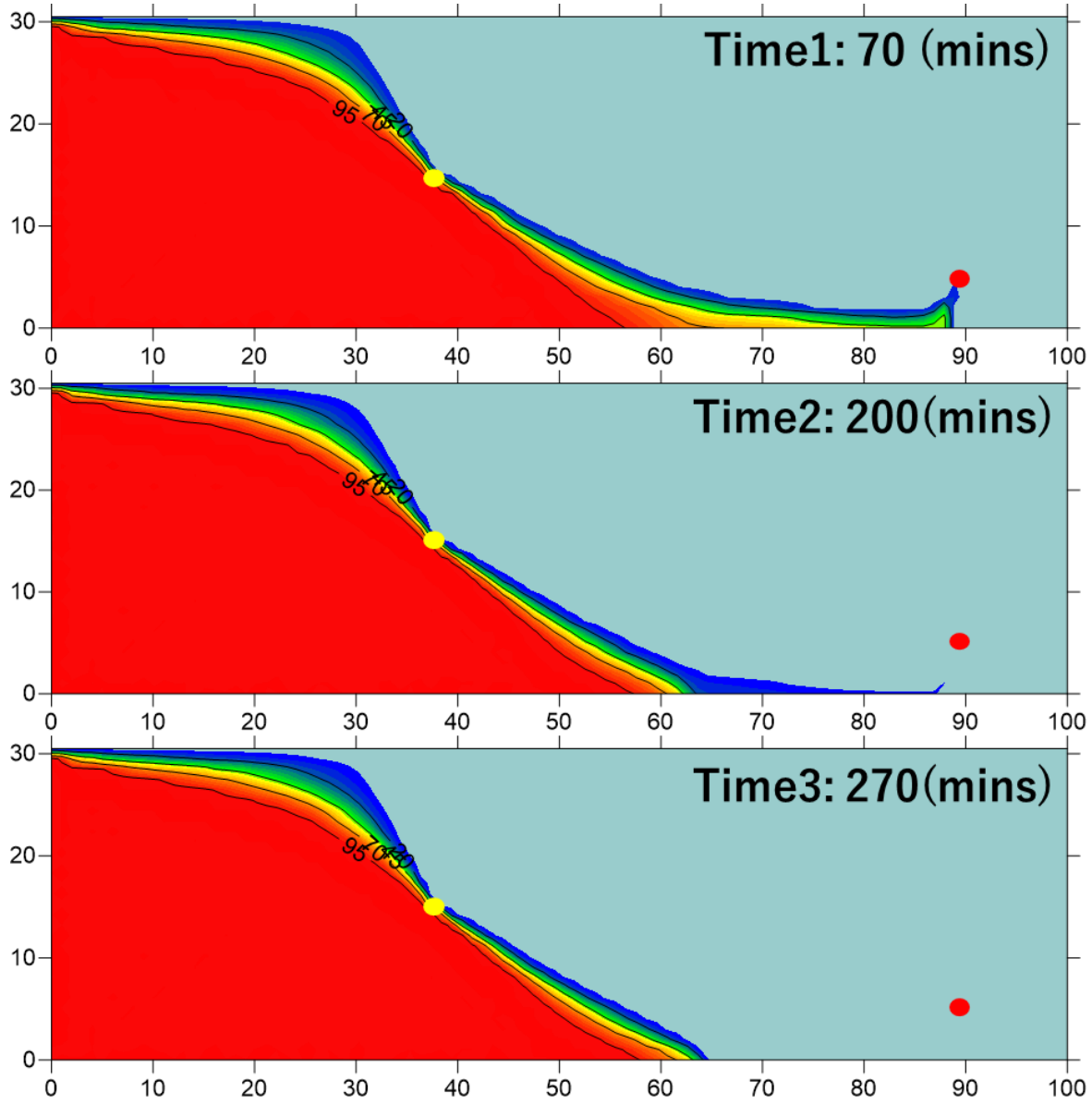

Figure 1-a4: Salinity distribution at each time with the barrier at a4.

a5

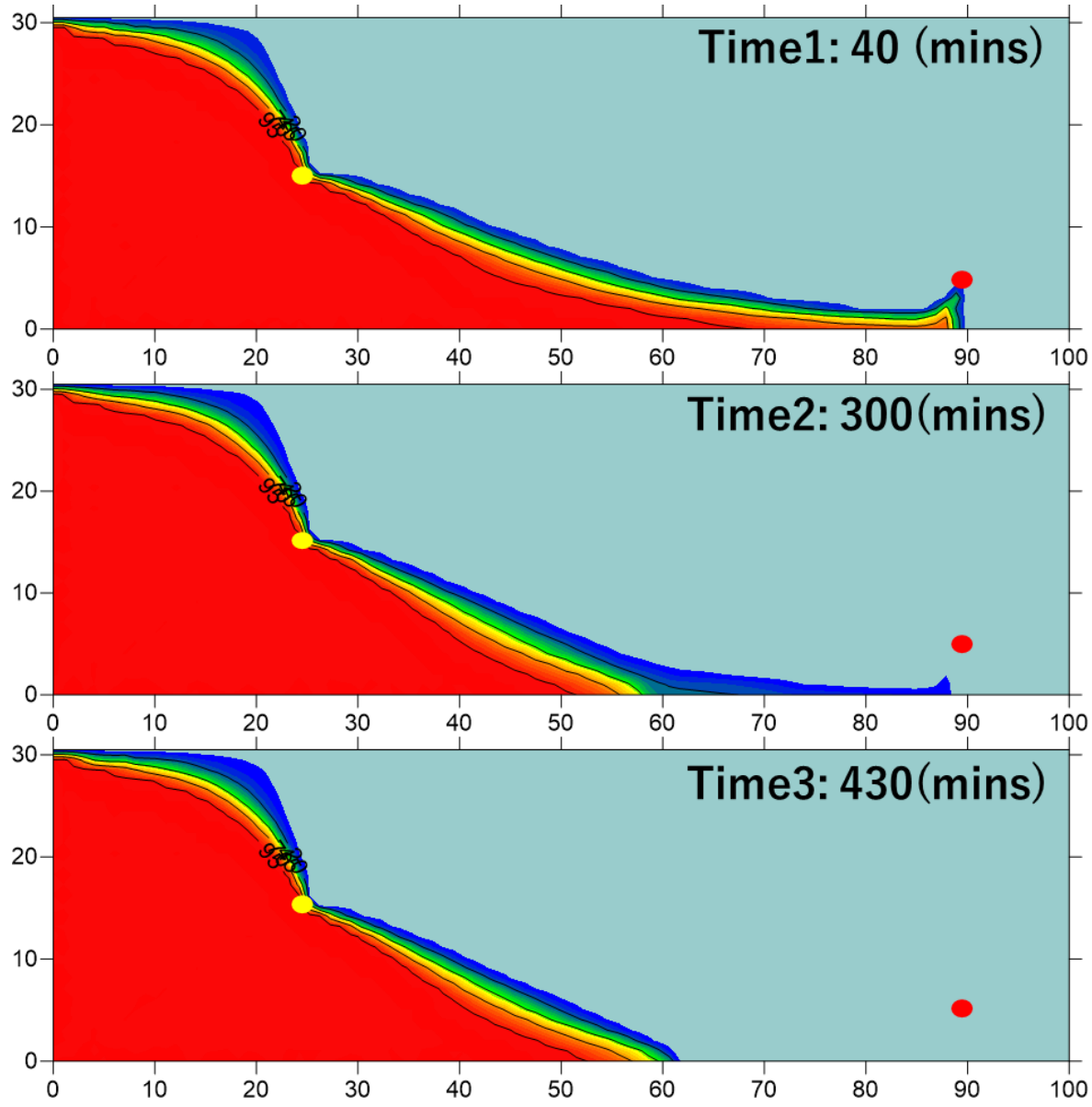

Figure 1-a5: Salinity distribution at each time with the barrier at a5.

a6

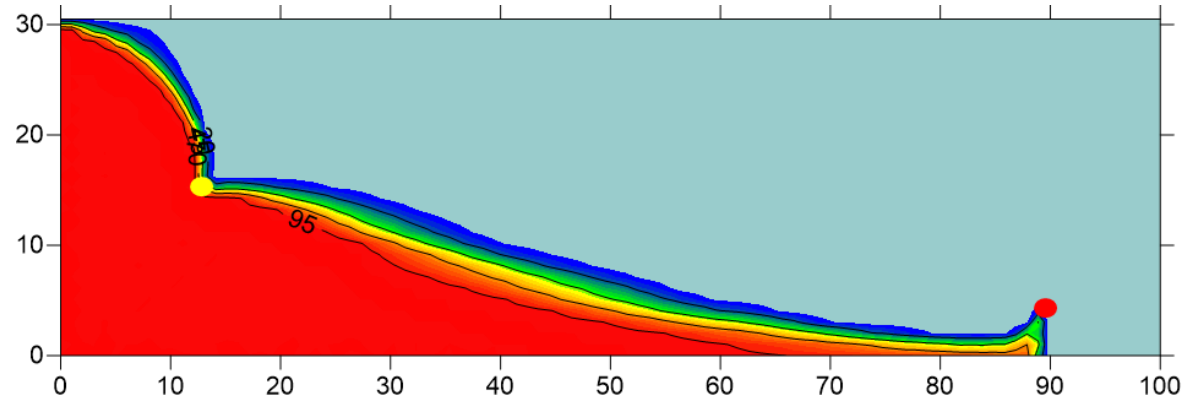

Figure 1-a6: Salinity distribution in 200 (mins) with the barrier at a6.

a7

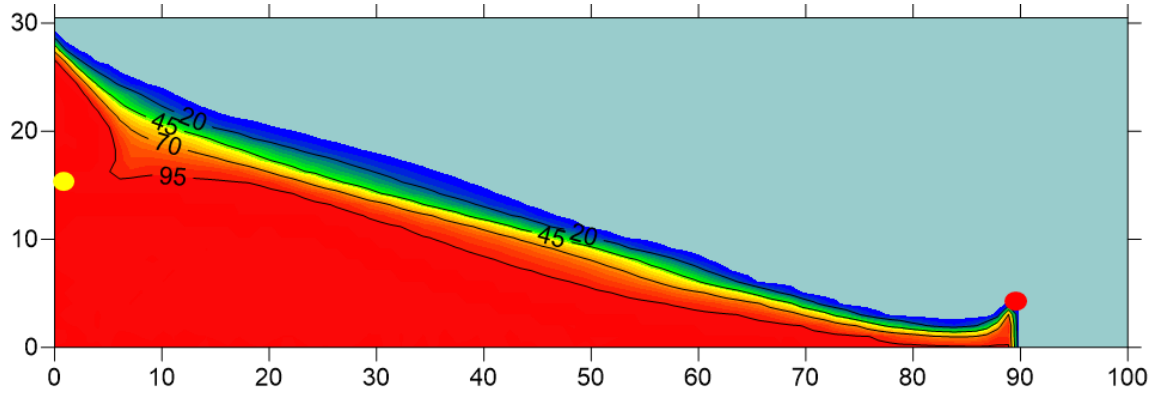

Figure 1-a7: Salinity distribution in 200 (mins) with the barrier at a7.

1-2 Barrier wells at depth b

b1

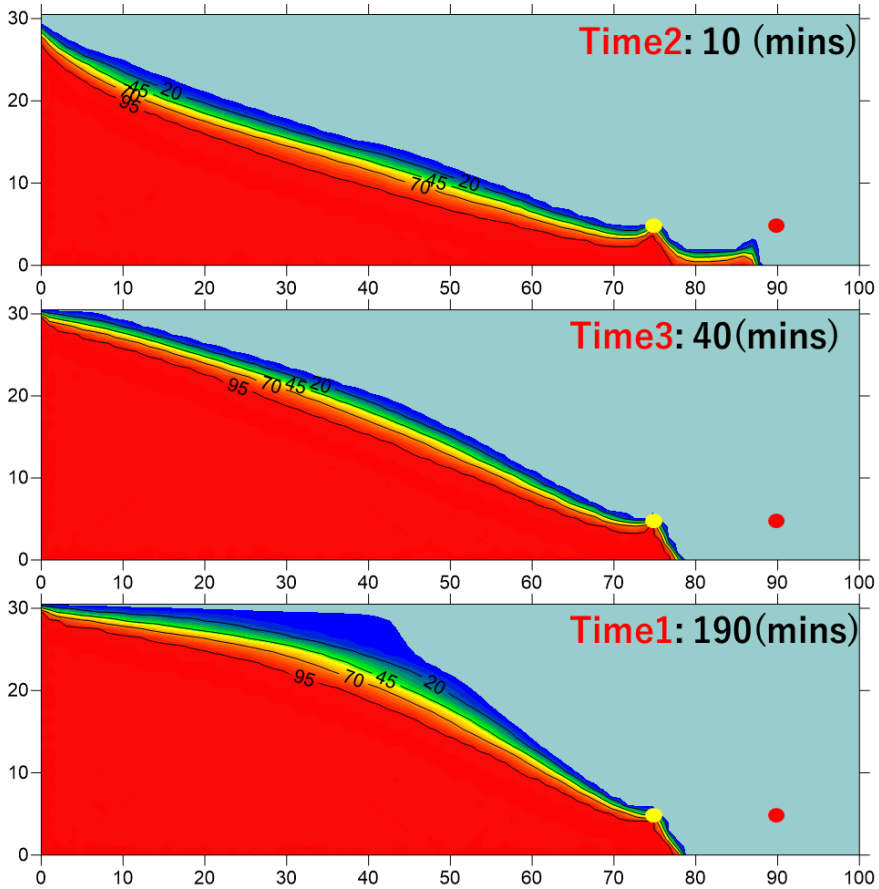

Figure 1-b1: Salinity distribution at each time with the barrier at b1.

As shown in Figure 1-b1, the barrier well at b1 restored the production quality in 10 mins and the remediation completed in 40 mins. However, the coastal salinization continued until 190 mins. Therefore, the order of the times (Time1, 2, and 3) was different from the others. This also happened at b2 for 31.5 cm groundwater level and at b1 for 31.0 cm groundwater level, as shown in Figure 1-b2 and 2-b1.

b2

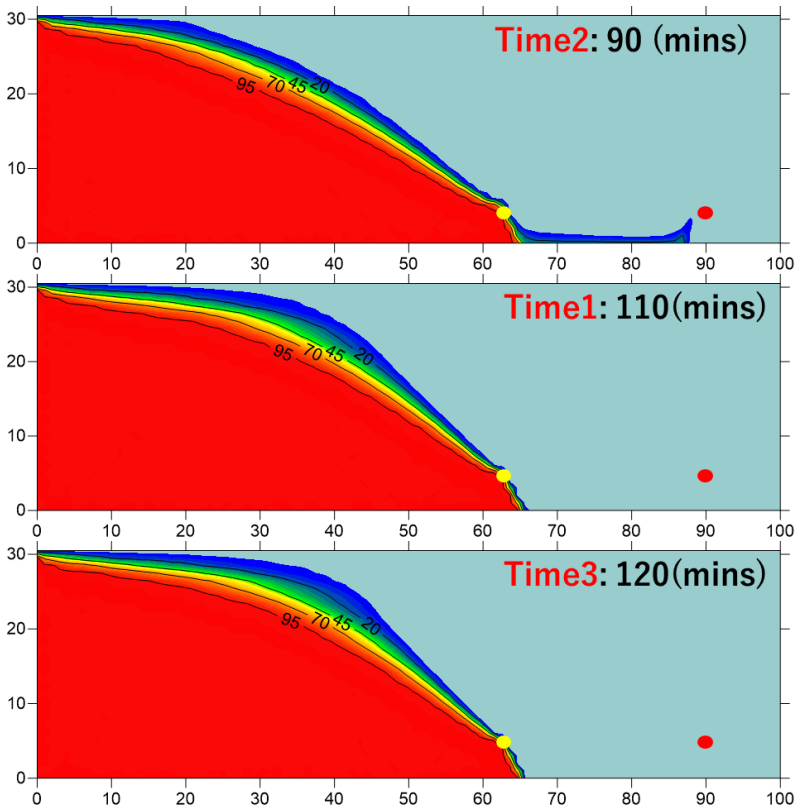

Figure 1-b2: Salinity distribution at each time with the barrier at b2

b3

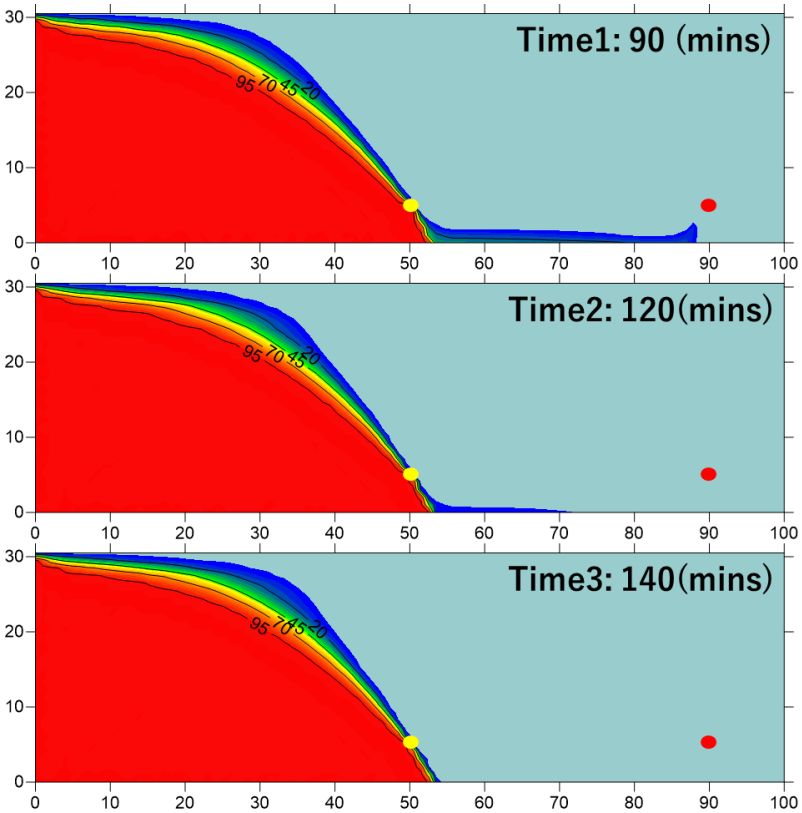

Figure 1-b3: Salinity distribution at each time with the barrier at b3

b4

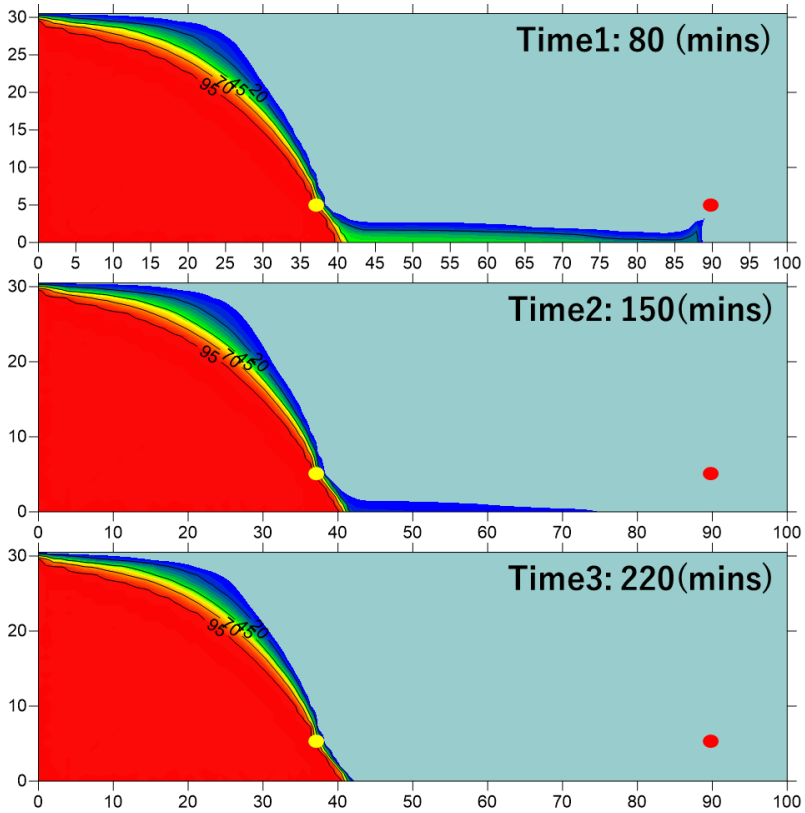

Figure 1-b4: Salinity distribution at each time with the barrier at b4

b5

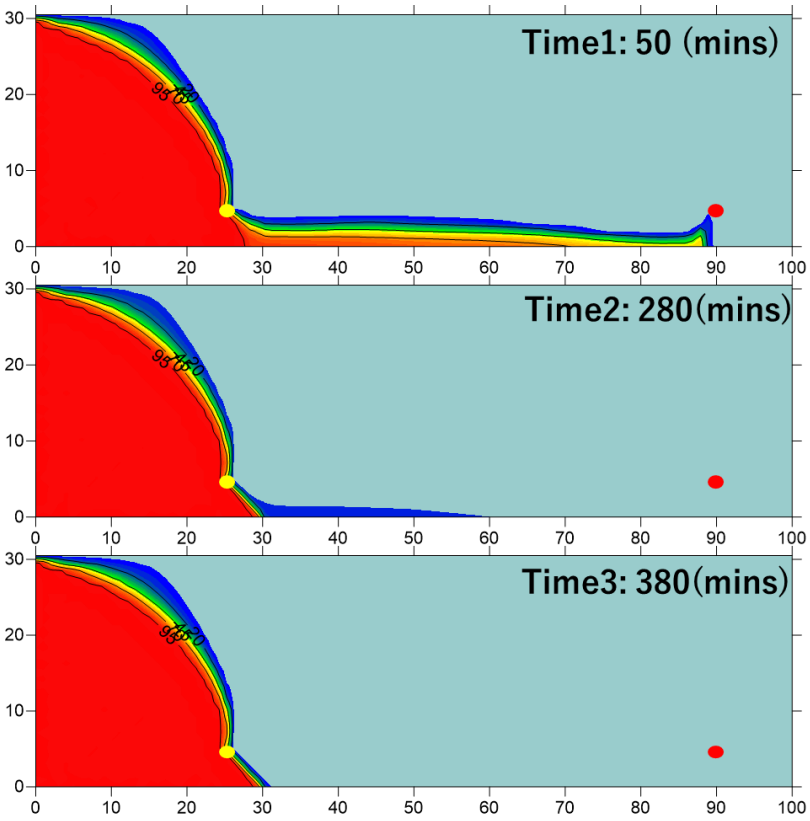

Figure 1-b5: Salinity distribution at each time with the barrier at b5

b6

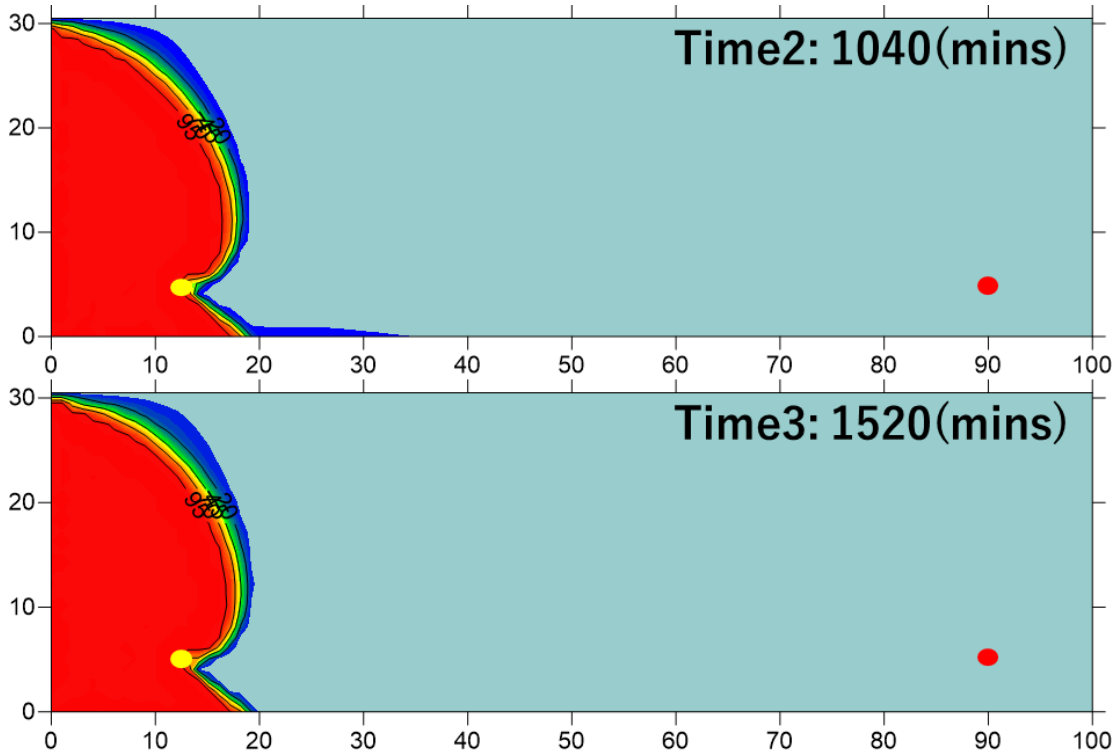

Figure 1-b6: Salinity distribution at each time with the barrier at b6

b7

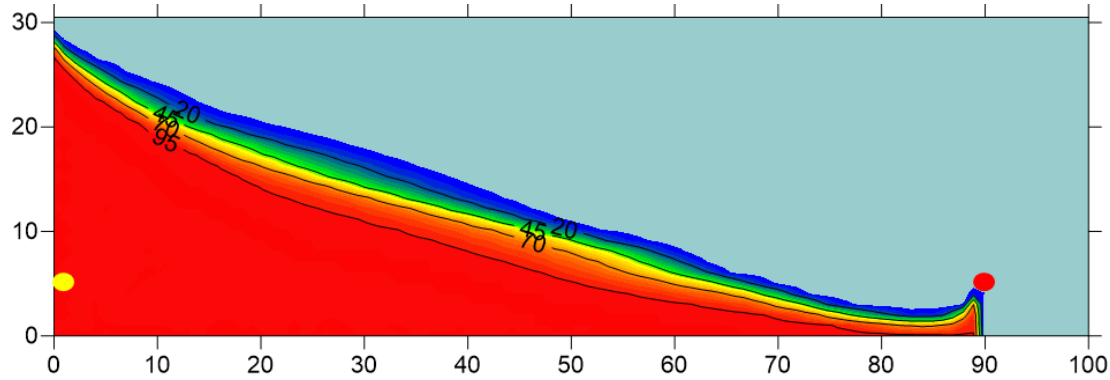

Figure 1-b7: Salinity distribution in 200 (mins) with the barrier at b7.

2 Simulation results for 31.0 cm groundwater level

2-1 Barrier wells at depth a

a1

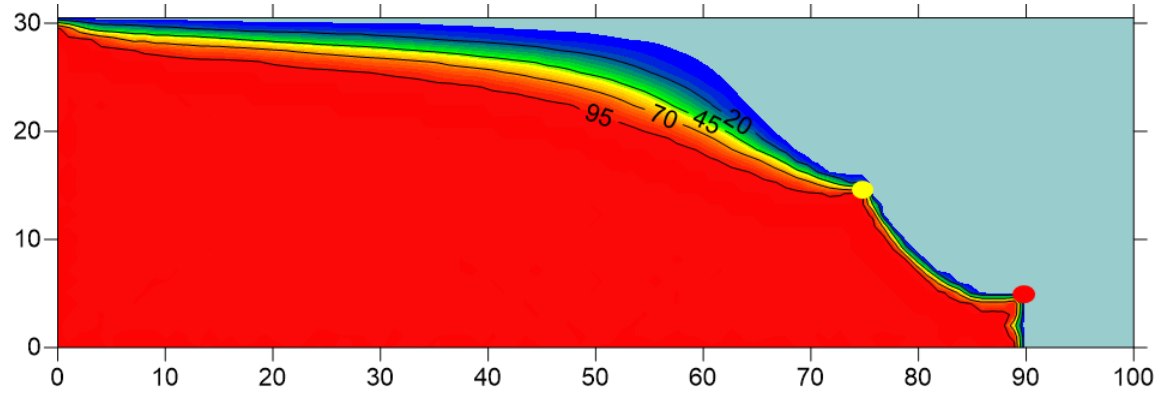

Figure 2-a1: Salinity distribution in 200 (mins) with the barrier at a1.

a2

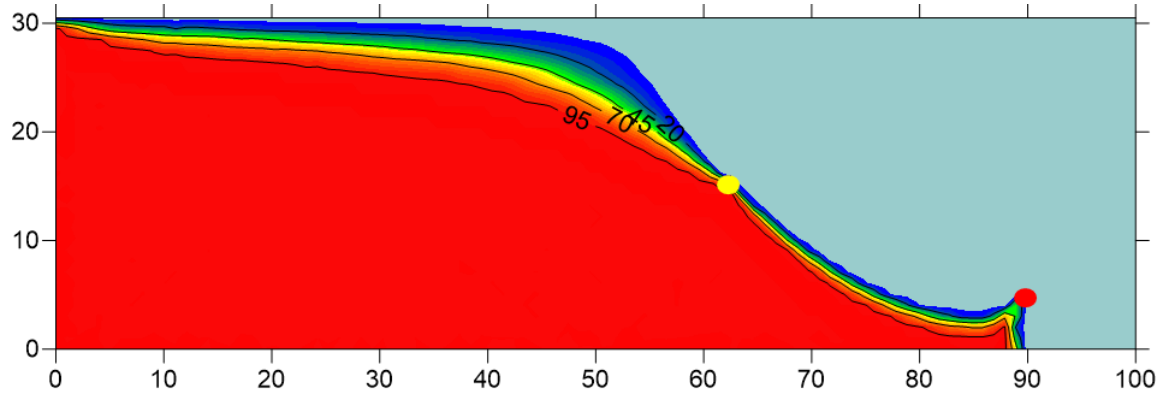

Figure 2-a2: Salinity distribution in 200 (mins) with the barrier at a2.

a3

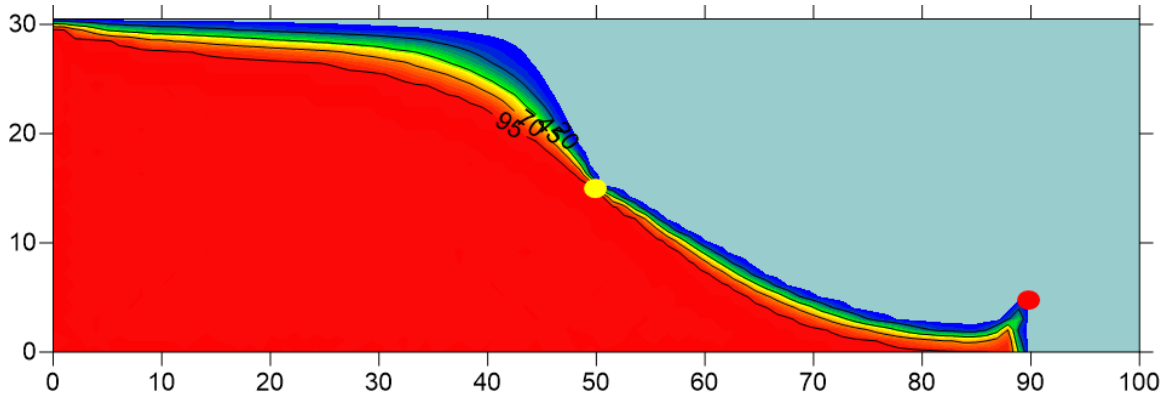

Figure 2-a3: Salinity distribution in 200 (mins) with the barrier at a3.

a4

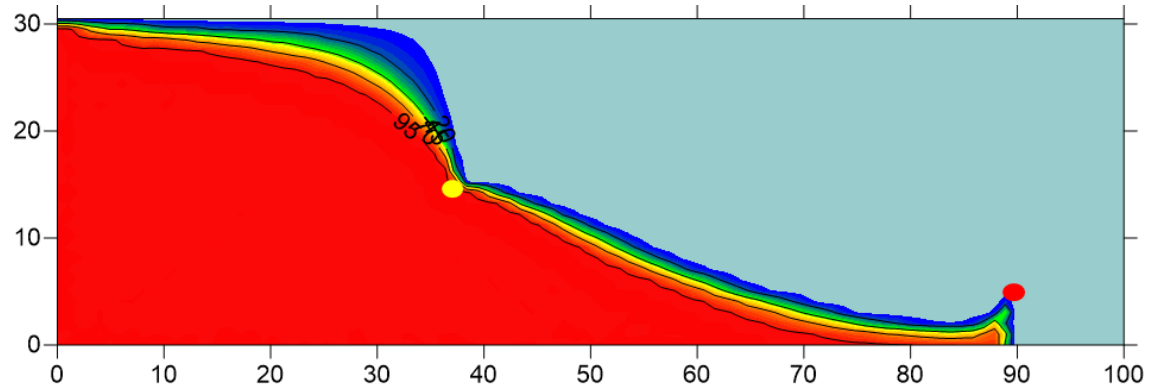

Figure 2-a4: Salinity distribution in 200 (mins) with the barrier at a4.

a5

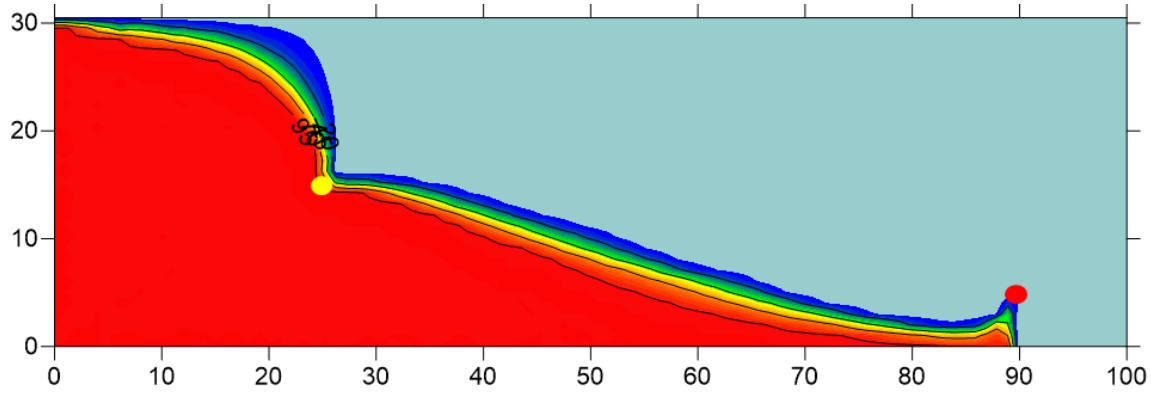

Figure 2-a5: Salinity distribution in 200 (mins) with the barrier at a5.

a6

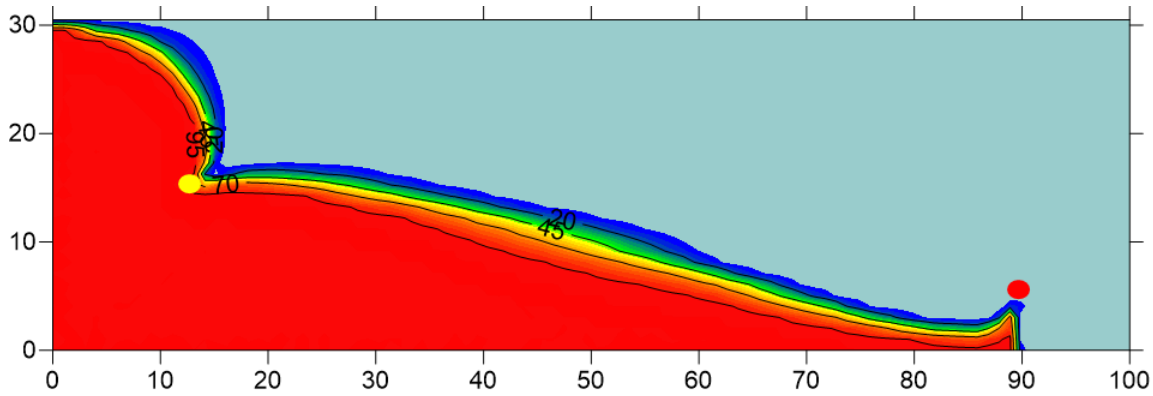

Figure 2-a6: Salinity distribution in 200 (mins) with the barrier at a6.

a7

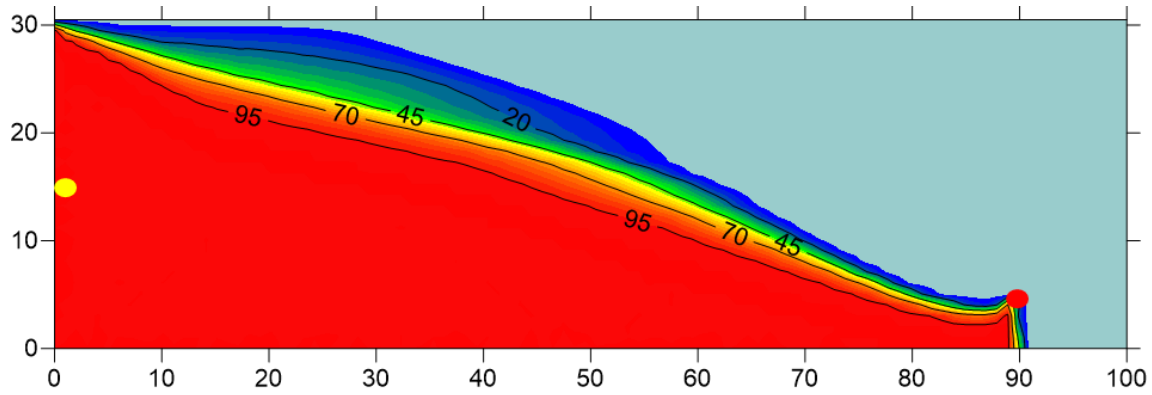

Figure 2-a7: Salinity distribution in 200 (mins) with the barrier at a7.

2-2 Barrier wells at depth b

b1

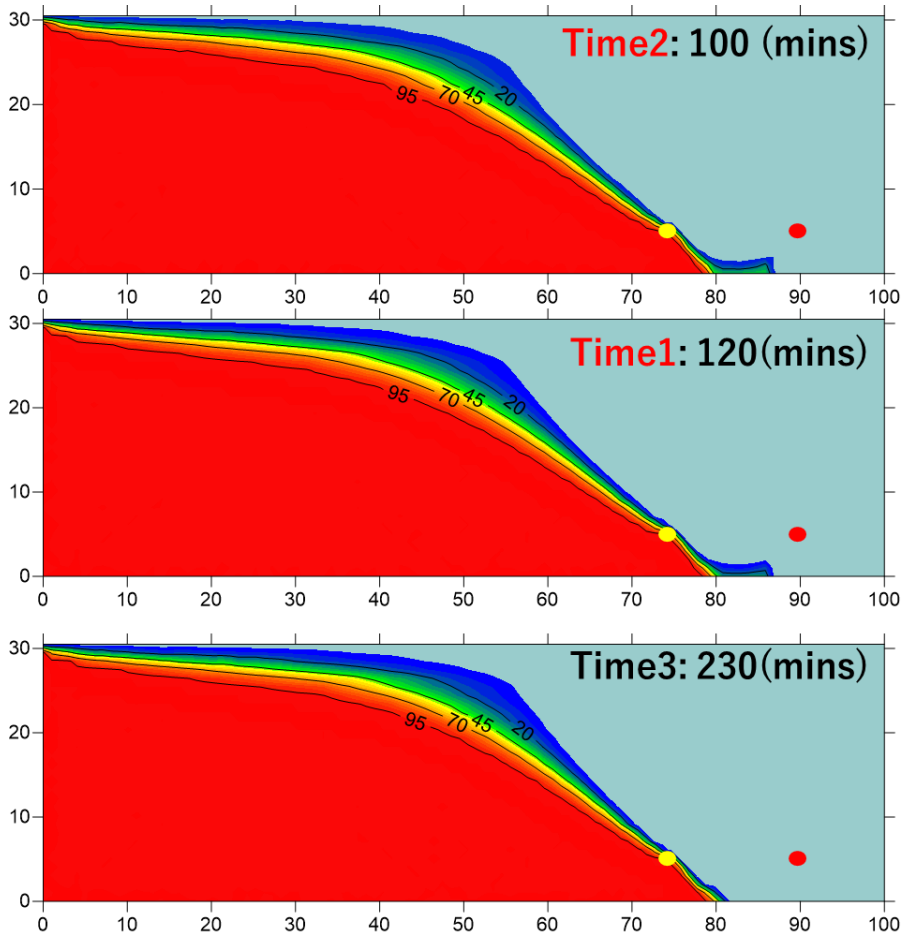

Figure 2-b1: Salinity distribution at each time with the barrier at b1

b2

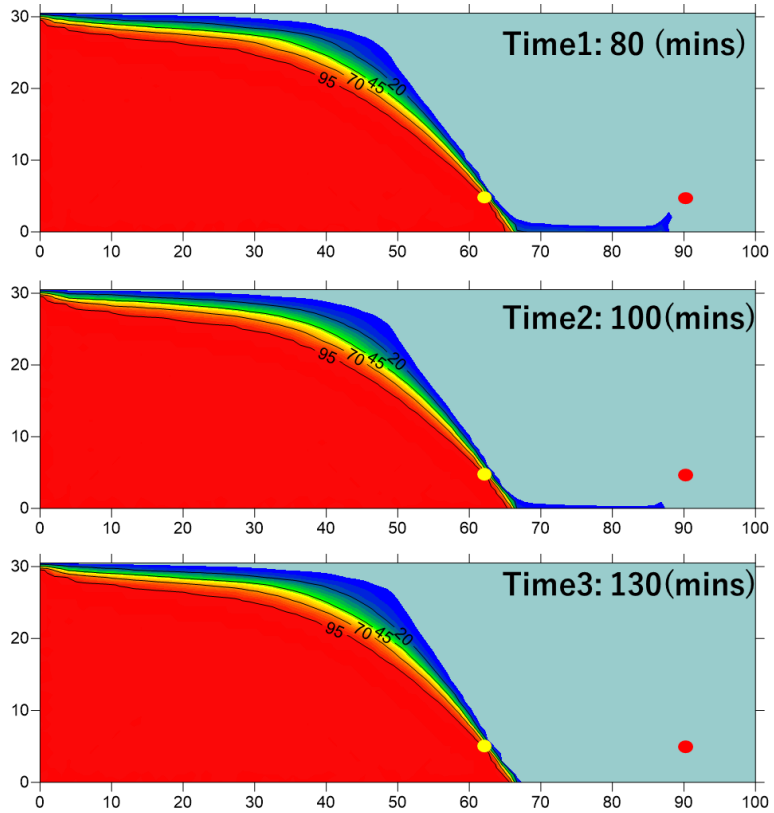

Figure 2-b2: Salinity distribution at each time with the barrier at b2

b3

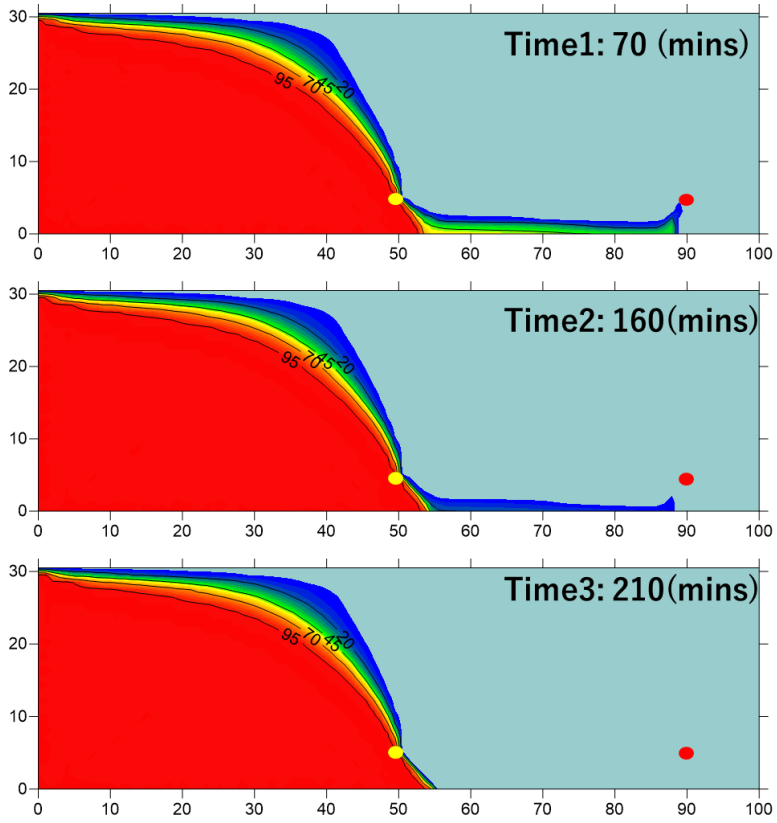

Figure 2-b3: Salinity distribution at each time with the barrier at b3

b4

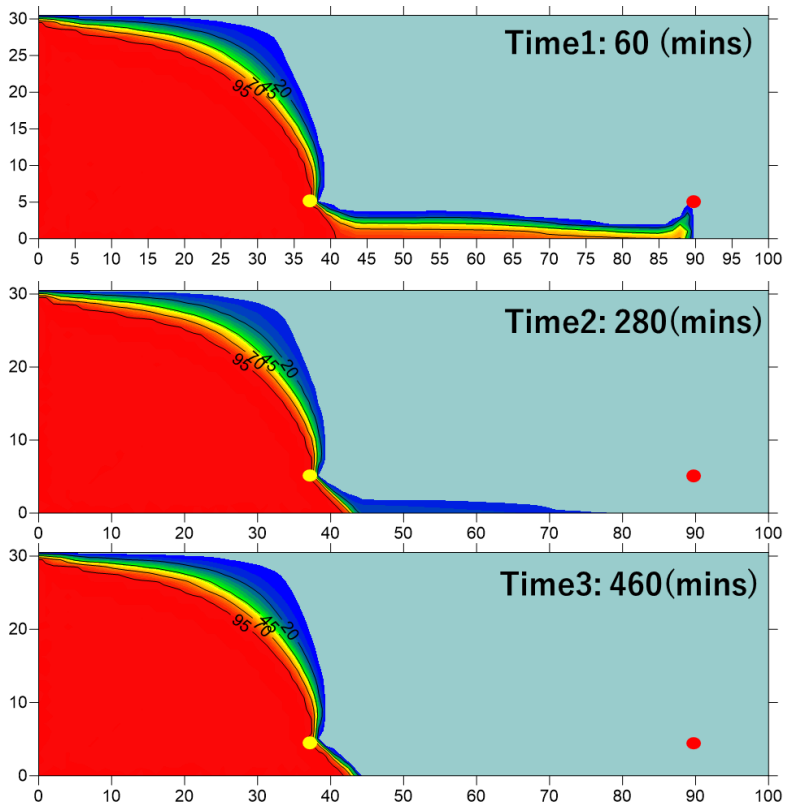

Figure 2-b4: Salinity distribution at each time with the barrier at b4

b5

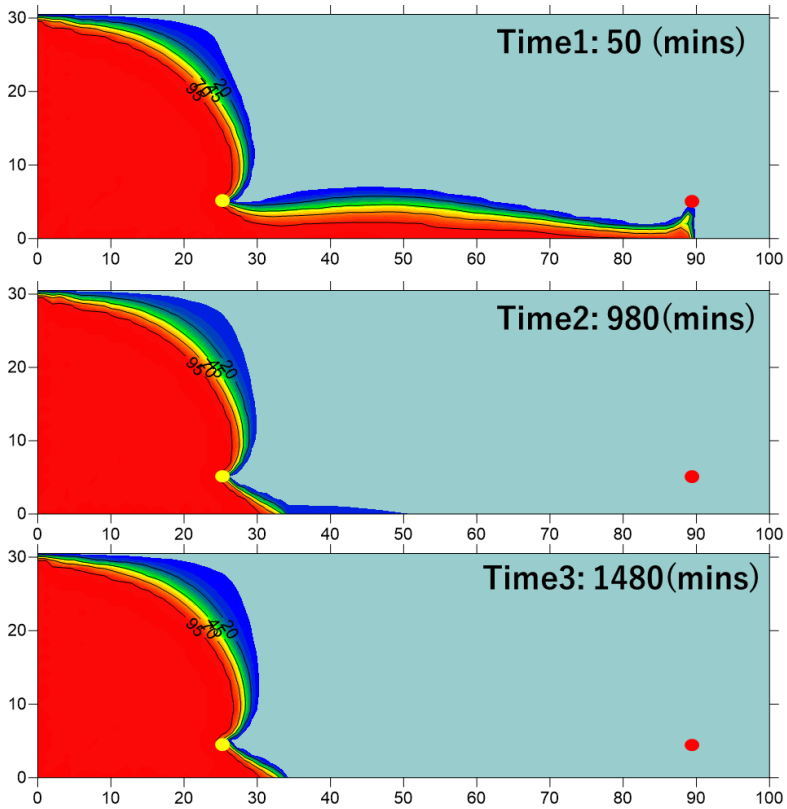

Figure 2-b5: Salinity distribution at each time with the barrier at b5

b6

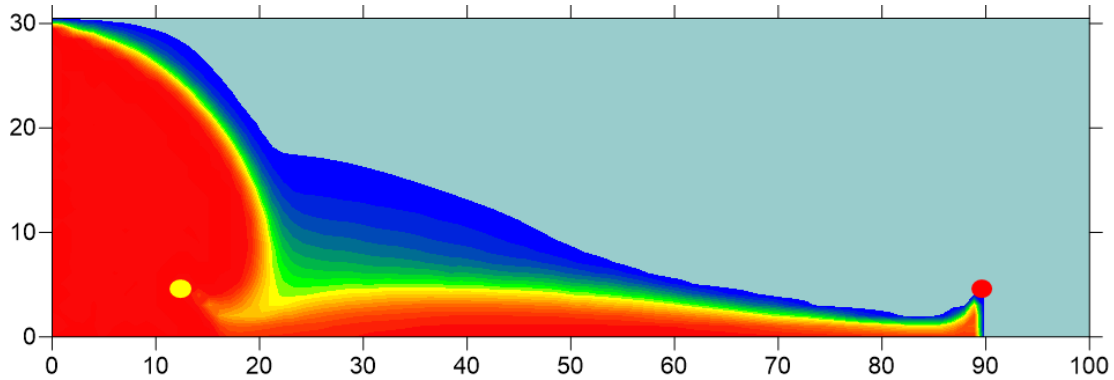

Figure 2-b6: Salinity distribution at each time with the barrier at b6

b7

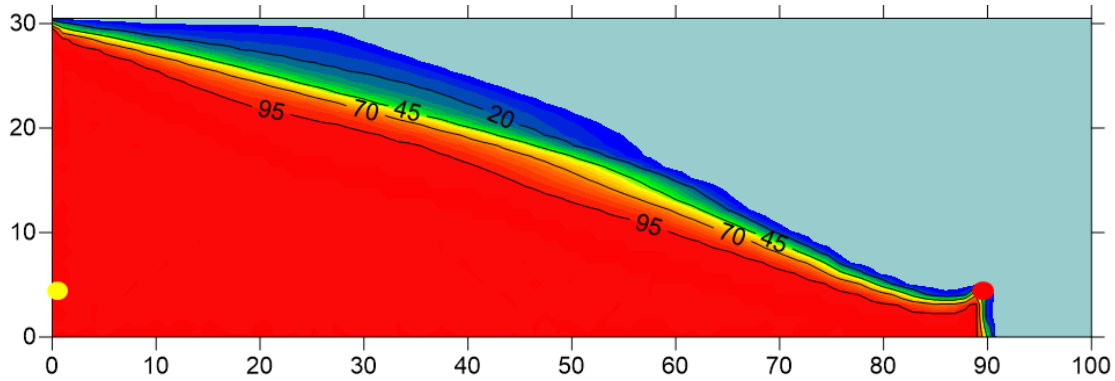

Figure 2-b7: Salinity distribution at each time with the barrier at b7